

ISSN: 2408-2384 (Online)

ISSN: 1686-5456 (Print)

Environment and Natural Resources Journal

Volume 19, Number 4, July - August 2021



Scopus® Clarivate
Analytics



DOAJ DIRECTORY OF
OPEN ACCESS
JOURNALS



TCI
THAI JOURNAL CITATION INDEX CENTRE

Environment and Natural Resources Journal (EnNRJ)

Volume 19, Number 4, July - August 2021

ISSN: 1686-5456 (Print)

ISSN: 2408-2384 (Online)

AIMS AND SCOPE

The Environment and Natural Resources Journal is a peer-reviewed journal, which provides insight scientific knowledge into the diverse dimensions of integrated environmental and natural resource management. The journal aims to provide a platform for exchange and distribution of the knowledge and cutting-edge research in the fields of environmental science and natural resource management to academicians, scientists and researchers. The journal accepts a varied array of manuscripts on all aspects of environmental science and natural resource management. The journal scope covers the integration of multidisciplinary sciences for prevention, control, treatment, environmental clean-up and restoration. The study of the existing or emerging problems of environment and natural resources in the region of Southeast Asia and the creation of novel knowledge and/or recommendations of mitigation measures for sustainable development policies are emphasized.

The subject areas are diverse, but specific topics of interest include:

- Biodiversity
- Climate change
- Detection and monitoring of polluted sources e.g., industry, mining
- Disaster e.g., forest fire, flooding, earthquake, tsunami, or tidal wave
- Ecological/Environmental modelling
- Emerging contaminants/hazardous wastes investigation and remediation
- Environmental dynamics e.g., coastal erosion, sea level rise
- Environmental assessment tools, policy and management e.g., GIS, remote sensing, Environmental Management System (EMS)
- Environmental pollution and other novel solutions to pollution
- Remediation technology of contaminated environments
- Transboundary pollution
- Waste and wastewater treatments and disposal technology

Schedule

Environment and Natural Resources Journal (EnNRJ) is published 6 issues per year in January-February, March-April, May-June, July-August, September-October, and November-December.

Publication Fees

There is no cost of the article-processing and publication.

Ethics in publishing

EnNRJ follows closely a set of guidelines and recommendations published by Committee on Publication Ethics (COPE).

EXECUTIVE CONSULTANT TO EDITOR

Associate Professor Dr. Kampanad Bhaktikul

(Mahidol University, Thailand)

Associate Professor Dr. Sura Pattanakiat

(Mahidol University, Thailand)

EDITOR

Associate Professor Dr. Benjaphorn Prapagdee

(Mahidol University, Thailand)

ASSOCIATE EDITOR

Dr. Witchaya Rongsayamanont

(Mahidol University, Thailand)

Dr. Piangjai Peerakiatkhajohn

(Mahidol University, Thailand)

EDITORIAL BOARD

Professor Dr. Anthony SF Chiu

(De La Salle University, Philippines)

Professor Dr. Chongrak Polprasert

(Thammasat University, Thailand)

Professor Dr. Gerhard Wiegler

(Brandenburgische Technische Universität Cottbus, Germany)

Professor Dr. Hermann Knoflacher

(University of Technology Vienna, Austria)

Professor Dr. Jurgen P. Kropp

(University of Potsdam, Germany)

Professor Dr. Manish Mehta

(Wadia Institute of Himalayan Geology, India)

Professor Dr. Mark G. Robson

(Rutgers University, USA)

Professor Dr. Nipon Tangtham

(Kasetsart University, Thailand)

Professor Dr. Pranom Chantaranothai

(Khon Kaen University, Thailand)

Professor Dr. Shuzo Tanaka

(Meisei University, Japan)

Professor Dr. Sompon Wanwimolruk

(Mahidol University, Thailand)

Professor Dr. Tamao Kasahara

(Kyushu University, Japan)

Professor Dr. Warren Y. Brockelman

(Mahidol University, Thailand)

Professor Dr. Yeong Hee Ahn

(Dong-A University, South Korea)

Associate Professor Dr. Kathleen R Johnson

(Department of Earth System Science, USA)

Associate Professor Dr. Marzuki Ismail

(University Malaysia Terengganu, Malaysia)

Associate Professor Dr. Sate Sampattagul

(Chiang Mai University, Thailand)

Associate Professor Dr. Takehiko Kenzaka

(Osaka Ohtani University, Japan)

Associate Professor Dr. Uwe Strotmann

(University of Applied Sciences, Germany)

Assistant Professor Dr. Devi N. Choesin

(Institut Teknologi Bandung, Indonesia)

Assistant Professor Dr. Said Munir

(Umm Al-Qura University, Saudi Arabia)

Dr. Mohamed Fassy Yassin

(University of Kuwait, Kuwait)

Dr. Norberto Asensio

(University of Basque Country, Spain)

Dr. Thomas Neal Stewart

(Mahidol University, Thailand)

ASSISTANT TO EDITOR

Associate Professor Dr. Kanchana Nakhapakorn

Dr. Kamalaporn Kanongdate

Dr. Paramita Punwong

JOURNAL MANAGER

Isaree Apinya

JOURNAL EDITORIAL OFFICER

Nattakarn Ratchakun

Parynya Chowwiwattanaporn

Editorial Office Address

Research Management and Administration Section,

Faculty of Environment and Resource Studies, Mahidol University

999, Phutthamonthon Sai 4 Road, Salaya, Phutthamonthon, Nakhon Pathom, Thailand, 73170

Phone +662 441 5000 ext. 2108 Fax. +662 441 9509-10

Website: <https://ph02.tci-thaijo.org/index.php/ennrj/index>

E-mail: ennrjournal@gmail.com

CONTENT

- Effectivity of Indonesian Rice Husk as an Adsorbent for Removing Congo Red from Aqueous Solutions** 255
*Neza Rahayu Palapa, Normah, Tarmizi Taher, Risfidian Mohadi, Addy Rachmat, and Aldes Lesbani**
- Impact of Climate Change on Reservoir Reliability: A Case of Bhumibol Dam in Ping River Basin, Thailand** 266
Allan Sriratana Tabucanon, Areeya Rittima, Detchakit Raveephinit, Yutthana Phankamolsil, Wudhichart Sawangphol, Jidapa Krajangka, Yutthana Talaluxmana, Varawoot Vudhivanich, and Wenchao Xue*
- Bioaccumulation of Lead by Pepper Elder (*Peperomia pellucida* (L.) Kunth) in a Lead-Contaminated Hydroponic System** 282
Jessica O. Tablang, Florenda B. Temanel, Ron Patrick C. Campos, and Helen C. Ramos*
- Effects of Campaign-Based Soil and Water Conservation Practice on Soil Properties: The Case of Workamba Watershed, Debark District, North Ethiopia** 292
Mulneh Bogale, Getnet Wondie, and Abdrahman Shafi*
- In Vitro* Removal of Electronic and Electrical Wastes by Fungi Isolated from Soil at Annaba Area in Northeast of Algeria** 302
Ghania Bourzama, Nadjet Iratni, Nadjet Ennaghra, Houria Ouled-Haddar, Boudjema Soumati, Khouloud Amour, and Khouloud Bechiri*
- Environmental and Microbial Influences on Corrosion of Selected Types of Petroleum Industry Steel** 310
Anwuli U. Osadebe, Dorcas C. Olorondu, and Gideon C. Okpokwasili*
- Characterization and Application of Mangosteen Peel Activated Carbon for Ammonia Gas Removal** 320
Zarah Arwienny Hanami and Puji Lestari*
- Removal of Iron from Groundwater by Ozonation: The Response Surface Methodology for Parameter Optimization** 330
*Apiradee Sukmilin and Ratsamee Sangsirimongkolying**

Effectivity of Indonesian Rice Husk as an Adsorbent for Removing Congo Red from Aqueous Solutions

Neza Rahayu Palapa¹, Normah², Tarmizi Taher³, Risfidian Mohadi^{1,2}, Addy Rachmat^{1,2}, and Aldes Lesbani^{1,4*}

¹Graduate School of Mathematics and Natural Sciences, Universitas Sriwijaya, Palembang, South Sumatera 30139, Indonesia

²Department of Chemistry, Faculty of Mathematics and Natural Sciences, Universitas Sriwijaya, Ogan Ilir, South Sumatera 30662, Indonesia

³Department of Environmental Engineering, Institut Teknologi Sumatera, Kecamatan Jati Agung, Lampung Selatan 35365, Indonesian

⁴Research Center of Inorganic Materials and Complexes, Universitas Sriwijaya, Ogan Ilir, South Sumatera 30662, Indonesia

ARTICLE INFO

Received: 13 Oct 2020
Received in revised: 15 Dec 2020
Accepted: 28 Jan 2021
Published online: 17 May 2021
DOI: 10.32526/enrj/19/2020232

Keywords:

Low-cost adsorbent/ Biomass/ Congo red/ Adsorption process/ Dyes

* Corresponding author:

E-mail:
aldeslesbani@pps.unsri.ac.id

ABSTRACT

Indonesian rice husk biochar (RH-BC) was prepared by pyrolysis method at 500°C and characterized using X-ray diffraction, Fourier-transform infrared spectroscopy, surface-area-specific analysis by Brunauer-Emmett-Teller, and scanning electron microscopy. The RH-BC were used as adsorbents for enhancing the adsorption of Congo red compared to pristine rice husk (RH) in aqueous solutions. The results of characterization through surface-area-specific analysis showed the surface area of RH-BC (72.25 m²/g) was ten times higher than RH (7.08 m²/g) owing to high-temperature treatment. The results of the adsorption study showed that the RH and RH-BC followed the pseudo-second-order kinetic model and the Freundlich isotherm equation with maximum adsorption capacities of 85.470 mg/g and 72.993 mg/g for the RH-BC and RH, respectively. The thermodynamic parameters of adsorption indicated spontaneous and endothermic processes. The reusability of the adsorbents (RH and RH-BC) showed that they are potentially suitable for extracting Congo red from aqueous solution up to three adsorption-desorption cycles. Their performance sharply decreases after the fourth and fifth cycles.

1. INTRODUCTION

Indonesia has many industries, such as plastics, textiles, pulps, papers, pharmaceuticals, and cosmetics that produce waste pollutants, such as dyes, that are released into the environment. The presence of dyes in aquatic systems can cause severe environmental problems (Saini, 2017; Vinsiah et al., 2017; Malik et al., 2020). These dyes are carcinogenic, non-biodegradable, and toxic to humans and biota in environmental systems (Hassaan and Nembr, 2017; Yaseen and Scholz, 2019). Several methods for removing dyes from wastewater have been developed to decrease their impact on health and environment (Banerjee and Chattopadhyaya, 2017). These methods include adsorption (Palapa et al., 2021), coagulation/flocculation (Mozumder and Islam, 2010), electrochemical (Cotillas et al., 2018), microbial decomposition (Patil et al., 2016), sonochemical

(Gholami et al., 2019), wet air oxidation, ozonation (Banerjee and Chattopadhyaya, 2017), and ion exchange (Choi et al., 2020).

Among these methods, adsorption is a well-known separation method that provides an effective process for dye removal from wastewater. The adsorption performance is based on the properties of the adsorbent materials. (Han et al., 2008; Banerjee and Chattopadhyaya, 2017). Several adsorbents have been tested for dye removal from wastewater, such as activated zeolites, clays, bentonite, chitin, chitosan, cellulose, algae, and carbon-based materials (Kandisa et al., 2016; Momina et al., 2018; Boulaiche et al., 2019; Rabie et al., 2020).

Activated carbon is an effective adsorbent for dye removal; however, the high cost of activated carbon limits its application (Azargohar and Dalai, 2006). Recently, agricultural wastes, such as orange

Citation: Palapa NR, Normah, Taher T, Mohadi R, Rachmat A, Lesbani A. Effectivity of Indonesian rice husk as an adsorbent for removing Congo red from aqueous solutions. Environ. Nat. Resour. J. 2021;19(4):255-265 (<https://doi.org/10.32526/enrj/19/2020232>)

peel (Annadurai et al., 2002), longan peel (Wang et al., 2016), limetta peel (Shakoor and Nasar, 2016), and rice husk (RH) (Liu and Zhang, 2009), have been used as feedstock for adsorbents. RH is agricultural waste feedstock produced from the rice milling industry, and it contains chemical compounds, such as lignin, cellulose, and hemicellulose, which can be used as active-site adsorbents for dye removal (Connor et al., 2018). However, the RH has a low adsorption capacity. Thus, to increase this adsorption capacity, they should be activated by carbonization (Bamroongwongdee et al., 2019; Milla et al., 2013).

Malik et al. (2020) also reported comparative comparison of RH, RH char, and chemically modified RH used as adsorbents for the removal of the Congo red dye. This study reported that the adsorption capacities of the RH, RH char, and chemically modified RH char (CMRHC) are 1.58 mg/g, 1.28 mg/g, and 2.04 mg/g, respectively, for Congo red dye removal. This comparative study indicated that the adsorption efficiency of the CMRHC was higher than that of the RH and RH char. Herlina and Masri (2017) reported that the adsorption of Congo red using the RH occurred in an optimum contact time of 30 min, with an adsorption percentage of 91.99%. The adsorption capacity was 7.19 mg/g. Gad et al. (2016) also used the RH as an adsorbent of metal ion Co(II) from wastewater, which resulted in a maximum adsorption capacity of 75.70 mg/g, and it followed the Langmuir isotherm model.

In this study, the RH and RH-BC-based local Indonesian feedstock were used as adsorbents of Congo red from aqueous solutions. The factors influencing the adsorption process, such as adsorption time, concentration of Congo red, and temperature adsorption, were studied in detail. The kinetics of adsorption, isotherm, and thermodynamics of the adsorption process of Congo red onto the RH and RH-BC are discussed in this article.

2. METHODOLOGY

2.1 Chemical and instrumentation

Analytical grade (p.a.) chemicals such as sodium hydroxide, ethanol, hydrochloric acid, and congo red (>75%) were purchased from Merck (Darmstadt, Germany). Water was supplied by the Research Center of Inorganic Materials and Complexes, FMIPA Universitas Sriwijaya. Distilled water was obtained after purify using a Pureit®, which removed undesirable ionic, organic, and bacterial contaminants from the water. Further, this water was

prepared for washing the RH from rice mills in Bukataorganics, Indonesia. The RH was washed with distilled water and dried at 60°C in an oven for 8 h. Production of the RH-BC by pyrolysis method was done by placing RH in the reactor and then heating at 600°C for 1 h. The RH and RH-BC was characterized using X-ray diffraction (XRD; Rigaku miniflex-6000). The RH and RH-BC were scanned from 5° to 80° at a scan rate of 1° min⁻¹. The functional groups were analyzed using Fourier-transform infrared (FT-IR) spectroscopy (Shimadzu Prestige-21) at 400-4,000 cm⁻¹ and a KBr pellet. The adsorption-desorption of N₂ was performed using a Quantachrome Micrometric ASAP adsorption analyzer. Morphology analysis was performed using a scanning electron microscopy (SEM; Quanta-650 Oxford). The concentration of Congo red was determined through an ultraviolet-visible (UV-Vis) spectrophotometer (Biobase BK-UV 1800 PC) at 501 nm.

2.2 Adsorption process

The adsorption process was studied in a batch system by varying the adsorption time, Congo red concentration, and temperature for three replication measurements. The initial pH of Congo red is 5.3, and the adsorbents were sieved through 80 mesh. The variation in the adsorption times was performed with 50 mg/L of Congo red dye. Further, 25 mL of the Congo red dye was placed in a glass beaker, 0.025 g of the adsorbent was added to it, and the mixture was stirred by a horizontal shaker for 5-180 min at 250 rpm. The mixing solution was centrifuged at 1,000 rpm before scanning at 501 nm using a UV-Vis spectrophotometer. The kinetic adsorption was calculated using the kinetic adsorption models, such as pseudo-first-order (PFO) and pseudo-second-order (PSO) kinetic models, as presented in equations 1 and 2.

$$\log (q_e - q_t) = \log q_e - \left(\frac{k_1}{2.303} \right) t \quad (1)$$

$$\frac{t}{q_t} = \frac{1}{k_2 q_e^2} + \frac{1}{q_e} t \quad (2)$$

Where; q_e is the adsorption capacity at equilibrium (mg/g); q_t is the adsorption capacity (mg/g) at t , which is the adsorption time (min); k_1 and k_2 denote the adsorption kinetic rates at PFO kinetics (min⁻¹) and PSO kinetics (g/mg·min), respectively.

The Congo red concentration was determined at dye concentrations of 50, 75, 100, 125, and 150 mg/L using 0.025 g of the adsorbents and 25 mL of Congo

red. Moreover, the mixture was stirred by a horizontal shaker for 100 min at 250 rpm at different adsorption temperatures of 303, 313, 323, and 333 K. The concentration of the Congo red was analyzed using the UV-Vis spectrophotometer at a maximum wavelength of 501 nm. Thereafter, the thermodynamic parameters were obtained from the Langmuir and Freundlich equations. The Langmuir adsorption model is assumed to be the chemical and monolayer adsorption processes, while the Freundlich adsorption model is assumed to be the physical and multilayer adsorption processes. Equations 3, 4, and 5 represent the Langmuir adsorption model, Freundlich adsorption model, and thermodynamic equations, respectively.

$$\frac{c}{m} = \frac{1}{bK_{ML}} + \frac{c}{b} \quad (3)$$

Where; C is the saturated concentration of the adsorbate, m is the amount of adsorbate, b is the maximum adsorption capacity (mg/g), and K_{ML} is the Langmuir constant (L/mg).

$$\log q_e = \log K_F + 1/n \log C_e \quad (4)$$

Where; q_e is the adsorption capacity at equilibrium (mg/g), C_e is the concentration of adsorbate at equilibrium (mg/L), and K_F is the Freundlich constant.

$$\ln K_d = \frac{\Delta S}{R} - \frac{\Delta H}{RT} \quad (5)$$

Where; R is the rate gas constant, T is the temperature of the adsorption process (K), K_d is the thermodynamic equilibrium constant, ΔH is the enthalpy (kJ/mol), and ΔS is the entropy (J/mol·K).

2.3 Desorption and reusability process

Based on the amount of adsorbed dye, the amount of desorbed dye can be calculated using the following equation.

$$\% D = \frac{C_{ads}}{C_{dsp}} \times 100\% \quad (6)$$

Where; C_{ads} is the concentration of adsorbed Congo red (mg/L), C_{dsp} is the concentration of desorbed Congo red (mg/L), and %D is the percentage of the desorption process.

The regeneration efficiency is determined using the equation:

$$\% \text{ regeneration} = \frac{Q_r}{Q_0} \times 100\% \quad (7)$$

Where; Q_r is the adsorption capacity of reusability (mg/g) and Q_0 is the adsorption capacity of the initial reusability (mg/g).

The desorption process was used to test each adsorbent using 1 g of RH and RH-BC, followed by the addition of 50 mL of the Congo red solution. Then, the mixture was stirred for 2 h. The used adsorbent was desorbed by taking 0.01 g of RH and RH-BC, respectively, and adding 10 mL of solvent (sodium hydroxide (0.01 M), hydrochloric acid (0.01 M), absolute ethanol, and distilled water) and stirring the mixture for 2 h for each conical flask. The reusability process was performed with the desorbed adsorbent reused to adsorb 100 mg/L of Congo red. The adsorption was performed for 2 h using a batch system and analyzed by UV-Vis spectrophotometry. The reusability of the adsorbent was evaluated in three cycles of the adsorption process.

3. RESULTS AND DISCUSSION

3.1 Adsorbent characterization

Figure 1 shows the XRD powder patterns of the RH and RH-BC characterization at 2θ diffraction peaks shown in the range of 16° - 29° . A previous study (Suyanta and Kuncaka, 2011) reported that there were no diffraction peaks, except one of approximately 23° with reflection (002) at 2θ diffraction. These diffractions indicate the presence of silica in an amorphous state from the RH and RH-BC (Milla et al., 2013). The XRD powder pattern of the RH exhibited diffraction at 23° . Another 2θ peak (101) at 18° disappeared after heating the RH at a high temperature (600°C) due to decomposition of cellulose (Rosa et al., 2012). As reported by De Bhowmick et al. (2018), the change in the peak occurred due to the destruction of the biomass structure by pyrolysis.

The FT-IR spectra of the RH and RH-BC are shown in Figure 2. The vibration peak at $3,448\text{ cm}^{-1}$ corresponds to the -OH group. The peak at $1,620\text{ cm}^{-1}$ indicates the presence of C-O bonds in the carboxylate group. The peak at wavenumber 794 cm^{-1} corresponds to the presence of Si-O bond (Bamroongwongdee et al., 2019). The vibration at $1,103\text{ cm}^{-1}$ refers to C-H stretching of lignin in the RH and RH-BC (Gad et al., 2016). Furthermore, the intensity of the water molecule (OH vibration) and carboxylate group (CO vibration) in the RH decreased after heating at 600°C to form the RH-BC.

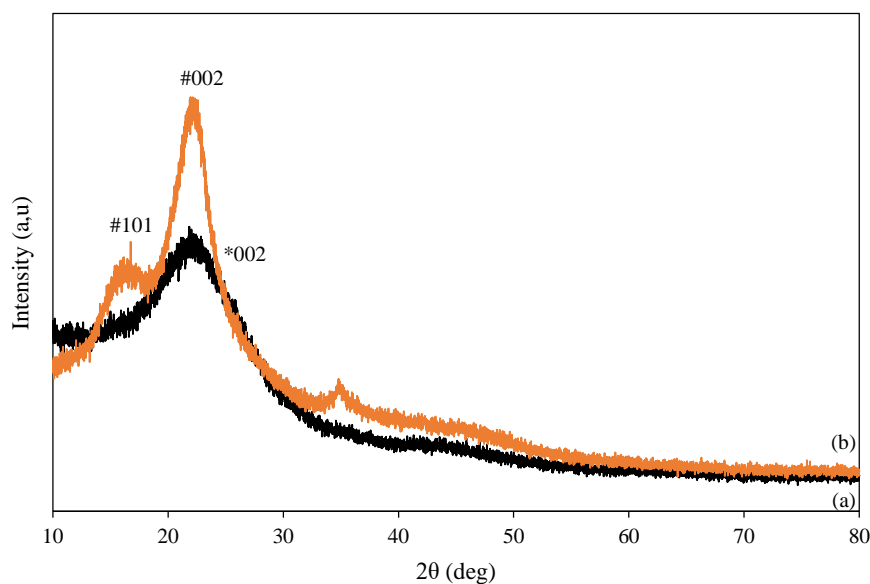


Figure 1. XRD powder patterns of (a) RH-BC and (b) RH

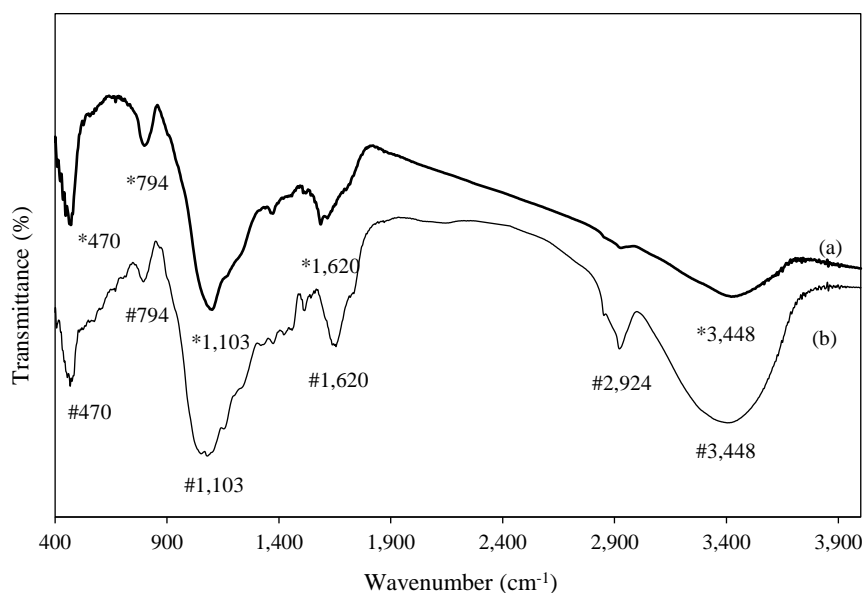


Figure 2. FT-IR spectra of (a) RH-BC and (b) RH

Table 1 shows the Brunauer-Emmett-Teller (BET) surface analyses of the RH and RH-BC. The RH-BC has a larger surface area than that of the RH because of the use of high temperatures during RH-BC pyrolysis. These temperatures can open the pore channels of the RH during thermal process to form the RH-BC (Fernandes et al., 2016). As shown in Table 1, the larger pore size can affect the higher adsorption capacity due to the increasing pore volume. This was also reported by Mangun et al. (1998). They also reported that the pore size and volume size can affect the adsorption capacity.

Table 1. Surface properties of RH and RH-BC

Adsorbent	Surface area (m ² /g)	Pore size (nm)	Pore volume (cm ³ /g)
RH-BC	72.25	3.33	0.060
RH	7.08	3.14	0.011

SEM-energy-dispersive X-ray (EDX) analysis revealed the elemental composition of the RH and RH-BC. The SEM-EDX analyses of the RH and RH-BC are shown in Figure 3(a) and 3(b), respectively. The morphology of the RH (Figure 3(a)) shows a uniform

size with a round stem shape. However, the RH-BC has an irregular pore size, as shown in [Figure 3\(b\)](#) ([Leng et al., 2015](#)). As expected from the results of the BET analysis, the opening of pores increases the surface area of the RH-BC. Furthermore, the EDX results showed that both the RH-BC and RH contain

C, Si, O, S, P, N, and Al. The main contents of the RH are C, O, and Si, which are obtained from SiO_2 and the carboxylate groups. The main components of the RH-BC are C and Si. The elements Al, P, S, and N are obtained through plants as non-essential elements ([Wang et al., 2017](#)).

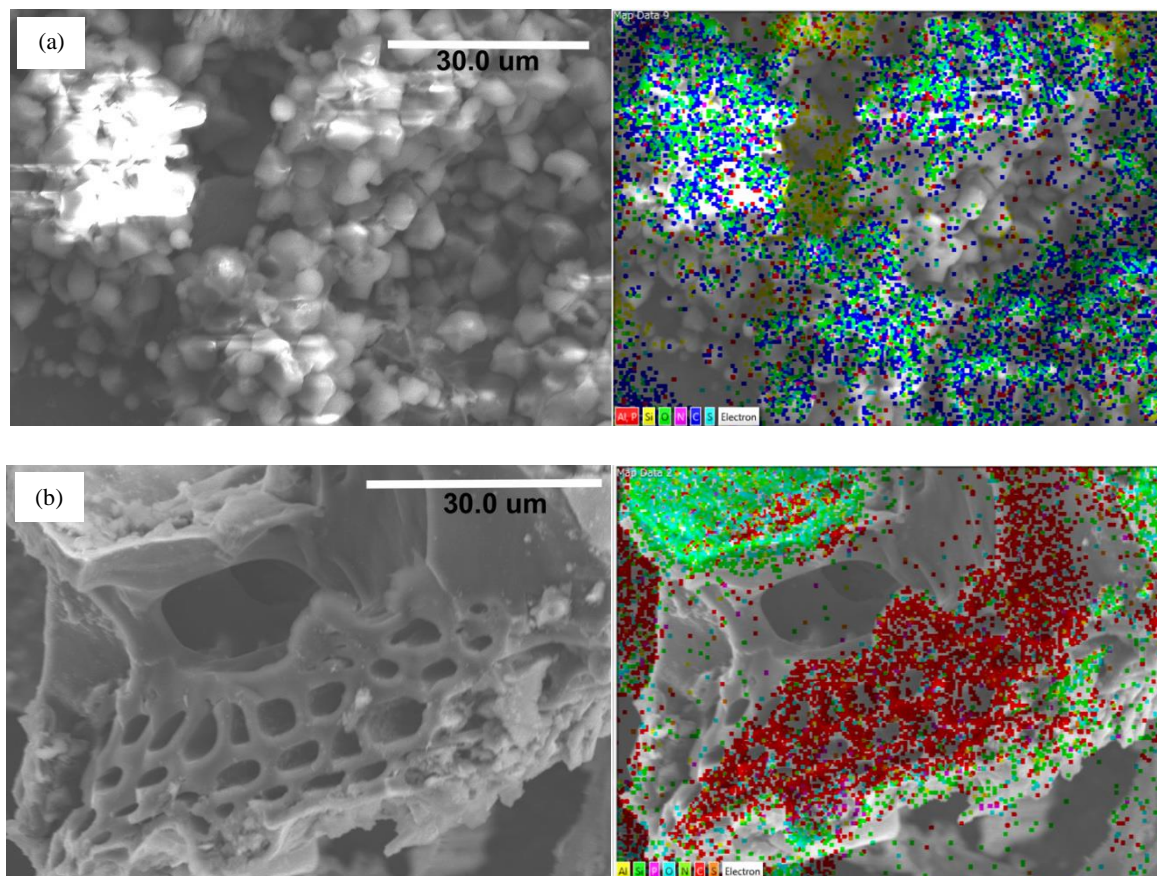


Figure 3. SEM-EDX analysis of (a) RH and (b) RH-BC

3.2 Adsorption study

The RH and RH-BC were used as adsorbents for the adsorption of Congo red from aqueous solutions. First, the adsorption was studied based on the adsorption time, as shown in [Figure 4](#) and [Table 2](#). The adsorption of Congo red on the RH and RH-BC increased sharply with the increasing adsorption time for both the adsorbents, and it reached equilibrium after 100 min of adsorption. The adsorption time data were calculated to obtain the kinetic parameters using the PFO and PSO kinetic models, as described by Equations 1 and 2. The adsorption of Congo red follows the PSO kinetic model, with a correlation coefficient $R^2 > 0.995$. The RH-BC has a larger adsorption capacity (31.619 mg/g) than that of the RH

(22.008 mg/g) because of its large surface area, which indicates sorbent-sorbate electrostatic attraction. According to [Bamroongwongdee et al. 2019](#) the PSO kinetic model also confirmed that the adsorption process involves a chemisorption stage, which constitutes the rate-limiting process.

Second, the effects of the Congo red concentration and temperature on the equilibrium of the adsorption process were studied. [Figure 5](#) shows the difference in the Congo red concentration and adsorption temperature in the case of RH and RH-BC. The figure also shows that the adsorption capacity increases with increasing temperature of the adsorption process.

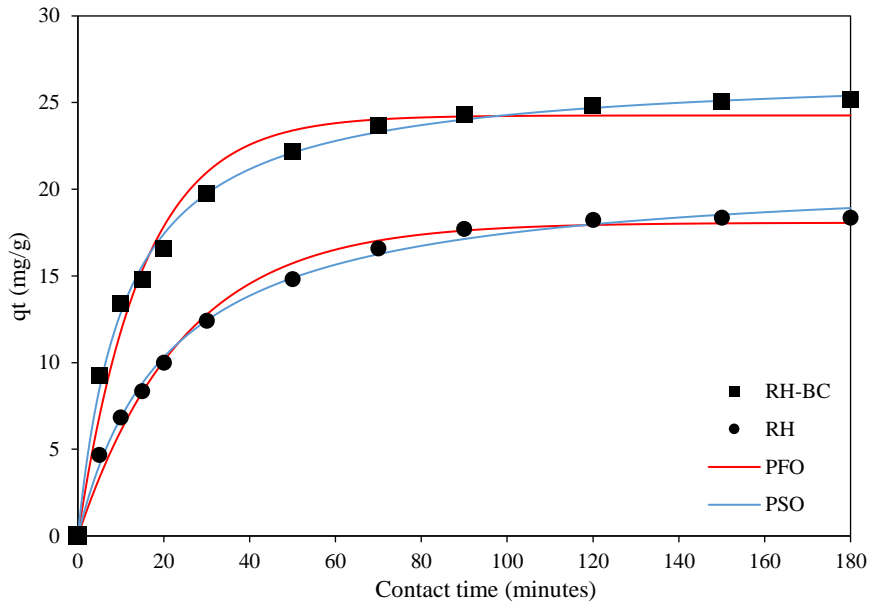


Figure 4. The plot of the fitted kinetics model against the experimental data

Table 2. Kinetic adsorption of Congo red on the RH and RH-BC

Adsorbent	Initial concentration (mg/L)	Q _e experiment (mg/g)	PFO			PSO		
			Q _e Calc (mg/g)	R ²	k ₁	Q _e Calc (mg/g)	R ²	k ₂
RH-BC	51.492	31.619	29.573	0.995	0.032	36.231	0.997	0.023
RH	51.492	22.008	19.037	0.979	0.029	25.062	0.994	0.021

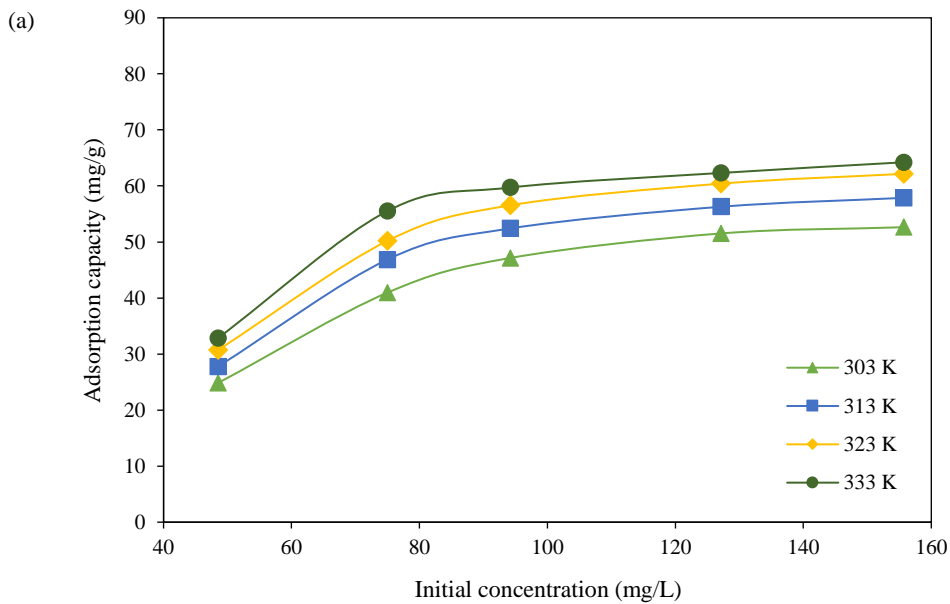


Figure 5. Effects of Congo red dye concentration on the adsorption capacities of (a) RH and (b) RH-BC

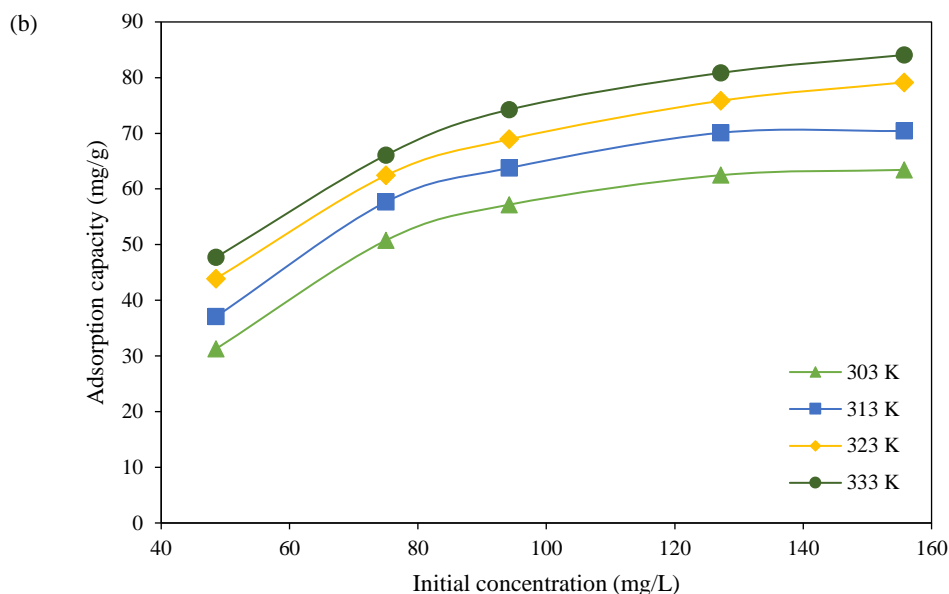


Figure 5. Effects of Congo red dye concentration on the adsorption capacities of (a) RH and (b) RH-BC (cont.)

Table 3 presents the Langmuir and Freundlich data, which were obtained from the data provided in Figure 5. According to the data in Table 3, the adsorption on the RH and RH-BC is appropriate with the Freundlich isotherm model with $R^2 > 0.99$, which suggests that the adsorption process is physisorption and occurs through multilayer (Wijayanti et al., 2018). However, this is in contrast to the PSO equation, which indicated that the adsorption process involves chemisorption. This finding suggests that physico-chemical adsorption occurred in the adsorption process. This conforms with the enthalpy results listed

in Table 4, which indicate that the adsorption of Congo red has low enthalpy. Further, according to IUPAC, physisorption with the enthalpy in the range of 4-40 kJ/mol and >40 kJ/mol corresponds to chemisorption (Thommes et al., 2015; Oktriayanti et al., 2019). The increasing dye uptake with the increasing temperature decreased the viscosity of the solution, increased the porosity, or interlayer, resulting in the enhancement of active sites form (Zhu et al., 2005). According to the results summarized in Table 4, the adsorption capacity of Congo red removal using the RH-BC is slightly higher than that for other adsorbents.

Table 3. Isotherm models of Congo red adsorption on RH and RH-BC

	Isotherm	Parameters	303 K	313 K	323 K	333 K
RH-BC	Langmuir	Qmax	77.519	79.365	83.333	85.470
		k_L	0.058	0.112	0.219	0.480
		R^2	0.971	0.992	0.999	0.998
	Freundlich	n	1.909	4.361	1.448	1.444
		k_F	7.034	1.328	3.631	3.928
		R^2	0.999	0.996	0.993	0.999
RH	Langmuir	Qmax	60.606	72.993	74.627	75.188
		k_L	0.067	0.088	0.039	0.058
		R^2	0.997	0.976	0.956	0.969
	Freundlich	N	1.071	10.953	5.688	9.497
		k_F	1.295	1.455	1.386	1.441
		R^2	0.999	0.979	0.983	0.994

Table 4. Comparison of Congo red adsorption using different adsorbents.

Adsorbent	Q _e (mg/g)	Refs
Na-bentonite	35.84	(Vimonses et al., 2009)
Bagasse fly ash	11.88	(Mall et al., 2005)
<i>Spirulina algae</i>	3.11	(Mohadi et al., 2017)
m-cell/Fe ₃ O ₄ /ACCs	66.09	(Zhu et al., 2011)
Magnetic Fe ₃ O ₄ @graphene	33.66	(Inyang et al., 2012)
<i>Funalia trogii</i>	83.70	(Bayramoglu and Arica, 2018)
RH-BC	85.47	This research
RH	75.188	This research

The thermodynamic parameters of the Congo red adsorption on the RH and RH-BC adsorbents, such as ΔH (enthalpy), ΔG (Gibbs free energy), and ΔS (entropy), are shown in Table 5. The positive values of ΔS indicate an increase in the degree of irregularity

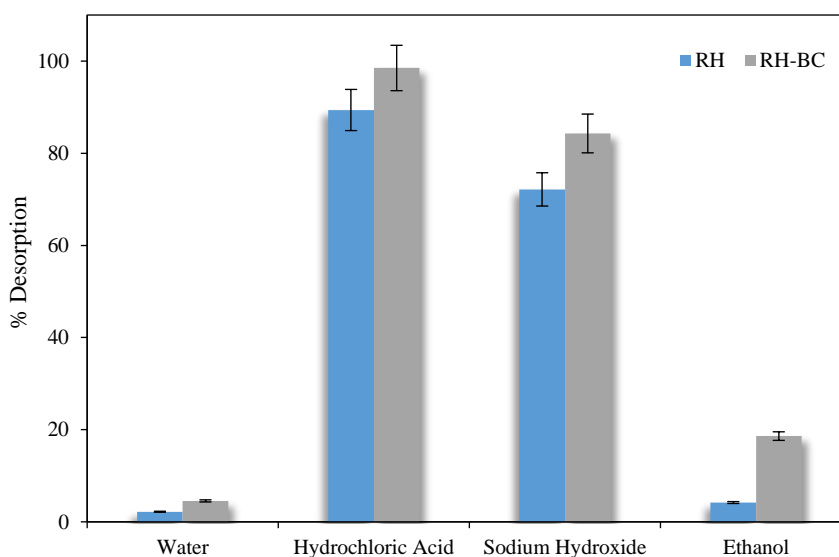
between the adsorbate and adsorbent. The positive value of ΔH indicates that the Congo red adsorption on the RH and RH-BC is endothermic. The negative value of ΔG indicates that the Congo red adsorption is spontaneous (Naushad et al., 2019).

Table 5. Thermodynamic parameters of Congo red adsorption on RH and RH-BC

Concentration	T (K)	Q _e (mg/g)	ΔH (kJ/mol)	ΔS (kJ/mol)	ΔG (kJ/mol)
48.524 mg/L	303	31.270	9.544	3.200	-0.070
	313	37.063		-0.387	
	323	43.889		-0.704	
	333	47.698		-1.022	
48.524 mg/L	303	24.841	19.565	6.500	-0.132
	313	27.778		-0.782	
	323	30.714		-1.432	
	333	32.857		-2.082	

Desorption of the adsorbent was studied using several solvents on the RH and RH-BC after the adsorption of Congo red, and the results are shown in Figure 6, which indicate that hydrochloric acid as a

solvent can give higher results in the desorption process of Congo red. This is because the H⁺ ion from the hydrochloric acid releases the Congo red dye anion by interacting with the adsorbent. Congo red prefers

**Figure 6.** Desorption of Congo red on the RH and RH-BC

lower number of H^+ ions than those present in hydrochloric acid because of greater electrostatic interactions than adsorbents (Palapa et al., 2020). The reusability of the adsorbent was evaluated using hydrochloric acid as a desorption reagent to release Congo red after the adsorption process.

The reusability study was conducted for five adsorption cycles, as demonstrated in Figure 7. The adsorption capacity of Congo red on both the adsorbents decreased sharply after three cycles, i.e., during the fourth and fifth adsorption processes. The first reusabilities of the RH and RH-BC were 58.88%

and 54.32%, and the second reusabilities were 53.44% and 47.33% for the RH and RH-BC, respectively. The third reusability was more stable with reusability values of 47.91% for RH and 44.24% for RH-BC. However, the adsorption capacity decreased significantly in the fourth and fifth adsorption processes. Thus, the RH and RH-BC are suitable adsorbents for the Congo red adsorption in three adsorption cycles. Furthermore, these adsorbents can be reused, although their adsorption capacity is slightly reduced.

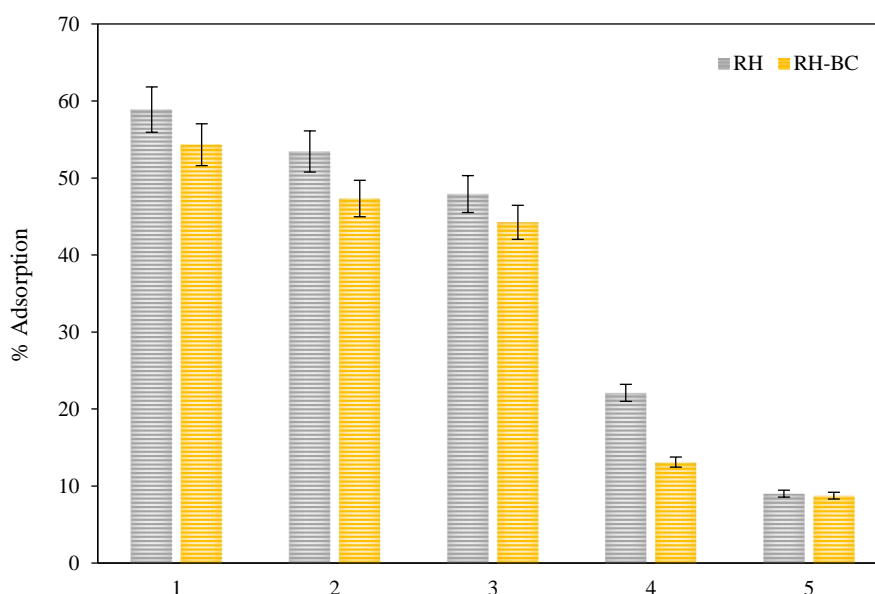


Figure 7. Reusability of the RH and RH-BC for Congo red adsorption

4. CONCLUSION

In this study, characterization of RH and RH-BC using XRD indicated the presence of silica molecules at a diffraction peak of 23° . The FT-IR spectra of the RH and RH-BC showed Si-O vibrations at 794 cm^{-1} , and the peak at $1,103\text{ cm}^{-1}$ corresponded to the C-H strain, which indicated the presence of lignin on the RH and RH-BC. The BET analysis showed that the surface areas of the RH and RH-BC were $72.25\text{ m}^2/\text{g}$ and $7.08\text{ m}^2/\text{g}$, respectively. The adsorption of Congo red on the RH and RH-BC followed the PSO kinetics model with optimum adsorption after 100 min and the Freundlich equation model with a maximum adsorption capacity of 85.470 mg/L . The RH-BC was more effective at Congo red dye removal than the RH. The thermodynamic parameters indicated that the Congo red was adsorbed spontaneously on the RH and RH-BC, and this adsorption was an endothermic process. The

reusability of the adsorbents indicated that the RH and RH-BC had a decreasing adsorption capacity after three cycles of adsorption. Furthermore, these experimental results are useful to increase the use of biomass as a potential adsorbent for wastewater treatment. The studied adsorbents are suitable to remove Congo red in an aqueous solution. In addition, the use of agricultural wastes as one source of adsorbents has the potential to further help to reduce agricultural waste in the environment.

ACKNOWLEDGEMENTS

This study was supported by “Hibah Profesi” Universitas Sriwijaya in fiscal year 2020-2021 by the financial support program for research with contact number 0687/UN9/SK.BUK.KP/2020. Special thanks for Research Center of Inorganic Materials and Complexes, Faculty of Mathematic and Natural

Science, Universitas Sriwijaya for analysis and instrumental measurement.

REFERENCES

- Annadurai G, Juang RS, Lee DJ. Use of cellulose-based wastes for adsorption of dyes from aqueous solutions. *Journal of Hazardous Materials* 2002;92(3):263-74.
- Azargohar R, Dalai AK. Biochar as a precursor of activated carbon. *Applied Biochemistry and Biotechnology* 2006;129-132:762-73.
- Bamroongwongdee C, Suwannee S, Kongsomsaksiri M. Adsorption of Congo red from aqueous solution by surfactant-modified rice husk: Kinetic, isotherm and thermodynamic analysis. *Songklanakarin Journal of Science and Technology* 2019;41(5):1076-83.
- Banerjee S, Chattopadhyaya MC. Adsorption characteristics for the removal of a toxic dye, tartrazine from aqueous solutions by a low cost agricultural by-product. *Arabian Journal of Chemistry* 2017;10:S1629-38.
- Bayramoglu G, Arica MY. Adsorption of Congo red dye by native amine and carboxyl modified biomass of *Funalia trogii*: Isotherms, kinetics and thermodynamics mechanisms. *Korean Journal of Chemical Engineering* 2018;35:1303-11.
- De Bhowmick G, Sarmah AK, Sen R. Production and characterization of a value added biochar mix using seaweed, rice husk and pine sawdust: A parametric study. *Journal of Cleaner Production* 2018;200:641-56.
- Boulaiche W, Hamdi B, Trari M. Removal of heavy metals by chitin: Equilibrium, kinetic and thermodynamic studies. *Applied Water Science* 2019;9:39.
- Choi Y, Gurav R, Kim HJ, Yang Y, Bhatia SK. Evaluation for simultaneous removal of anionic and cationic dyes onto maple leaf-derived biochar using response surface methodology. *Applied Sciences* 2020;10:2982.
- Connor DO, Peng T, Li G, Wang S, Duan L, Mulder J, et al. Sulfur-modified rice husk biochar: A green method for the remediation of mercury contaminated soil. *Science of the Total Environment* 2018;621:819-26.
- Cotillas S, Llanos J, Cañizares P, Clematis D, Cerisola G, Rodrigo MA, et al. Removal of Procion red MX-5B dye from wastewater by conductive-diamond electrochemical oxidation. *Electrochimica Acta* 2018;263:1-7.
- Fernandes IJ, Calheiro D, Kieling AG, Moraes CAM, Rocha TLAC, Brehm FA, et al. Characterization of rice husk ash produced using different biomass combustion techniques for energy. *Fuel* 2016;165:351-9.
- Gad HM, Omar H, Aziz A, Hassan M, Khalil M. Treatment of rice husk ash to improve adsorption capacity of cobalt from aqueous solution. *Asian Journal of Chemistry* 2016;28(2):385-94.
- Gholami P, Dinpazhoh L, Khataee A, Hassani A, Bhatnagar A. Facile hydrothermal synthesis of novel Fe-Cu layered double hydroxide/biochar nanocomposite with enhanced sonocatalytic activity for degradation of cefazolin sodium. *Journal of Hazardous Materials* 2019;381:120742.
- Han R, Ding D, Xu Y, Zou W, Wang Y, Li Y, et al. Use of rice husk for the adsorption of congo red from aqueous solution in column mode. *Bioresource Technology* 2008;99(8):2938-46.
- Hassaan MA, Nemr A El. Health and environmental impacts of dyes: Mini review. *American Journal of Environmental Science and Engineering* 2017;1(3):64-7.
- Herlina R, Masri MS. Adsorption study of rice bran against Congo red dyes in Wajo. *Journal Chemical* 2017;18(1):16-25.
- Inyang M, Gao B, Yao Y, Xue Y, Zimmerman AR, Pullammanappallil P, et al. Removal of heavy metals from aqueous solution by biochars derived from anaerobically digested biomass. *Bioresource Technology* 2012;110:50-6.
- Kandisa RV, Kv NS, Shaik KB, Gopinath R. Dye removal by adsorption: A review. *Journal of Bioremediation and Biodegradation* 2016;7(6):371.
- Leng L, Yuan X, Zeng G, Shao J, Chen X, Wu Z, et al. Surface characterization of rice husk bio-char produced by liquefaction and application for cationic dye (Malachite green) adsorption. *Fuel* 2015;155:77-85.
- Liu Z, Zhang FS. Removal of lead from water using biochars prepared from hydrothermal liquefaction of biomass. *Journal of Hazardous Materials* 2009;167(1-3):933-9.
- Malik A, Khan A, Natasha A, Naeem M. A comparative study of the adsorption of Congo red dye on rice husk, rice husk char and chemically modified rice husk char from aqueous media. *Bulletin of the Chemical Society of Ethiopia* 2020; 34(1):41-54.
- Mall ID, Srivastava VC, Agarwal NK, Mishra IM. Adsorptive removal of malachite green dye from aqueous solution by bagasse fly ash and activated carbon-kinetic study and equilibrium isotherm analyses. *Colloids and Surfaces A: Physicochemical and Engineering Aspects* 2005;264(1-3): 17-28.
- Mangun CL, Daley MA, Braatz RD, Economy J. Effect of pore size on adsorption of hydrocarbons in phenolic-based activated carbon fibers. *Carbon* 1998;36(1-2):123-9.
- Milla OV, Rivera EB, Huang W, Chien C, Wang Y. Agronomic properties and characterization of rice husk and wood biochars and their effect on the growth of water spinach in a field test. *Journal of Soil Science and Plant Nutrition* 2013;13(2):251-66.
- Mohadi R, Hanafiah Z, Hermansyah H, Zulkifli H. Adsorption of procion red and congo red dyes using microalgae *Spirulina* sp. *Science and Technology Indonesia* 2017;2(4):102-4.
- Momina, Shahadat M, Isamil S. Regeneration performance of clay-based adsorbents for the removal of industrial dyes: A review. *RSC Advances* 2018;8:24571-87.
- Mozumder MSI, Islam MA. Development of treatment technology for dye containing industrial wastewater. *Journal of Scientific Research* 2010;2(3):567-76.
- Naushad M, Abdullah A, Abdullah Z, Hotan I, Saad M, Mohammed A. Adsorption kinetics, isotherm and reusability studies for the removal of cationic dye from aqueous medium using arginine modified activated carbon. *Journal of Molecular Liquids* 2019;293:111442.
- Oktriyanti M, Palapa NR, Mohadi R, Lesbani A. Modification of Zn-Cr layered double hydroxide with keggin ion. *Indonesian Journal of Environmental Management and Sustainability* 2019;3(3):93-9.
- Palapa NR, Taher T, Rahayu BR, Mohadi R, Rachmat A, Lesbani A. CuAl LDH/rice husk biochar composite for enhanced adsorptive removal of cationic dye from aqueous solution. *Bulletin of Chemical Reaction Engineering and Catalysis* 2020;15(2):525-37.
- Palapa NR, Taher T, Mohadi R, Rachmat A, Lesbani A. Preparation of copper aluminum-biochar composite as adsorbent of malachite green in aqueous solution. *Journal of Engineering Science and Technology* 2021;16(1):259-74.

- Patil NP, Bholay AD, Kapadnis BP, Gaikwad VB. Biodegradation of model azo dye methyl red and other textile dyes by isolate *Bacillus circulans* npp1. *Journal of Pure and Applied Microbiology* 2016;10(4):2793-800.
- Rabie AM, Abukhadra MR, Rady AM, Ahmed SA, Labena A, Mohamed HSH, et al. Instantaneous photocatalytic degradation of malachite green dye under visible light using novel green Co-ZnO/algae composites. *Research on Chemical Intermediates* 2020;46:1955-73.
- Rosa SML, Rehman N, De Miranda MIG, Nachtigall SMB, Bica CID. Chlorine-free extraction of cellulose from rice husk and whisker isolation. *Carbohydrate Polymers* 2012;87(2):1131-8.
- Saini RD. Textile organic dyes: Polluting effects and elimination methods from textile waste water. *International Journal of Chemistry Engineering Research* 2017;9(1):121-36.
- Shakoor S, Nasar A. Removal of methylene blue dye from artificially contaminated water using citrus limetta peel waste as a very low cost adsorbent. *Journal of the Taiwan Institute of Chemical Engineers* 2016;66:154-63.
- Suyanta, Kuncaka A. Utilization of rice husk as raw material in synthesis of mesoporous silicates mcm-41. *Indonesian Journal of Chemistry* 2011;11(3):279-84.
- Thommes M, Kaneko K, Neimark AV, Olivier JP, Rodriguez-Reinoso F, Rouquerol J, et al. Physisorption of gases, with special reference to the evaluation of surface area and pore size distribution (IUPAC technical report). *Pure and Applied Chemistry* 2015;87(9-10):1051-69.
- Vimonses V, Lei S, Jin B, Chow CWK, Saint C. Kinetic study and equilibrium isotherm analysis of Congo red adsorption by clay materials. *Chemical Engineering Journal* 2009;148(2-3):354-64.
- Vinsiah R, Mohadi R, Lesbani A. Performance of graphite for Congo red and direct orange adsorption. *Indonesian Journal of Environmental Management and Sustainability* 2020;4: 125-32.
- Wang F, Pan Y, Cai P, Guo T, Xiao H. Single and binary adsorption of heavy metal ions from aqueous solutions using sugarcane cellulose-based adsorbent. *Bioresource Technology* 2017;241:482-90.
- Wang Y, Zhu L, Jiang H, Hu F, Shen X. Application of longan shell as non-conventional low-cost adsorbent for the removal of cationic dye from aqueous solution. *Spectrochimica Acta Part A: Molecular and Biomolecular Spectroscopy* 2016; 159:254-61.
- Wijayanti A, Susatyo EB, Kurniawan C. Adsorpsi logam Cr(VI) dan Cu(II) pada tanah dan pengaruh penambahan pupuk organik. *Indonesian Journal of Chemical Science* 2018;7(3):242-8 (in Indonesian).
- Yaseen DA, Scholz M. Textile dye wastewater characteristics and constituents of synthetic effluents: A critical review. *International Journal of Environmental Science and Technology* 2019;16:1193-226.
- Zhu J, He J, Du X, Lu R, Huang L, Ge X. A facile and flexible process of β -cyclodextrin grafted on Fe_3O_4 magnetic nanoparticles and host-guest inclusion studies. *Applied Surface Science* 2011;257(21):9056-62.
- Zhu MX, Li YP, Xie M, Xin HZ. Sorption of an anionic dye by uncalcined and calcined layered double hydroxides: A case study. *Journal of Hazardous Materials* 2005;120(1-3):163-71.

Impact of Climate Change on Reservoir Reliability: A Case of Bhumibol Dam in Ping River Basin, Thailand

Allan Sriratana Tabucanon¹, Areeya Rittima^{2*}, Detchasit Raveephinit², Yutthana Phankamolsil³,
Wudhichart Sawangphol⁴, Jidapa Krajangka⁴, Yutthana Talaluxmana⁵,
Varawoot Vudhivanich⁶, and Wenchao Xue⁷

¹Faculty of Environment and Resource Studies, Mahidol University, Nakhon Pathom 73170, Thailand

²Faculty of Engineering, Mahidol University, Nakhon Pathom 73170, Thailand

³Environmental Engineering and Disaster Management Program, Mahidol University, Nakhon Pathom 73170, Thailand

⁴Faculty of Information and Communication Technology, Mahidol University, Nakhon Pathom 73170, Thailand

⁵Faculty of Engineering, Kasetsart University, Bangkok 10900, Thailand

⁶Faculty of Engineering at Kamphaeng Saen, Kasetsart University, Nakhon Pathom 73140, Thailand

⁷Department of Energy, Environment and Climate Change, School of Environment, Resources and Development, Asian Institute of Technology, Pathum Thani 12120, Thailand

ARTICLE INFO

Received: 21 Jan 2021
Received in revised: 18 Mar 2021
Accepted: 16 Apr 2021
Published online: 18 May 2021
DOI: 10.32526/enrj/19/2021012

Keywords:

Bhumibol Dam/ Climate change/
Hydrological model/ Ping River
Basin/ Reservoir reliability

* Corresponding author:

E-mail: areeya.rit@mahidol.ac.th

ABSTRACT

Bhumibol Dam is the largest dam in the central region of Thailand and it serves as an important water resource. The dam's operation relies on reservoir operating rules that were developed on the basis of the relationships among rainfall-inflow, water balance, and downstream water demand. However, due to climate change, changing rainfall variability is expected to render the reliability of the rule curves insecure. Therefore, this study investigated the impact of climate change on the reliability of the current reservoir operation rules of Bhumibol Dam. The future scenarios from 2000 to 2099 are based on EC-EARTH under RCP4.5 and RCP8.5 scenarios downscaled by RegCM4. MIKE11 HD was developed for the inflow simulation. The model generates the inflow well ($R^2=0.70$). Generally, the trend of increasing inflow amounts is expected to continue in the dry seasons from 2000-2099, while large fluctuations of inflow are expected to be found in the wet seasons, reflecting high uncertainties. In the case of standard deviations, a larger deviation is predicted under the RCP8.5 scenario. For the reservoir's operation in a climate change study, standard operating procedures were applied using historical release records to estimate daily reservoir release needed to serve downstream water demand in the future. It can be concluded that there is high risk of current reservoir operating rules towards the operation reliability under RCP4.5 (80% reliability), but the risk is lower under RCP8.5 (87% reliability) due to increased inflow amounts. The unmanageability occurs in the wet season, cautioning the need to redesign the rules.

1. INTRODUCTION

Anthropogenic greenhouse gas emissions have been regarded as the cause for 1.0°C of global warming above pre-industrial levels. The global warming phenomenon has been scientifically related to changing rainfall variability patterns (IPCC, 2018). The IPCC (2012) concluded that climate change is causing the emergence of statistically significant trends in the number of heavy rainfall events, as well

as more intense and longer droughts. These findings are also consistent with statistical long-term records of Thailand, including increasing extreme temperature indices (Limsakul, 2020), as well as less frequent but more intense rainfall events (Limsakul and Singhruck, 2016). Raneesh (2014) proposed a variety of factors arising from the challenges in water resources planning and management. The major factor will be the impact of climate change through the alteration of

Citation: Tabucanon AS, Rittima A, Raveephinit D, Phankamolsil Y, Sawangphol W, Krajangka J, Talaluxmana Y, Vudhivanich V, Xue W. Impact of climate change on reservoir reliability: A case of Bhumibol Dam in Ping River Basin, Thailand. Environ. Nat. Resour. J. 2021;19(4):266-281. (<https://doi.org/10.32526/enrj/19/2021012>)

the hydrological cycle, which affects quantity and quality of regional water resources, especially in Asia. These consequences will be further exacerbated by population growth, economic factors, and land use changes (including urbanization). [Shiferaw et al. \(2014\)](#) and [Miyani \(2015\)](#) found that these changes impact the vulnerable and poor, especially those related to agricultural activities. A major reason for the impact is the uncertainty of the capability of reservoir operating rules for dams influenced by the impacts of climate change ([Kang et al., 2007](#); [Kim et al., 2009](#); [Ehsani et al., 2017](#)). Reservoir operating rules are generally developed based on the relationship between rainfall-inflow, water balance, and downstream water demand. The rules are applied to ensure appropriate management of flood in the wet season and water scarcity in the dry season. Therefore, understanding future changes of inflow into the dam is important for adaptive management of the rules ([Raneesh, 2014](#); [Koontanakulvong et al., 2020](#)).

The objective of this study was to investigate the impact of climate change on the reliability of the current reservoir operating rules of Bhumibol Dam, the largest dam in Thailand, which is an important water resource for agriculture in the central region, especially in the dry season ([Kitpaisalsakul, 2018](#); [Koontanakulvong et al., 2020](#)). This is one of two major dams regulating the Chao Phraya River, the major river in Thailand. From a historical perspective, floods frequently occur in Thailand and the 2011 flood was the largest experienced by the country, which was triggered by successive storms that forced the dam to fully release its stored water. The 2011 flood was responsible for economic losses totaling 45.5 billion USD ([World Bank, 2012](#)). In contrast, due to inadequate rainfall, there was a severe drought in 2020. It was anticipated that production of sugarcane, off-season rice and cassava were decreased by 27%, 21% and 7%, respectively. This resulted in an extensive decline of the farmers' overall income. The most seriously impacted region was in the central part of the country and was influenced by critically low water level in the dams ([Siam Commercial Bank, 2020](#)). The start of the problems in 2020 can be traced to November 2019, when the total reservoir storage of Bhumibol Dam was at a critical level of only 22% ([Thana-dachophol et al., 2020](#)).

[Kitpaisalsakul \(2018\)](#), and [Sharma and Babel \(2013\)](#) conducted a climate change impact study on the inflow and water storage of the dam. However, their study lacked consideration of a number of updated

climate change scenarios to sufficiently address future uncertainties and reliability of the current reservoir operating rule curves under climate change scenarios. Furthermore, [Kure et al. \(2013\)](#) applied MIKE11 to estimate annual inflow to the Bhumibol Dam, in which a significant increase was detected. Moreover, according to our extensive literature reviews, the research of reservoir operating reliability under recently developed climate change scenarios in the South East Asia (SEA) region is still very limited. In this study, we used MIKE11 rainfall-runoff (RR) and MIKE11 Hydrodynamic (HD) for inflow simulation of the current situation and we incorporated the climate change scenarios that were developed by Ramkhamhaeng University Center of Regional Climate Change and Renewable Energy (RU-CORE). The prediction was based on the simulation of EC-EARTH under RCP4.5 and RCP8.5 scenarios for future inflow simulation. The reliability of the future inflows was then examined, based on the standard operating procedure (SOP) of reservoir operating rules.

The additional information derived from this study can inform water management-related agencies to redesign reservoir operating rules under climate change scenarios to minimize future flood and drought risks. The current incidents and damage impacts triggered by unsatisfactory operation of major dams are evidence of the importance and necessity of redesigning reservoir operation rules with adaptive management strategies under climate change to minimize these disaster risks.

2. METHODOLOGY

2.1 Study area

Bhumibol Dam is located at 17°14'33"N Latitude and 98°58'20"E Longitude in Sam Ngao District in Tak Province in the northern region of Thailand, as shown in [Figure 1](#). It is a concrete arch gravity dam, with a storage capacity of 13,462 million m³ (MCM) to receive inflow from the Ping River Basin with an area of 25,370 km². The dam is designed for a hydroelectric power plant with a total installed capacity of 779.2 MW. According to [Koontanakulvong et al. \(2020\)](#), the long-term annual inflow over the period between 1969 and 2019 averaged 5,637 MCM. Nevertheless, their study indicated a trend of decreasing inflow after the 2011 flood, with an average annual inflow of only 3,960 MCM between 2012-2019. This highlights the challenge of reservoir management of the Bhumibol Dam, both currently and in the future. A flowchart of

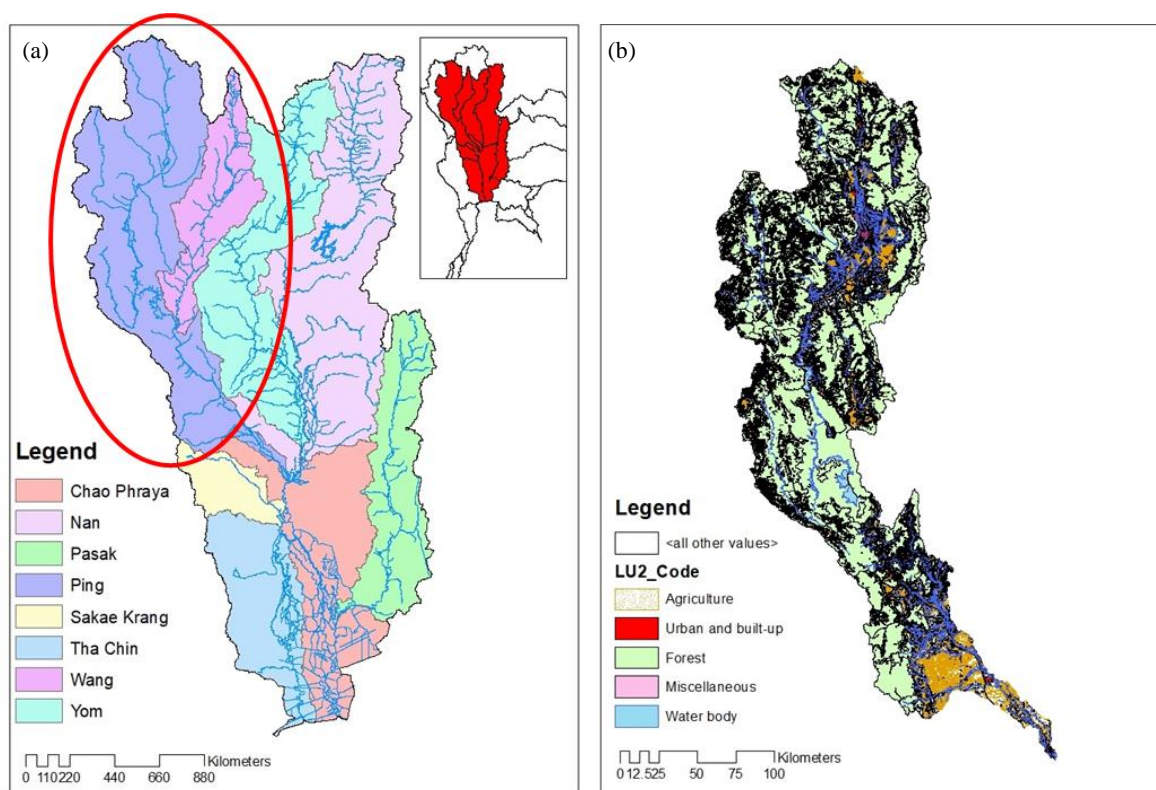


Figure 1. The Greater Chao Phraya River Basin (a) and land use of Ping River Basin in 2013 (b)

the methodology used in this study is given in [Figure 2](#). The methods and tools that were used are described in detail in the following sections.

2.2 Development of hydrological models

The platform of MIKE11 Zero Version 2016, developed by the Danish Hydraulic Institute (DHI), was adopted for simulation of inflow into Bhumibol Dam. The package consists of a variety of hydrological-hydraulic models for use, depending upon the nature of the problem and solution objective. In this study, we selected MIKE11 (Rainfall-runoff) RR NAM model and MIKE11 Hydrodynamics (HD) for inflow simulation. The MIKE11 RR NAM model, the lumped model, was applied for rainfall-runoff simulation in the Ping River Basin. As shown in [Figure 3\(a\)](#), 30 sub-basins were delineated in accordance with the recommendation of the Royal Irrigation Department (RID), as well as Thiessen polygons of 22 daily rainfall stations, namely 070731 and 170181 derived from RID, and 20 stations, namely 300201, 300202, 303201, 303301, 310201, 327301, 327501, 328201, 328202, 328301, 32920,1 373201, 373301, 376201, 376202, 376203, 376301, 376401, 380201, and 400201 derived from the Thailand Meteorological Department (TMD). In addition, daily evaporation data in the study area was obtained from

TMD station 48376. The simulated runoff was compared with the observed runoff at RID discharge stations, namely P.4A (Mat Taeng station), P.20 (Chiang Dao station), P.21 (Mae Rim station), P.24A (Mae Klang station), and P.26A (Klong Suan Mak station), as shown in [Figure 3\(b\)](#) for the model setup. The list and adjustment methods of rainfall-runoff parameters can be found in [DHI \(2017\)](#). The adjusted parameters include maximum water content in surface storage (U_{max}), maximum water content in root zone storage (L_{max}), overland flow runoff coefficient (CQOF), time constant for interflow (CKIF), time constants for routing overland flow (CK1,2), root zone threshold value for overland flow (TOF), root zone threshold value for interflow (TIF), time constant for routing baseflow (CKBF), and root zone threshold value for ground water recharge (TG). In this study, the period for model calibration was between 2000 and 2010, in which the auto-calibration function of MIKE11 RR was first applied and followed by manual adjustment to find the best fit with the observations, while the verification period was independently simulated between 2010 and 2018.

The developed MIKE11 RR model was then incorporated with MIKE11 HD. The data input for MIKE11 HD includes MIKE11 RR runoffs and 128 river cross-sections along Ping River, obtained from

RID and Hydro-Informatics Institute (HAI) for hydrodynamic simulation of the inflow into Bhumibol Dam. The model calculation is based on one- dimension flow Saint Venant equation. Furthermore, the river discharge record at P.20 station and water level at P.17 derived from RID were set as upstream and downstream boundaries, respectively. The record of reservoir storage of the dam on 1 January 2000 (9,508.49 MCM) was set as an initial storage condition.

As for MIKE11 HD, Manning’s coefficients of river channels and flood plains were adjusted to improve the fitness of inflow between simulation and observation.

To evaluate the model’s performance, the coefficient of determination (R^2) was applied. In addition, the Q-Q plots of wet season (May-October) and dry season (November-April) were also used to evaluate the simulated inflow performance.

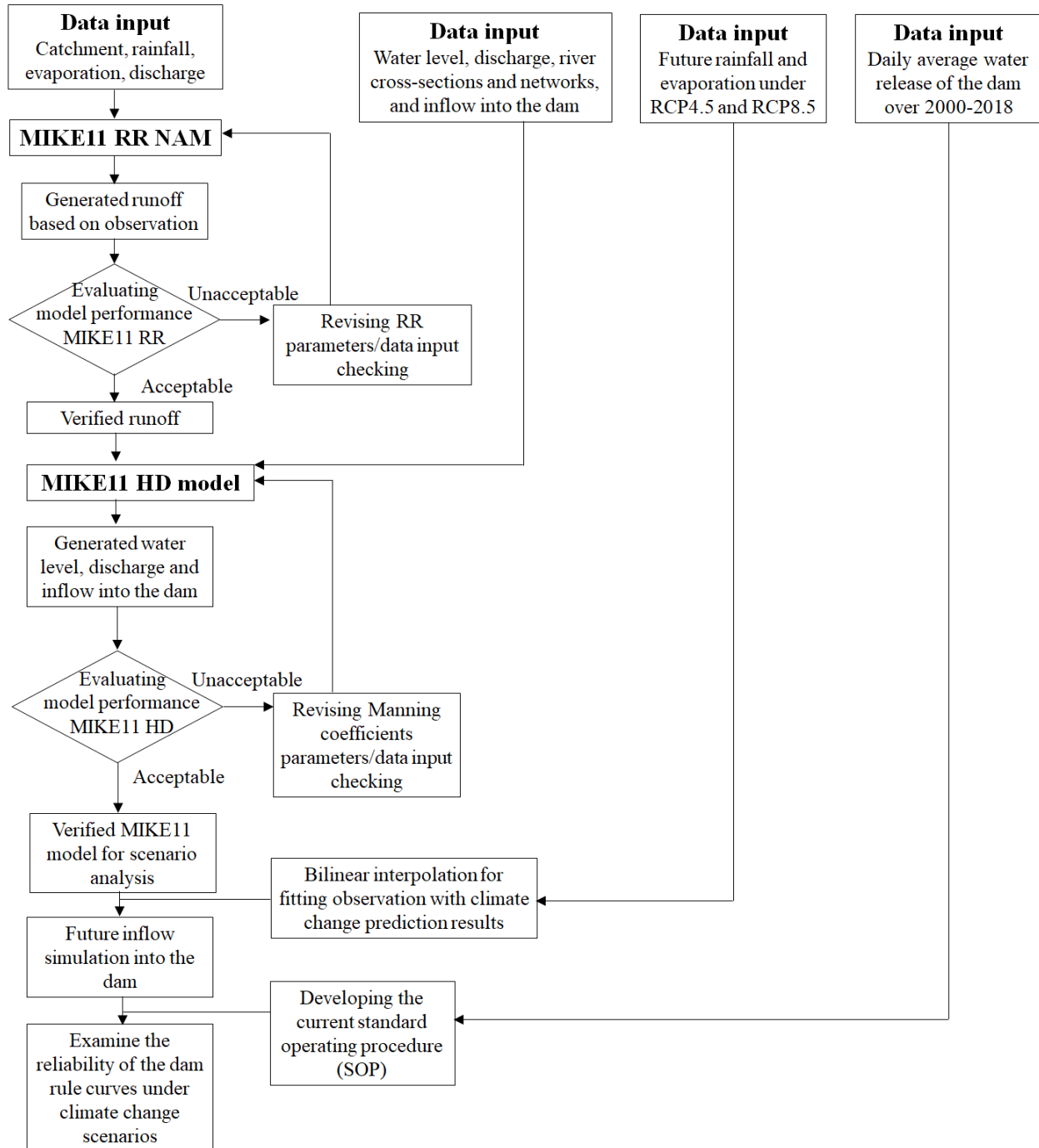


Figure 2. Flowchart of the methodology used in this study

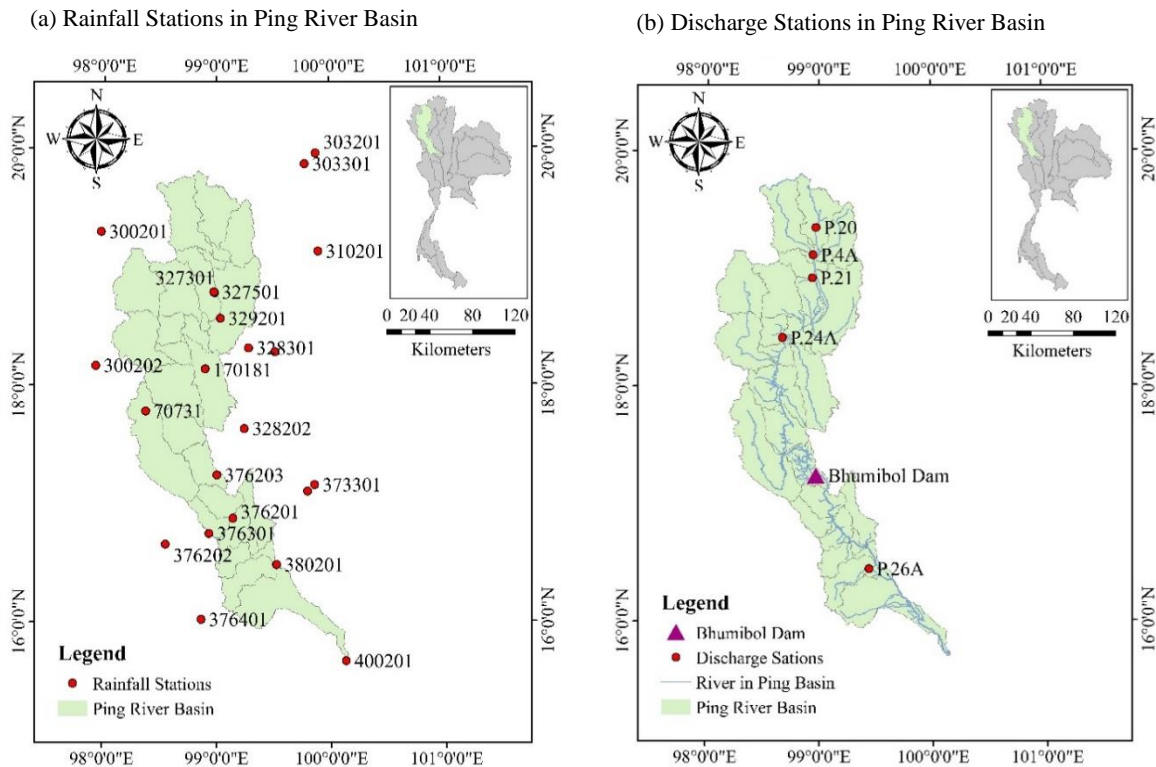


Figure 3. 30-subbasins delineated, selected rainfall (a) and selected discharge stations (b)

2.3 Climate change scenarios

Prediction of rainfall and evaporation under climate change scenarios was extracted from RU-CORE. The prediction was based on the simulation of EC-EARTH under RCP4.5 and RCP8.5 scenarios regionally downscaled by RegCM4 with 25 km × 25 km grid size over the study area (Ngo-Duc et al., 2017; Cruz et al., 2017; Tangang et al., 2019). According to the IPCC glossary, RCP stands for representative concentration pathways, providing possible future scenarios regarding long-term concentrations of greenhouse gases (Moss et al., 2010). RCP4.5 indicates that radiative forcing is stabilized at approximately 4.5 W/m² (intermediate intensity level of global warming), while RCP8.5 shows radiative forcing greater than 8.5 W/m² by 2100 and continues to rise afterwards (highest possible intensity level of global warming). Rainfall and evaporation data at the stations described in Section 2.2 were extracted in reference to the average values of four grids neighboring the targeted station grid. Murphy (1999) indicated that this method provided more precise rainfall data than the grid over the targeted station. In addition, bilinear interpolation was applied to correct the predicted values, as shown in the following equation:

$$P_{corrected\ i} = P_{RU-CORE\ i} \times \frac{\mu_{P_{observed\ i}}}{\mu_{P_{RU-CORE\ i}}}$$

Where; $P_{corrected\ i}$ is the corrected daily prediction data in month i , $P_{RU-CORE\ i}$ is the average value of four grids neighboring the targeted meteorological station grid in month i , $\mu_{P_{observed\ i}}$ is the monthly average of observed value over the targeted period between 2000 and 2018 in month I , and $\mu_{P_{RU-CORE\ i}}$ is the monthly average of predicted value over the targeted period between 2000 and 2018 in month i . In this study, predictions were temporally separated into five periods-namely 2000-2020 (baseline), 2021-2040, 2041-2060, 2061-2080, and 2081-2099 to investigate the changes in comparison with the baseline value. The statistical parameters for the analysis include average, standard deviation and the storage at the end of wet season, representing water security in the dry season.

2.4 The reservoir operating policy used in this study

The reservoir operating rules of Bhumibol Dam, developed in 2012, were obtained from the Electricity Generating Authority of Thailand (EGAT). The previous rules were redesigned after the 2011 flood event in Thailand. The procedure to evaluate the reliability of the current rules under climate change scenarios is described as follows.

1) Daily reservoir release was based on the record between 2000-2018. Annual inflow into the

dam was fitted with Gumbel Distribution (Rittima, 2018). The behavior of daily reservoir release was set to be constant across a respective month. The record of annual inflow over 2000-2018 was first categorized into three groups, namely low inflow year (<20th percentile), normal inflow year (20th-80th percentile) and high inflow year (>80th percentile). Each group had its own constant daily release behavior in the respective month, dependent upon inflow year groups, as shown in Table 1. This was done to represent the daily release behavior based on expected amount of river inflow in the following year.

Table 1. Daily release of Bhumibol Dam based on the respective months and inflow year groups

	Daily reservoir release (MCM)		
	Low inflow year	Normal inflow year	High inflow year
Jan	15.77	24.85	19.75
Feb	19.17	27.40	21.58
Mar	17.46	24.26	19.21
Apr	16.22	20.59	16.40
May	24.20	13.59	11.61
Jun	21.08	9.24	9.57
Jul	10.16	9.98	8.67
Aug	7.35	7.57	11.82
Sep	3.54	4.95	9.30
Oct	3.70	3.52	24.30
Nov	10.04	8.11	20.69
Dec	10.70	18.48	25.87
Annual	4832.41	5223.55	6041.38

2) The concept of standard operating procedure (SOP) of reservoir operating rule curves was applied with the following four conditions:

2.1) When storage of the previous day (S_{t-1}) is lower than the value specified by the lower rule curve, the release is regulated to a rate of 5 MCM/day, this value is set to maintain the vitality of downstream ecosystems.

2.2) When S_{t-1} is in the range between the value of lower and upper rule curves, the release is regulated based on daily reservoir release behaviors that was previously described.

2.3) When S_{t-1} is higher than the value specified by the upper rule curve, the release is regulated to a rate of 69.76 MCM/day, which is the maximum release capacity of the dam.

2.4) When S_{t-1} is higher than the normal high-water level value of the dam, which is 13,462 MCM, the exceedance value above 13,462 MCM is regarded as spilled water and the storage of the following day will remain at 13,462 MCM.

The reliability of reservoir operation was calculated by the following equation (Rittima, 2018);

$$Rl = 1.00 - \frac{FL}{n}$$

Where; Rl is the reservoir reliability, FL is the failure of reservoir storage to maintain in the range between lower and upper rule curves, and n is the total number operation days.

3. RESULTS AND DISCUSSION

3.1 Performance of the developed hydrological models

The results of MIKE11 RR calibration and verification are, respectively, shown in Figure 4 and Figure 5. For calibration, R^2 ranged between 0.29 and 0.55. It was apparent that there is an overestimation of runoff at P.21 at low runoff periods and an underestimation at high runoff periods. These may be due to a limited number of rainfall stations representing the sub-basin. Other factors may include unknown hydraulic structures in the P.21 sub-basin that can decelerate runoff and also correction of sub-basin delineation size by the governments. Therefore, an additional field survey is required for improvement. In addition, MIKE11 RR can capture the observed runoff patterns at other stations well. Considering the verification period, R^2 ranged between 0.39 and 0.53. To be consistent with calibration results, the runoff simulation at P.21 was still problematic. Furthermore, runoff simulation at P.4A and P.20 was overestimated while simulated runoff at P.26A and P.24A can capture the observed runoff patterns well. Additional information regarding a number of rainfall stations and operations of weirs and small-to-middle sized reservoirs can improve the results in this section.

Concerning MIKE11 HD, adjusted Manning's coefficients of channel flow ranged between 0.040 in downstream and 0.066 in upstream areas, which are consistent with the study of Sriwongsitanon (1997). In the case of flood plain flows, the values were between 0.060 in downstream and 0.100 in upstream areas.

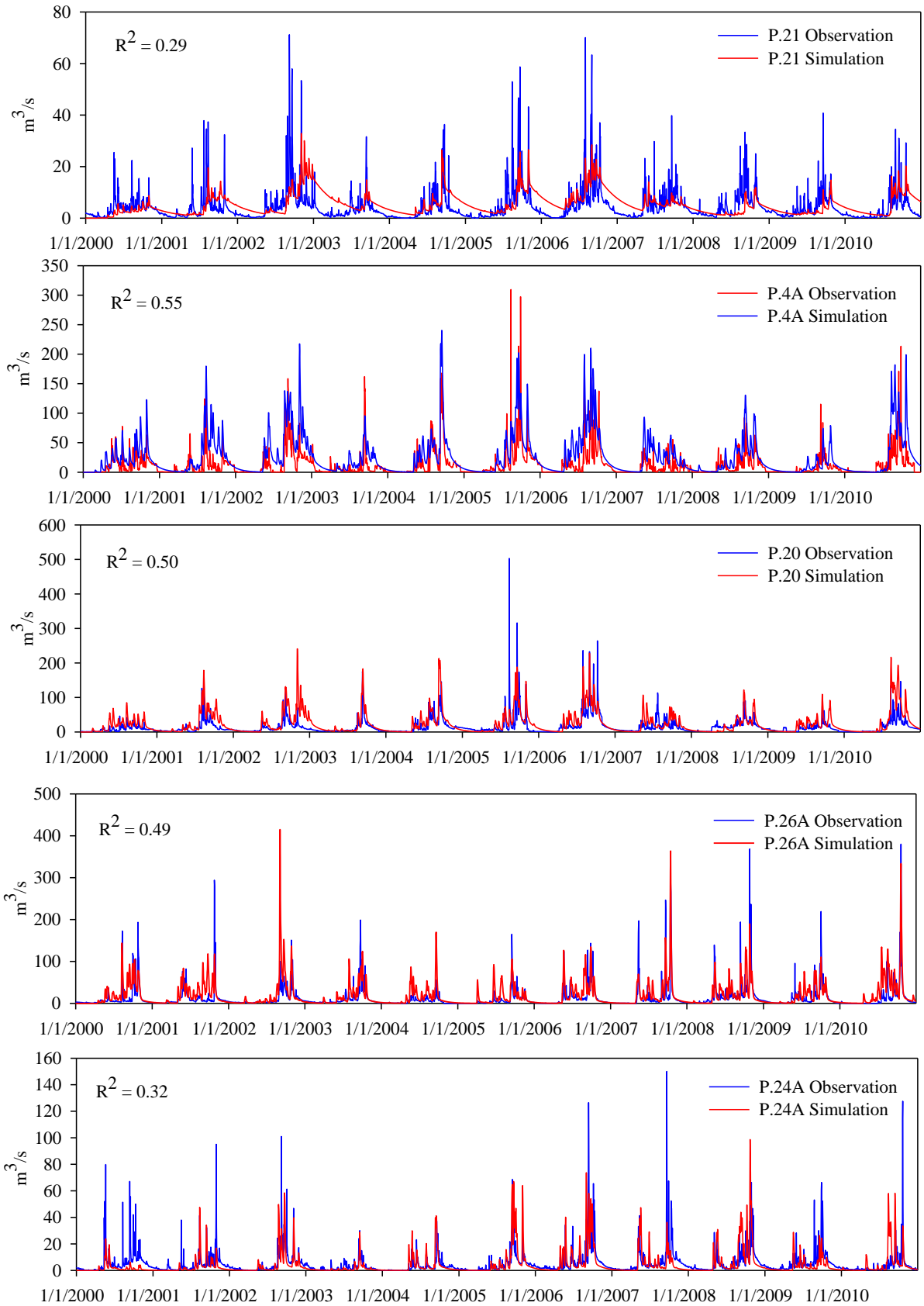


Figure 4. Calibration results of MIKE11 RR

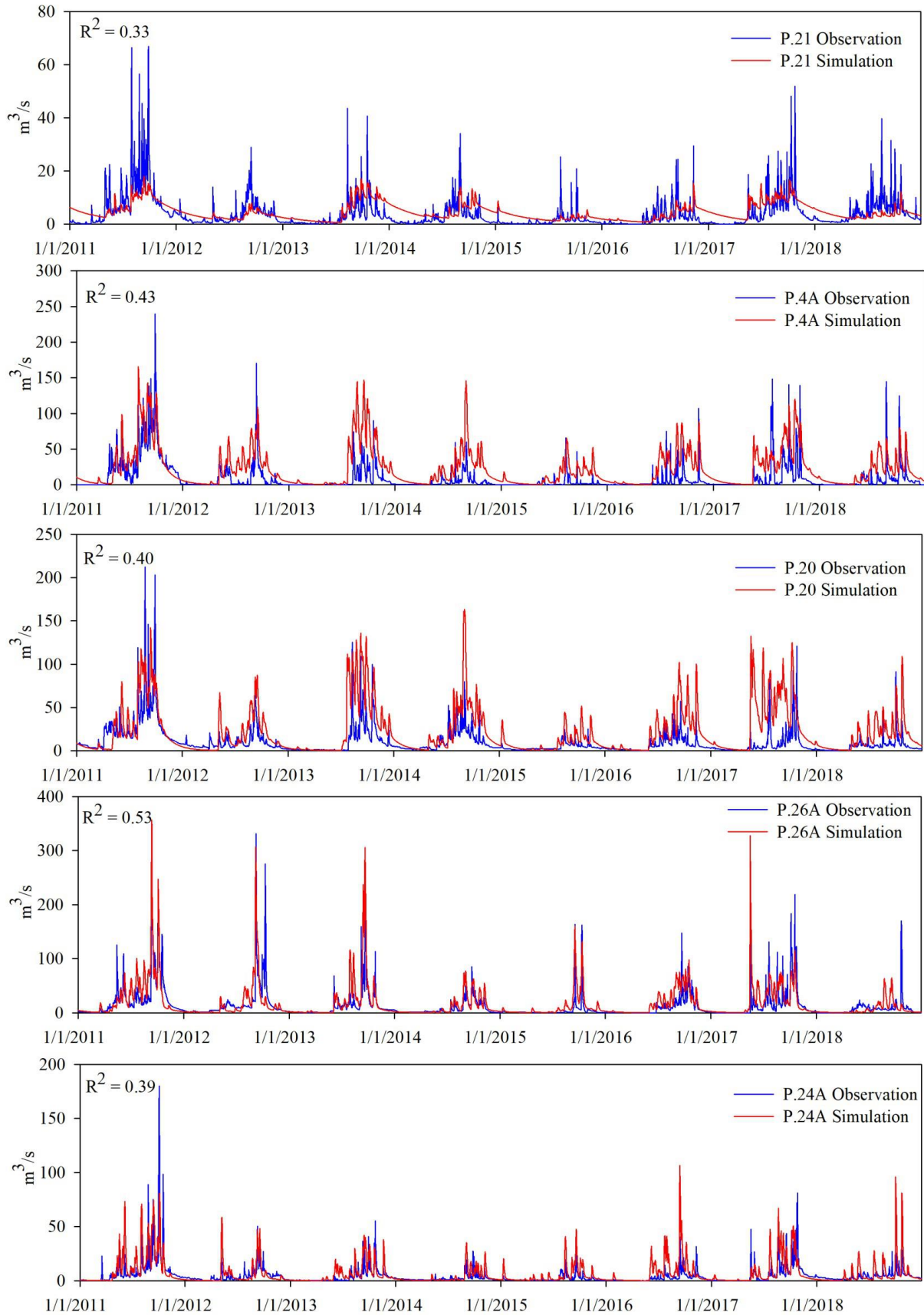


Figure 5. Verification results of MIKE11 RR

According to our land use data collection in Ping River Basin between 1989 and 2016 as shown in Figure 6, we found gradual changes in land uses. Therefore, Manning’s coefficients were not different from Sriwongsitanon (1997). According to the results of the simulated daily inflow into Bhumibol Dam as shown in Figure 7, the predicted inflow matched the actual inflow well over the period between 2000 and 2018 ($R^2=0.70$). Nevertheless, the simulation was not capable of capturing high inflow rate periods, which are typical limitations for hydrological modelling,

especially for daily rainfall input. To simulate extreme events, hourly rainfall data is necessary. The results of seasonal inflow Q-Q plot are shown in Figure 8. It was found that the model can calculate monthly inflows in the wet season well, and the model only underestimated the values in extreme events. However, in the dry season, the simulated inflow was overestimated. This was due to the unknown characteristics of the operated weirs and small-to-middle sized reservoirs in the study area, which can decelerate the river flow rate.

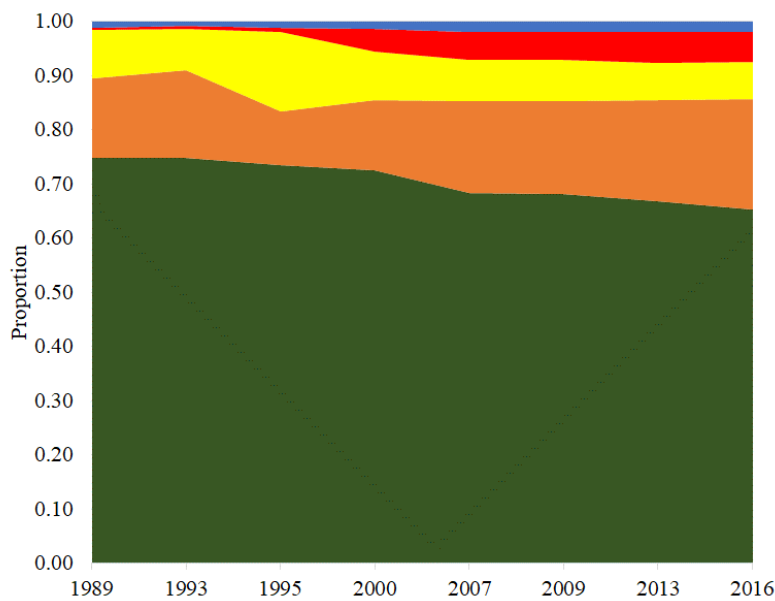


Figure 6. Proportion of land use change between 1989 and 2016. Blue, red, yellow, orange and green denote percentage proportion of water, urban, paddy land, upland agriculture and forest, respectively. (Source: Land Use Development Department, Thailand)

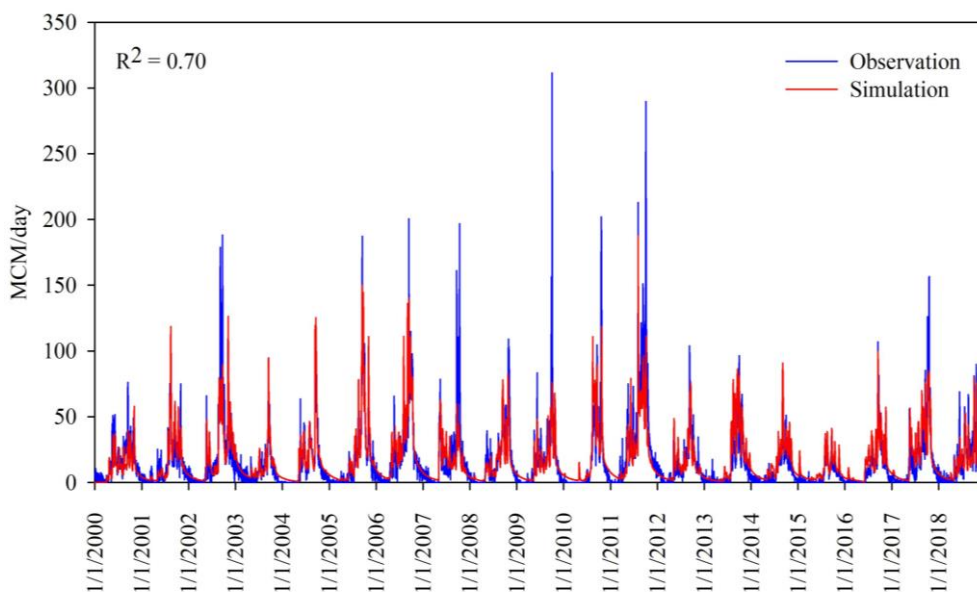


Figure 7. Comparison of simulated and observed inflows into Bhumibol Dam between 2000 and 2018 based on MIKE 11 HD

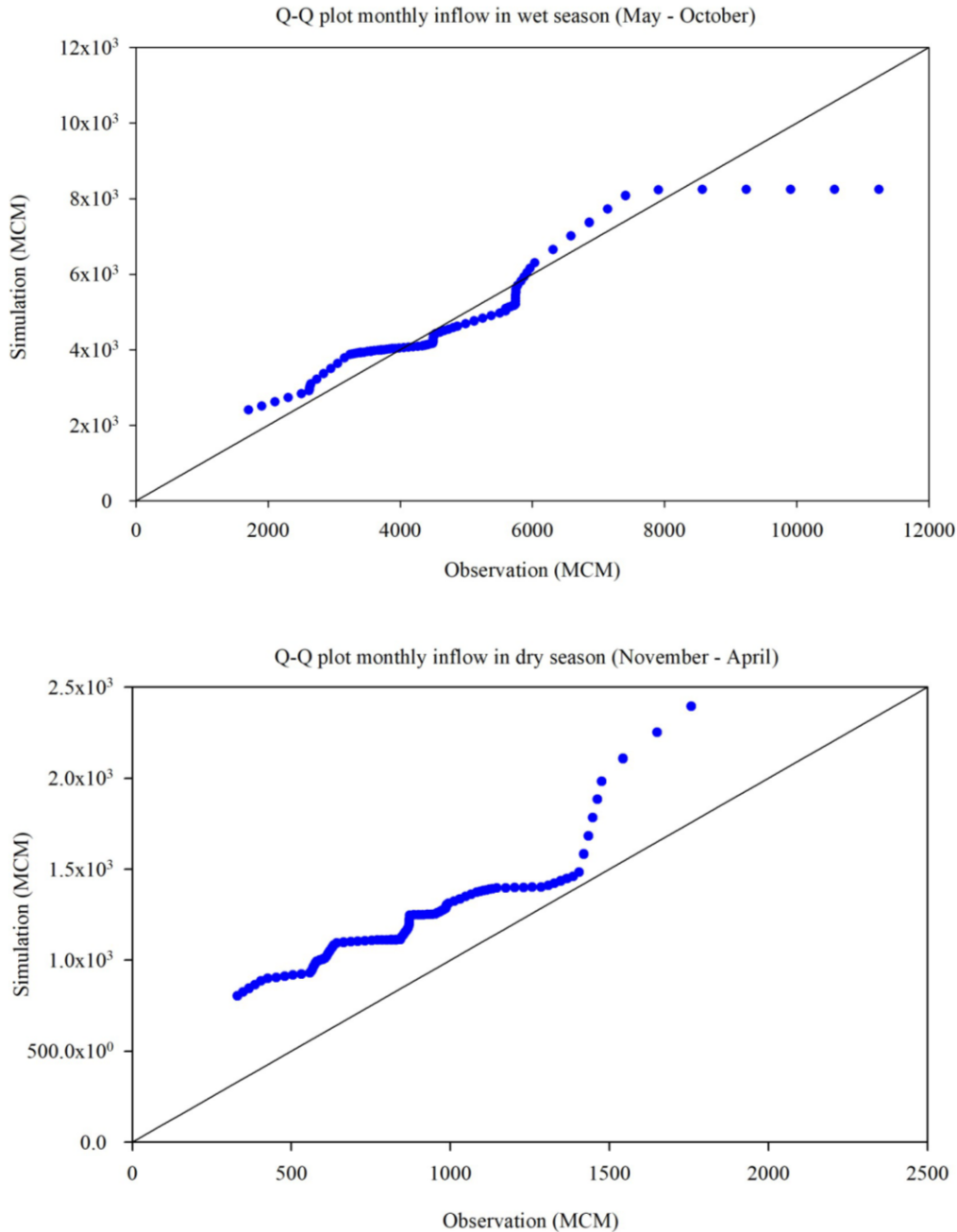


Figure 8. Q-Q plot of monthly inflow into Bhumibol Dam in wet (upper) and dry seasons (lower) between 2000 and 2018

3.2 Changes in monthly and seasonal inflow

The prediction of inflow into Bhumibol Dam under RCP4.5 and RCP8.5 is summarized in Tables 2 and 3, respectively. In comparison with the baseline period (2000-2020), RCP4.5 scenarios indicate increases in inflow in dry season by +0.07%, +10.00%, +15.42%, and +6.25% in 2021-2040, 2041-2060, 2061-2080, and 2081-2099, respectively. However, the results are generally converse in the wet season because the changes are expected to be -10.44%, +9.60%, -13.01%, and -2.63%, respectively. In the RCP8.5 scenario, the results in dry season are generally consistent with RCP4.5 in which the

changes compared with the baseline period are expected to be -5.03%, +8.14%, +8.15%, and +22.71% in 2021-2040, 2041-2060, 2061-2080, and 2081-2099, respectively. In contrast to RCP4.5, RCP8.5 in the wet season also shows fluctuating results which are projected to be -4.68%, +20.17%, -10.13%, and +18.04%, respectively. The findings in this study do not correspond with Kitpaisalsakul (2018), who applied bias corrected MRI-GCM climate data and concluded a slightly decreasing trend of annual inflow into Bhumibol Dam in both seasons through the near future (2015-2039) at the slope rate of -5.744 MCM/year and the far future (2075-2099) at

Table 2. Summary of percentage change in statistical indicators compared with the baseline period (2000-2020) under RCP4.5

Year	Average														
	Jan	Feb	Mar	Apr	May	Jun	Jul	Aug	Sep	Oct	Nov	Dec	Annual	Wet	Dry
2021-2040	-0.64%	-1.89%	-8.67%	45.44%	44.21%	-32.29%	-11.48%	-19.49%	-12.34%	-5.35%	-1.30%	-6.61%	-8.74%	-10.44%	0.07%
2041-2060	7.09%	5.44%	8.29%	28.22%	77.19%	54.53%	-3.22%	-2.53%	5.08%	-1.55%	12.83%	3.65%	9.67%	9.60%	10.00%
2061-2080	9.04%	1.56%	133.76%	35.26%	23.83%	-16.32%	-19.88%	-7.40%	-21.51%	-10.33%	1.87%	6.64%	-8.40%	-13.01%	15.42%
2081-2099	10.97%	2.79%	-7.63%	17.20%	16.42%	9.42%	0.15%	-10.31%	-0.71%	-8.71%	9.16%	0.60%	-1.19%	-2.63%	6.25%
	Standard deviation														
2021-2040	12.58%	12.55%	-18.63%	58.56%	82.67%	-9.40%	45.47%	-35.76%	38.98%	23.64%	-4.85%	3.59%	-2.53%	12.75%	8.49%
2041-2060	6.78%	3.49%	-3.55%	39.79%	134.19%	77.73%	-11.10%	-42.74%	37.37%	2.79%	41.81%	-11.05%	6.18%	14.43%	19.38%
2061-2080	54.55%	36.45%	911.78%	45.86%	34.77%	13.69%	-23.50%	-44.10%	23.93%	3.18%	73.54%	96.97%	-2.10%	-5.71%	146.93%
2081-2099	15.78%	-11.28%	-44.44%	74.93%	71.72%	88.84%	29.47%	-41.97%	34.00%	-18.97%	-14.19%	-36.42%	-9.61%	9.63%	-4.19%
	Storage at the end of wet season														
2021-2040	-10.44%														
2041-2060	9.60%														
2061-2080	-13.01%														
2081-2099	-2.63%														

Table 3. Summary of percentage change in statistical indicators compared with the baseline period (2000-2020) under RCP8.5

Year	Average														
	Jan	Feb	Mar	Apr	May	Jun	Jul	Aug	Sep	Oct	Nov	Dec	Annual	Wet	Dry
2021-2040	-4.91%	-2.80%	-9.06%	-28.34%	-1.47%	-11.83%	-36.68%	2.28%	-14.92%	16.18%	-3.66%	0.80%	-4.74%	-4.68%	-5.03%
2041-2060	11.93%	13.35%	7.03%	-16.37%	8.42%	6.59%	3.30%	131.09%	3.00%	2.73%	10.65%	8.04%	18.20%	20.17%	8.14%
2061-2080	15.73%	8.90%	0.77%	-26.91%	-56.47%	-37.78%	-31.99%	17.52%	-12.32%	5.13%	15.08%	4.90%	-7.15%	-10.13%	8.15%
2081-2099	13.11%	15.64%	9.08%	61.47%	39.31%	10.19%	24.59%	76.45%	1.42%	6.95%	21.72%	23.88%	18.80%	18.04%	22.71%
	Standard deviation														
	Jan	Feb	Mar	Apr	May	Jun	Jul	Aug	Sep	Oct	Nov	Dec	Annual	Wet	Dry
2021-2040	5.86%	12.89%	-15.69%	-76.78%	17.93%	-25.30%	-23.38%	49.15%	18.73%	65.67%	-11.44%	28.26%	44.32%	16.79%	-18.71%
2041-2060	20.02%	23.62%	-6.75%	-70.15%	8.48%	-1.50%	-6.77%	346.47%	35.56%	27.10%	8.94%	29.00%	62.78%	53.03%	-6.81%
2061-2080	77.98%	43.98%	2.36%	-80.03%	-62.32%	-19.75%	-15.07%	95.60%	5.49%	80.80%	85.01%	38.75%	34.32%	14.94%	27.48%
2081-2099	30.26%	37.67%	3.69%	82.13%	113.54%	25.83%	69.48%	184.66%	10.92%	35.76%	49.55%	76.38%	73.58%	57.77%	55.40%
	Storage at the end of wet season														
2021-2040	-4.68%														
2041-2060	20.17%														
2061-2080	-10.13%														
2081-2099	18.04%														

the slope rate of -23.03 MCM/year. The results closely relate with predicted decreasing rainfall in those periods. Similarly, the results are dependent upon the studied location. For example, [Harraki et al. \(2020\)](#) indicated a decrease in the total average supply between 9% and 12% for mid-term scenario (2046-2065) and 20% to 27% for the long-term scenario (2081-2100) for the Sebou Basin in Morocco. Our results correspond with the work of [Sharma and Babel \(2013\)](#), especially in the dry season. The work applied bias corrected and downscaled ECHAM4/OPYC and indicated continuous decreases in inflow rate in the wet season by -29.0% in the period between 2023-2027 and -27.0% in 2093-2097 under A2, as well as -23.0% and -27.0% under B2. As for dry season, insistent increases in inflow rate were detected by +10.0% and +6.0% under A2, as well as +19.0% and +24.0% under B2. In addition, our study also had the same finding that the peak flows in the future would be shifted from September to October, which was more apparent in RCP8.5. [Giesen et al. \(2010\)](#) also found a shift of ending rainy season to later periods under climate change in the Volta Basin, West Africa.

In terms of inflow variation, a large change in standard deviation indicates increasing difficulty for reservoir managers to estimate and regulate appropriate release to control the storage within the range between lower and upper rule curves. Under RCP4.5, in comparison with the baseline period, the deviation will be less at the annual change rate of -2.53%, +6.18%, -2.10%, and -9.61% in 2020-2040, 2041-2060, 2061-2080, and 2081-2099, respectively. This implies more stability of water inflow into the dam, leading to better estimation for the appropriate release. In contrast, RCP8.5 is challenging due to a large increase in the deviation rate at +44.32%, +62.78%, +34.32%, and +73.58%, respectively.

Regarding the results of storage at the end of wet season (May-October), this indicates water security for utilization in the dry season, especially for agricultural activities. The results show high uncertainties in which RCP4.5 provides change rates of -10.44%, +9.60%, -13.01%, and -2.36% in 2020-2040, 2041-2060, 2061-2080, and 2081-2099, respectively. While for RCP8.5, the changes are expected to be -4.68%, +20.17%, -10.13%, and +18.04%, respectively. Therefore, with an understanding of climate change impacts, the adaptive or flexible management of the reservoir operating rule curves should be considered to be able to be

proactively redesigned under uncertain conditions ([Adeloye and Dau, 2019](#); [Fletcher et al., 2019](#)).

3.3 Reliability of current reservoir operating rules

Daily reservoir storage of Bhumibol Dam based on the standard operating rules under RCP4.5 and RCP8.5 is illustrated in [Figure 9](#). Under RCP4.5, the reliability of reservoir operation throughout 2000-2099 will be 80%. This indicates high failure risk (20%) in reservoir operation reliability quality, in which the acceptable percentage is 80% ([Rittima, 2018](#)). Interestingly, RCP8.5 indicates higher reliability with the rate of 87%. The results are consistent with the findings of [Park and Kim \(2014\)](#), who suggested that under the new climatic conditions, the reliability of water and hydropower supply from the Chungju Multipurpose Dam in South Korea would be generally improved as a consequence of increased dam inflow. In addition, the study of [Zolghadr-Asli et al. \(2019\)](#) found similar results in which the dam reliability for power generation will be generally improved through 2010-2099 due to climate change because of the increased inflow from four hydropower projects in the Karkheh River Basin in Iran.

Considering reservoir operation reliability, the dominant cases will be the storage below the lower rule curve accountable for 92% for RCP4.5 and 86% for RCP8.5. The monthly failure ratios are summarized in [Table 4](#). Under RCP4.5, the apparent failure rates above 10% would occur in January (11.87%), August (10.72%), September (11.50%), October (13.09%), November (14.20%), and December (13.93%). In case of failure of upper rule curve, the frequent flood risks would occur in June (20.80%), July (35.88%), August (12.65%), and October (10.75%). Under RCP8.5, the failure to be below the lower rule curve would apparently occur in July (11.01%), August (12.66%), September (12.01%), October (12.78%), November (15.25%), and December (12.31%), while the failure of upper rule curve management would be in June (14.88%), July (23.07%), August (22.77%), September (18.45%), and October (15.63%). The major cause of these failures would be due to high fluctuation of average and deviation rates of monthly rainfall between April and September through 2021 to 2099, in which the monthly rainfall pattern is relatively different from the current situation (2000-2020); as can be seen in [Tables 2](#) and [3](#). The results indicate that the failure of lower and upper rule curves generally

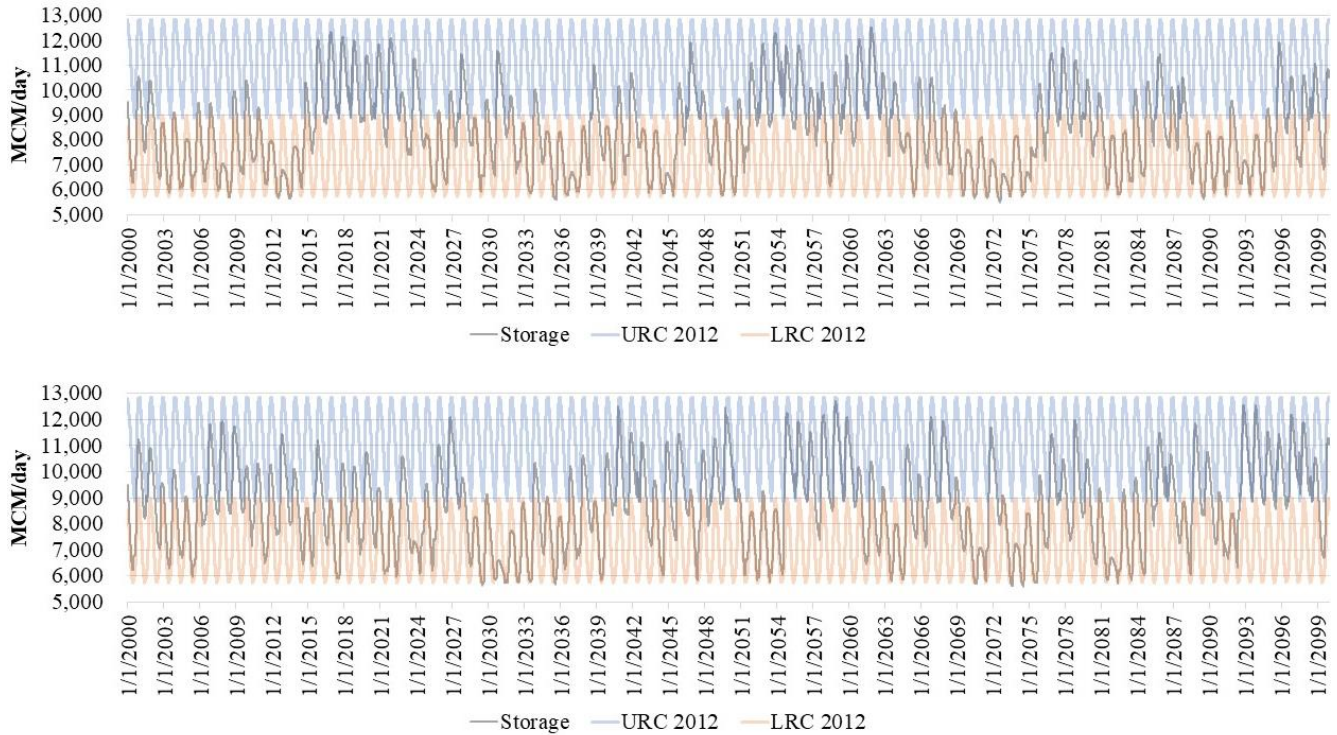


Figure 9. Simulated daily reservoir storage with current lower rule curve (LRC) and upper rule curve (URC) under RCP4.5 (upper) and RCP8.5 (lower) between 2000 and 2099.

Table 4. Monthly reservoir operation failure ratios under climate change scenarios (2000-2099)

	RCP4.5		RCP8.5	
	Lower	Upper	Lower	Upper
Jan	11.87%	0.00%	9.47%	0.00%
Feb	6.20%	0.00%	5.81%	0.00%
Mar	3.00%	0.00%	3.07%	0.00%
Apr	1.24%	0.00%	1.35%	0.45%
May	1.33%	1.56%	0.67%	3.42%
Jun	4.55%	20.80%	3.61%	14.88%
Jul	8.38%	35.88%	11.01%	23.07%
Aug	10.72%	12.65%	12.66%	22.77%
Sep	11.50%	17.68%	12.01%	18.45%
Oct	13.09%	10.75%	12.78%	15.63%
Nov	14.20%	0.69%	15.25%	1.34%
Dec	13.93%	0.00%	12.31%	0.00%
Total	100.00%	100.00%	100.00%	100.00%

occurs in the wet season, especially between the month of June and October. This suggests that the dam regulator should revise the rule curves, especially in the wet season.

Our study heavily relies on SOP, which may not be able to reflect the real reservoir release response situation. However, we can successfully demonstrate that SOP would be a relatively more inappropriate operation in the future. The Hedging Rule (HR), an

advanced/developed form of SOP, can also be considered for further study, in which operating rules can be designed to ration water supply in an appropriate preparation for potential low inflows in the near future (You and Cai, 2008). Hedging aims at distributing the anticipated water shortage uniformly to reduce severity in reservoir management so that it can cope well with impact of drought and consequent shortage in current and future water supply (Jain and

Singh, 2003). Advanced research and technology, including further climate change impact studies with various future scenarios and application of artificial intelligence (AI), could support improvement of water regulation through adaptive management of rule curves, which are highly recommended for further study. For example, Kompor et al. (2020) found that changing the reservoir operation plan with seasonal prediction adopted from Centre for Medium-Range Weather Forecasts could decrease the peak river discharge in the Chao Phraya River by 20% under the 2011 flood rainfall scenario. Therefore, integration of climate change scenarios should be further included in future studies to understand and minimize climate change uncertainties, which would be useful information for decision-makers in the development of appropriate rule curves.

4. CONCLUSION

According to the results of this study, it can be concluded that there is high risk of current reservoir operating rules moving towards reliability failure under RCP4.5, but the risk will be lower under RCP8.5 due to increased inflow amounts. The failures obviously occur in the wet season, due to a large fluctuation of the rainfall amount and standard deviation, which cautions the need to redesign the rules. Therefore, it is necessary to revisit the rule curves, especially in the wet season, to maximize reliability. A limitation of this study is the assumption of SOP representing reservoir release behaviors, which is fixed and inflexible. In addition, unknown future water demand in the downstream area was not considered. For future study, adaptive management of rule curves through application of artificial intelligence (AI), such as fuzzy logic model or neuro fuzzy optimization model, is a promising alternative to cope with high uncertainties under climate change.

ACKNOWLEDGEMENTS

This work is financially supported by the Thailand Science Research and Innovation and National Research Council of Thailand, under Grant No. SIP6230022. The authors would like to express their sincere gratitude to Thailand government agencies, including Electricity Generating Authority of Thailand, Royal Irrigation Department, Hydroinformatics Institute and Thai Meteorological Department, for their kind support and sharing of data input for analysis in this study.

REFERENCES

- Adeloye AJ, Dau QV. Hedging as an adaptive measure for climate change induced water shortage at the Pong Reservoir in the Indus Basin Beas River, India. *Science of The Total Environment* 2019;687:554-66.
- Cruz FT, Narisma GT, Dado JB, Singhruck P, Tangang F, Linarka UA, et al. Sensitivity of temperature to physical parameterization schemes of RegCM4 over the CORDEX-Southeast Asia region. *International Journal of Climatology* 2017;37:5139-53.
- Danish Hydraulic Institute (DHI.) MIKE 11 User Guide [Internet]. 2017 [cited 2021 Jan 12]. Available from: https://manuals.mikepoweredbydhi.help/2017/Water_Resources/MIKE11_UserManual.pdf.
- Ehsani N, Vörösmarty CJ, Fekete BM, Stakhiv EZ. Reservoir operations under climate change: Storage capacity options to mitigate risk. *Journal of Hydrology* 2017;555:435-46.
- Fletcher S, Lickley M, Strzepek K. Learning about climate change uncertainty enables flexible water infrastructure planning. *Nature Communications* 2019;10:1782.
- Giesen NVD, Liebe J, Jung G. Adapting to climate change in the Volta Basin, West Africa. *Current Science* 2010;98(8):1033-7.
- Harraki WEL, OUAZAR D, Bouziane A, Hasnaoui D. Climate change observations and trends overview: Focus on Morocco with a case-study of a future reservoir's response to climate change. *E3S Web Conference* 2020;150.
- Intergovernmental Panel on Climate Change (IPCC). *Global Warming of 1.5°C: An IPCC Special Report on the Impacts of Global Warming of 1.5°C Above Preindustrial Levels and Related Global Greenhouse Gas Emission Pathways, in the Context of Strengthening the Global Response to the Threat of Climate Change, Sustainable Development, and Efforts to Eradicate Poverty*. In Press; 2018.
- Intergovernmental Panel on Climate Change (IPCC). *Managing the Risks of Extreme Events and Disasters to Advance Climate Change Adaptation. A Special Report of Working Groups I and II of the Intergovernmental Panel on Climate Change*. Cambridge, England: Cambridge University Press; 2012.
- Jain SK, Singh, VP. *Water Resources Systems Planning and Management*. New York, USA: Springer; 2003.
- Kang B, Lee SJ, Kang DH, Kim YO. A flood risk projection for Yongdam Dam against future climate change. *Journal of Hydro-environment Research* 2007;1:118-25.
- Kim S, Tachikawa Y, Nakakita E, Takara K. Reconsideration of reservoir operations under climate change: case study with Yagisawa Dam, Japan. *Annual Journal of Hydraulics Engineering* 2009;53:115-20.
- Kitpaisalsakul T. Impact of climate change on irrigation water management by the Bhumibol Dam in Thailand. *Journal of Thai Interdisciplinary Research* 2018;13:49-54.
- Koontanakulvong S, Vudhivanich V, Rittima A, Phankamolsil Y, Tabucanon AS, Sawangphol W, et al. Lesson learnt from past to present and water storage potential in future for Bhumibol and Sirikit Dams. *Proceedings of the 13th THAICID National E-Symposium; 2020 Jul 31; Studio of Irrigation Development Institute, Bangkok: Thailand; 2020*.
- Kompor W, Yoshikawa S, Kanae S. Use of seasonal streamflow forecasts for flood mitigation with adaptive reservoir operation: A case study of the Chao Phraya River Basin, Thailand, in 2011. *Water* 2020;12(3210):1-19.
- Kure S, Tenakari T, Okabe M. Spatial and seasonal differences in the response of flow to climate change in the Chao Phraya

- River Basin, Thailand. *Journal of Japan Society of Civil Engineers, Ser.B1 (Hydraulic Engineering)* 2013;69(4):55-60.
- Limsakul A, Singhruck P. Long-term trends and variability of total and extreme precipitation in Thailand. *Atmospheric Research* 2016;169:301-17.
- Limsakul A. Trends in Thailand's extreme temperature indices during 1955-2018 and their relationship with global mean temperature change. *Applied Environmental Research* 2020; 42:94-107.
- Miyan MA. Droughts in Asian least developed countries: Vulnerability and sustainability. *Weather and Climate Extremes* 2015;7:8-23.
- Moss R, Edmonds J, Hibbard K, Manning M, Rose S, Vuuren D, et al. The next generation of scenarios for climate change research and assessment. *Nature* 2010;463:747-56.
- Murphy J. An evaluation of statistical and dynamical techniques for downscaling local climate. *Journal of Climate* 1999;12:2256-84.
- Ngo-Duc T, Tangang FT, Santisirisomboon J, Cruz F, Trinh-Tuan L, Nguyen-Xuan T, et al. Performance evaluation of RegCM4 in simulating extreme rainfall and temperature indices over the CORDEX- Southeast Asia region. *International Journal of Climatology* 2017;37:1634-47.
- Park JY, Kim SJ. Potential impacts of climate change on the reliability of water and hydropower supply from a multipurpose dam in South Korea. *Journal of the American Water Resources Association* 2014;50:1273-88.
- Raneesh J. Impact of climate change on water resources. *Earth Science and Climatic Change* 2014;5(3):1-5.
- Rittima A. *Reservoir Systems and Operation Planning*. Bangkok, Thailand: Mittrapopkarnpim; 2018.
- Sharma D, Babel MS. Application of downscaled precipitation for hydrological climate-change impact assessment in the upper Ping River Basin of Thailand. *Climate Dynamics* 2013; 41:2589-602.
- Shiferaw B, Tesfaye K, Kassie M, Abate T, Prasanna BM, Menkir A. Managing vulnerability to drought and enhancing livelihood resilience in sub-Saharan Africa: Technological, institutional and policy options. *Weather and Climate Extremes* 2014;3:67-79.
- Siam Commercial Bank. EIC evaluates that the 2020 drought could extend to June with severe impacts on sugarcane, off-season rice, and cassava [Internet]. 2020 [cited 2021 Jan 12]. Available from: https://www.scbeic.com/en/detail/file/product/6660/fl65yywwln/EIC-Note_drought_EN_20200302.pdf.
- Sriwongsitanon N. The study of the flood conditions of the Upper Ping River Basin by an application of MIKE 11 model (part 1). *Kasetsart Engineering Journal* 1997;11:74-87 (in Thai).
- Tangang F, Santisirisomboon J, Juneng L, Salimun E, Chung J, Supari S, et al. Projected future changes in mean precipitation over Thailand based on multi-model regional climate simulations of CORDEX Southeast Asia. *International Journal of Climatology* 2019;39:5413-36.
- Thana-dachophol T, Teamsuwan V, Udomsap L, Wongsamut W, Chamnankaw U. An analysis of water management in 2020 drought conditions. *Proceedings of the 13th THAICID national esymposium*; 2020 Jul 31; Studio of Irrigation Development Institute, Bangkok: Thailand; 2020.
- The World Bank. *Thai flood 2011, Rapid Assessment for Resilient Recovery and Reconstruction Planning*. The World Bank; 2012.
- You JY, Cai X. Hedging rule for reservoir operations: 1. A theoretical analysis. *Water Researches Research* 2008; 44:W01415.
- Zolghadr-Asli B, Bozorg-Haddad O, Chu X. Effects of the uncertainties of climate change on the performance of hydropower systems. *Journal of Water and Climate Change* 2019;10.3:591-609.

Bioaccumulation of Lead by Pepper Elder (*Peperomia pellucida* (L.) Kunth) in a Lead-Contaminated Hydroponic System

Jessica O. Tablang, Florenda B. Temanel, Ron Patrick C. Campos*, and Helen C. Ramos

College of Arts and Sciences, Isabela State University-Echague, 3309 Isabela, Philippines

ARTICLE INFO

Received: 28 Jan 2021
 Received in revised: 21 Mar 2021
 Accepted: 21 Apr 2021
 Published online: 25 May 2021
 DOI: 10.32526/enrj/19/2021010

Keywords:

Pepper elder/ *Peperomia pellucida*/ Phytoremediation/
 Heavy metal/ Lead

* Corresponding author:

E-mail:
 ronpatrick.campos@gmail.com

ABSTRACT

Lead (Pb) has become one of the most common heavy metal contaminants, demanding research on economical remediation approaches with minimal ecological impacts. Pepper elder (*Peperomia pellucida*) is a fast-growing plant that can be a candidate for bioaccumulation and phytoremediation. In this study, the lead bioaccumulation of *P. pellucida* was assessed by determining the growth response and absorptive capacity of the plant. Plants were grown in hydroponic solution spiked with 500 mg/L of Pb for 28 days. Growth response, absorptive capacity and tolerance of plants grown in contaminated nutrient solution were determined in comparison with control plants. After 28 days of exposure, lead phytotoxicity symptoms such as wilting, chlorosis and necrosis were observed on some plants. The control plants recorded 3.08 g total dry weight (DW) compared to the 1.35 g in Pb-contaminated plants. The tolerance index (TI) of *P. pellucida* was at 43.40%. The plants were able to absorb lead, with the concentration of lead in the roots (158.6 µg/g) being greater than the concentration of the metal in the shoots (43.2 µg/g). Meanwhile, bioconcentration factor (BCF) and translocation factor (TF) values were recorded at 0.40 and 0.27, respectively. BCF criterion indicates that the plant is not suitable for phytoextraction, but TF value shows that the plant can be a potential excluder. The findings of the study show that *P. pellucida* accumulated considerable amount of lead within its tissues, indicating that the plants may be further exploited for their capacity to absorb heavy metals by tweaking several factors that may affect its bioaccumulation ability.

1. INTRODUCTION

Global industrialization and human activity have caused the widespread contamination of persistent pollutants that resulted in the degradation of the environment (Lado et al., 2008). This is caused by contamination of inorganic and organic pollutants from various sources such as direct discharge of industrial effluents to soil, accidental spillage of chemicals, application of agrochemicals to soils and the percolation of contaminated surface water to subsurface stratum, or improper disposal of wastes (Mirsal, 2004). Many heavy metals can be considered essential to the life cycles of both flora and fauna, but may reach toxic levels when the number of pollutants exceeds the demand of the inherent biological systems (Mandkini et al., 2016). Furthermore, the non-biodegradability of heavy metal pollutants creates a

hazard when discharged in soils and bodies of water (Thayaparan et al., 2013).

Lead (Pb) has become one of the most common heavy metal contaminants in the soil (Thayaparan et al., 2013; Solidum et al., 2010). Lead contamination has become prevalent due to existing mining and smelting activities (Liu et al., 2010) and the disposal of sewage sludge and industrial wastes (Ona et al., 2006), as well as being a component of common products such as paints, gasoline and explosives.

Phytoremediation is a cheap and reliable technology that is utilized for the cleansing of polluted environments that can potentially address the problems of contaminated areas affected by urban and industrial activities (Mojiri, 2011). It is based on exploiting plant's natural mechanisms to detoxify and accumulate heavy metals within soil or from aquatic

Citation: Tablang JO, Temanel FB, Campos RPC, Ramos HC. Bioaccumulation of lead by pepper elder (*Peperomia pellucida* (L.) Kunth) in a lead-contaminated hydroponic system. Environ. Nat. Resour. J. 2021;19(4):282-291. (<https://doi.org/10.32526/enrj/19/2021010>)

environments (Mandkini et al., 2016). Plants can be used to either partially or substantially remediate different media including sludge, soil, groundwater, sediment and waste water contaminated with pollutants (Salt et al., 1998).

Owing to its physiological and morphological characteristics, *Peperomia pellucida* can be a candidate for bioaccumulation and phytoremediation. This plant, commonly referred to as shiny bush, clear weed or pepper elder, belongs to the family Piperaceae. It is an herbaceous plant found in many South American and Asian countries (Arquion et al., 2015) and is distinguished by its heart-shaped and fleshy leaves with lush and succulent stems, shallow roots and small flowers, which eventually develop into numerous tiny seeds attached on cord-like spikes (Tablang et al., 2020). In the Philippines, the plant has been listed as one of the clinically tested and approved alternative herbal medicines endorsed by the Department of Health (Tolentino et al., 2019). Traditionally, the plant is used in the treatment of different ailments such as convulsions, conjunctivitis, headache, fever, gout, skin diseases, and rheumatic pains (Tolentino et al., 2019; Mosango, 2008; Raghavendra and Kekuda, 2018).

Pepper elder possesses a number of remarkable qualities which makes it a candidate for phytoremediation. It is (1) a plant with fast growth rates (McIntyre, 2003); (2) produces large biomass above and below ground (Mosango et al., 2008); (3) establishes a vast niche for the development of rhizosphere microorganisms (Kirk et al., 2002); and (4) is widely distributed, well adapting to different climatic conditions. In a study by Anoliefo et al. (2006), *P. pellucida* was labelled as the plant species with the most engine oil-tolerant phytoremediation capacity in Benin City, Nigeria because it was found in every heavy metal contaminated site in the city. *P. pellucida* grown on lead, copper and manganese contaminated soils also showed accumulation of up to 1,769 ppm of copper, 2,478 ppm of lead and 621 ppm of manganese (Calawagan et al., 2012). Belonias (2009) further supported the capacity of the plant to bioaccumulate lead, concluding that *P. pellucida* can tolerate Pb levels as high as 400 ppm without affecting its growth. Moreover, it was reported that *P. pellucida* can contain high amount of toxic metals like lead (Pb) and cadmium (Cd) surpassing the limits allowed by the World Health Organization (De Guzman, 1999).

The deterioration of the environment due to lead contamination demands technology involving

economical approaches with minimal ecological impacts. Phytoremediation through bioaccumulation can be one of these approaches. With the objective of determining the lead-absorptive capacity and heavy metal tolerance of *P. pellucida*, this study was conducted to evaluate the potential of *P. pellucida* in the bioaccumulation of lead *ex situ* and determine the growth response of the plant upon exposure to Pb contamination in a hydroponic setting.

2. METHODOLOGY

2.1 Plant collection and acclimatization

Plant samples of *P. pellucida* were obtained from uncontaminated sites in Isabela State University, Echague, Isabela (16.7212° N, 121.6887° E). Young and healthy plants in uniform height were selected, and tested for initial heavy metal content to ensure absence of heavy metals prior to experimentation. Collected plants were transplanted individually in a sowing bed containing 50.8 mm-deep coconut coir dust. The plants were watered regularly for three (3) days. After which, each plant was transferred to individual growing pots and introduced to the nutrient solution for ten (10) days to allow the plants to adapt to the experimental conditions and to obtain substantial biomass prior to contamination.

2.2 Hydroponic system set-up and experimental set-up

This study employed the Simple Nutrient Addition Program (SNAP) hydroponics system, a non-circulating, passive aeration hydroponics system (Santos and Ocampo, 2005).

A treatment series of 0 mg/L (control) and 500 mg/L Pb (Pb-contaminated) was prepared on par with the regulatory standards for environmental levels of the heavy metal (USEPA, 1992). Lead stock solution was prepared using analytical grade Pb (NO₃)₂. After the 10-day acclimatization period, the nutrient solution was spiked with 500 mg/L of lead by dissolving 8.789 g of Pb (NO₃)₂ in every 11 litre-capacity culture boxes. Control plants were grown exclusively on nutrient solution.

In each treatment, four hydroponic culture boxes were set up, each containing eight (8) individual plants of *P. pellucida*. The schematic diagram of the hydroponic set up is presented in Figure 1. The experiment was conducted for 28 days and toxicity symptoms of plants were observed throughout the experiment.

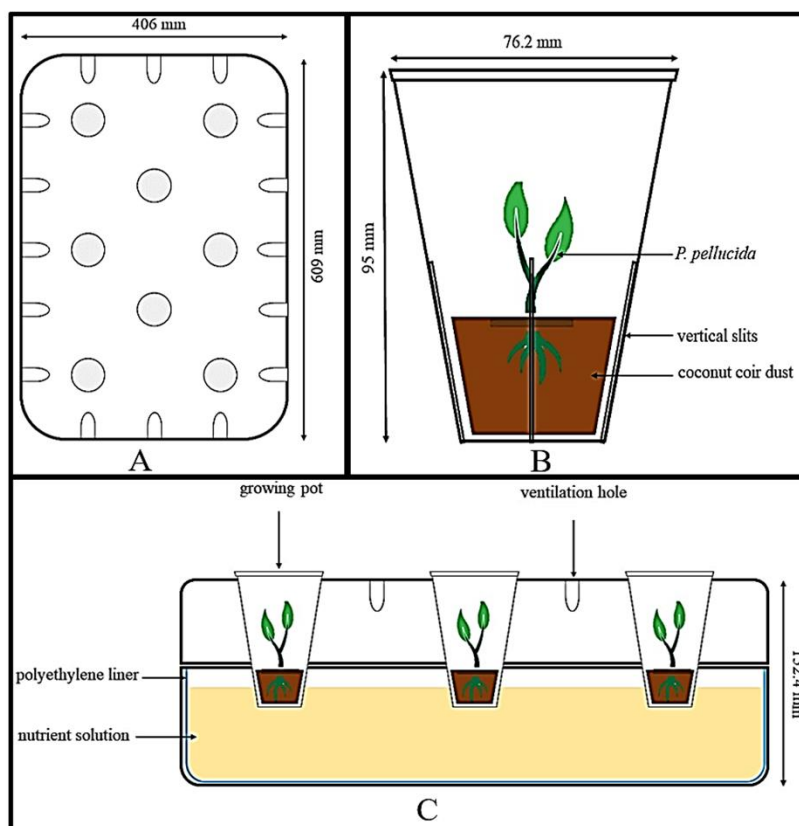


Figure 1. Schematic diagram of SNAP hydroponic system; (A) top view of the hydroponic culture box; (B) growing pots; (C) cross-section view of the hydroponic system

2.3 Monitoring of growth response

Growth response to lead contamination was determined by measuring the observable physical changes in the test plants, such as height, leaf area and number of leaves. Measurement was done periodically before and after Pb contamination. These factors are the indications that the tested plant species had undergone lead bioaccumulation in terms of physical changes. Dry weight of the plants was calculated using the formula:

$$\text{Dry Weight (g)} = \frac{\text{Total dry weight of plants in treatment (g)}}{\text{Total number of plants in treatment}}$$

2.4. Plant harvesting

At the end of the 28-day growth period, the *P. pellucida* plants were gently removed from each growing pot while carefully separating the coconut coir dust from roots. After which, they were rinsed with distilled water to remove adherent debris, taking extra caution to preserve as much root as possible. The roots of the plant were then gently separated from shoots (stems and leaves). Separately, the above ground and below ground parts were cut into smaller pieces and blot-dried. Root and shoot samples were

separately placed in microwavable containers, labelled and subjected to oven-drying at 80°C for 72 h. After which, the dried plant samples were weighed and acid-digested.

2.5 Sample preparation and analysis

The USEPA (2007) Method 7000B as modified by Atayese et al. (2009) was used in the preparation of plant tissues for lead-content analysis. Once the drying process is completed, the tissue was removed from the containers and ground using a mortar and pestle. Approximately, 0.5 g of homogenized powder (shoot or root) was transferred into a 100 mL conical flask and 5 mL of concentrated H₂SO₄ was added, followed by the addition of 25 mL of concentrated HNO₃. Then, the contents of the conical flask were heated on a heating plate at 100°C until a clear solution is obtained. After cooling, distilled water was added to the falcon tube to obtain a final volume of 25 mL. The filtered and rinsed solution was collected in a sterile, 25 mL capacity graduated falcon tube. Finally, the falcon tube was left to settle down for 24 h. Each tube was labelled and prepared for Flame Atomic Absorption Spectroscopy (Flame AAS) analysis.

2.6 Computation of absorptive capacity and tolerance parameters

In response to Pb exposure, the following heavy metal absorptive capacity and tolerance parameters were determined: survival rate (SR), tolerance index (TI), bioconcentration factor (BCF), translocation factor (TF) and lead metal uptake. These were calculated following the equations of Meeinkuirt et al. (2012), Zhivotovsky et al. (2011), Yaowakhan et al. (2005), Tanhan et al. (2007), Niu et al. (2007), and Vamerali et al. (2010):

1) *Survival rate (SR)*: This is percentage of plants still alive after the experimentation period computed as:

$$SR = \frac{\text{Final number of plants}}{\text{Initial number of plants}} \times 100$$

2) *Tolerance index (TI)*: This is the ratio of dry weight in plants grown on contaminated solution and control plants grown on uncontaminated solution, and is expressed as a percentage using the formula:

$$TI (\%) = \frac{\text{Dry weight of plant in Pb treatment (g)}}{\text{Dry weight of plant in control treatment (g)}} \times 100$$

3) *Bioconcentration factor (BCF)*: This was determined by the ratio of lead concentration in plant tissues to the total metal initial concentration expressed in mg/kg. This was obtained using the following equation (Wilson and Pyatt, 2007):

$$BCF = \frac{\text{Pb concentration in whole plant (mg/kg)}}{\text{Initial Pb concentration in solution (mg/L)}}$$

4) *Translocation factor*: This was used to evaluate the efficiency of *P. pellucida* in translocating the accumulated metal from its roots to shoots. The value was obtained by measuring the ratio in concentration in the aerial tissues and that in the roots, respectively, with the heavy metal content expressed as mg/kg. The following formula was used (Padmavathiamma and Li, 2007):

$$TF = \frac{\text{Heavy metal concentration in shoot (mg/kg)}}{\text{Pb concentration in root (mg/kg)}}$$

5) *Pb concentration*: This is the ratio of the product of AAS reading and dilution factor to the weight of sample used for acid digestion. This was calculated using the formula:

$$\text{Pb accumulation} = \frac{\text{AAS Reading } (\mu\text{g/mL}) \times \text{Dilution Factor (mL/g)}}{\text{Weight of sample (g)}}$$

6) *Pb uptake*: It is the ratio of the lead concentration in the tissues of *P. pellucida* and the dry biomass of the plant after experimentation. This is determined by the following formula:

$$\text{Pb uptake } (\mu\text{g/plant}) = \text{Pb accumulation } (\mu\text{g/g}) \times \text{dry weight (g/plant)}$$

2.7 Statistical analysis

Paired Student's t-test was used to evaluate the growth response of the plant on Pb exposure. The dry weight was also compared using the said test. For heavy metal absorptive capacity and tolerance parameters, the values were computed based on given formula.

3. RESULTS AND DISCUSSION

3.1 Growth response of *P. pellucida* on lead (Pb) contamination

The growth response and performance of *P. pellucida* in the presence of Pb can determine its viability as a phytoremediator. The physiological parameters and growth response of *P. pellucida* upon lead-exposure is presented in Figure 2-4.

Throughout the experimental growth period, *P. pellucida* plants grown exclusively on nutrient solution were constantly growing, as noticed in the gradual and continuous increase in plant height, leaf number and leaf area (Figure 2-4). On the other hand, *P. pellucida* plants exposed to 500 mg/L of Pb were growing relatively at the same rate as the unexposed plants during the first two weeks of experimentation; however, manifestation of lead phytotoxicity appeared during the third week, where biomass production was affected as implied in the reduction of plant height, leaf number and leaf area of lead-exposed plants.

Relative growth of uncontaminated and contaminated plants became divergent during the third week of experimentation. Plants grown solely on nutrient solution depicted an upward slope of relative growth, exhibiting constant linear increment in height, and leaf number and area; whereas lead-contaminated plants showed a curb in the figures of plant height, leaf number and leaf area during the third week of exposure (Figure 2-4), mainly due to the slowed

growth and death of some plants. Symptoms of lead phytotoxicity such as drooping, necrosis and leaf bleaching also started to manifest as early as the

second week, while the indications became more apparent during the third and fourth week where lead-exposed plants started to wilt, lose turgidity and die.

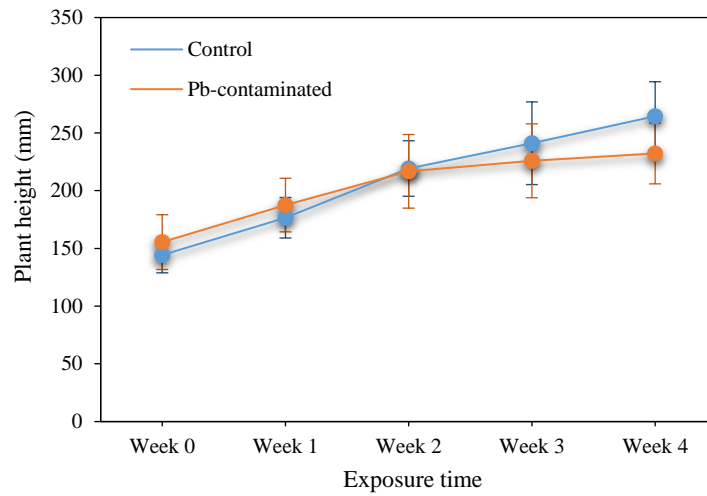


Figure 2. Effect of 500 mg/L Pb on the plant height of *P. pellucida*.

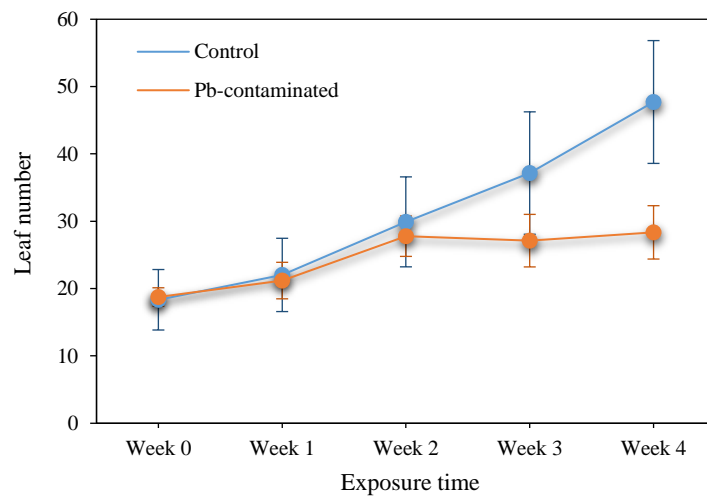


Figure 3. Effect of 500 mg/L Pb on the leaf number of *P. pellucida*.

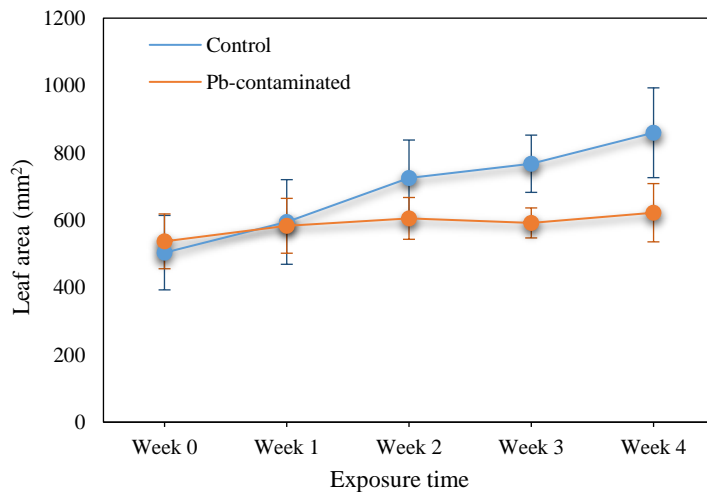


Figure 4. Effect of 500 mg/L Pb on the leaf area of *P. pellucida*.

Throughout the first two weeks of experimentation, the plant height, leaf number and leaf area of the plants were not significantly affected ($p>0.05$) by the presence of 500 mg/L of Pb concentration. This is because of the consistent increment of biomass produced in both treatments during the first two weeks. However, at the conclusion of the experimental period, final mean values for plant height, leaf number and leaf area were determined to be significantly different from each other ($p>0.05$) with respect to the presence or absence of 500 mg/L of Pb.

As plants grow in a contaminated environment, they tend to continue to absorb Pb and sequester the metal within their tissues, causing the toxicity symptoms in the plant to increase. In hydroponics experiment, *P. pellucida* grew well without the presence of Pb concentrations, and little to no morphological symptoms such as chlorosis and necrosis were observed. However, lead-exposed plants had reduced total biomass which is a result of decreased number of leaves, fresh and dry weight, and length of root and shoot. According to [Belonias](#)

(2009), *P. pellucida* can tolerate lead levels of up to 400 ppm, with Pb-treated plants and the control showing comparably uniform vigorous growth during a 3-week experimental period. However, in this study, the 500 mg/L concentration had significant effect on the growth response of the plant. Same results were obtained by some other studies at the calculated lead concentration on different plants; root, shoot and leaf growth, fresh and dry biomass were critically reduced in *Pisum sativum*, *Zea mays*, *Paspalum distichum*, *Cynodon dactylon*, *Lycopersicon esculentum*, *Ipomoea aquatica*, *Phaseolus vulgaris*, and *Lens culinaris* ([Nas and Ali, 2018](#); [Jaja and Odoemena, 2004](#); [Gothberg et al., 2004](#)).

The result of the study shows that manifestation of Pb effect on plant is evident after two to three weeks. Manifestations of toxicity became apparent as the plants were increasingly exposed to the Pb. Visual examination of the plants exposed to Pb also shows signs of toxicity such as necrosis of leaf tip and darkened shoot base, pale-colored leaves, drooped and shrunken shoots and short and dark roots, with heavily shrunken shoot base ([Figure 5](#)).



Figure 5. Lead-phytotoxicity symptoms during the four-week exposure period; (A) second week plants showing necrosis of leaf tip and darkened shoot base; (B) third week plants with pale-colored leaves and drooped and shrunken shoots; (C) final week plants showing short and dark roots, with heavily shrunken shoots base (top) and deceased plant (bottom).

These results and observations corroborate with the findings of by [Sharma and Dubey \(2005\)](#) and [Nas and Ali \(2018\)](#). According to them, the visual non-specific symptoms of Pb toxicity are rapid inhibition of root growth, stunted growth of the plant and chlorosis. This claim is also supported. They stated that Pb toxicity is manifested outwardly in the plant such as stunted growth, chlorosis and blackening of the root system. In addition, Pb inhibits photosynthesis, upsets mineral nutrition and balance, changes hormonal status and affects membrane structure and permeability. These disorders upset normal physiological activities of the plants ([Nas and Ali, 2018](#)).

It can also be noted in the result that symptoms of Pb toxicity were manifested by the plants in the later part of the experimental period. This may mean that the amount of Pb absorbed in the earlier part of the experiment is not yet considerable. According to [Putra et al. \(2016\)](#), the amount of Pb accumulation must be

in considerable amount to inhibit plant metabolism before showing a visible phytotoxic and oxidative damage effect.

3.2 Lead tolerance of *P. pellucida*

Tolerance is an organism’s ability to cope with heavy metals that are excessively accumulated within its body. The effect of lead on biomass production and the parameters for lead tolerance are presented in [Table 1](#).

Results showed that plants exposed to Pb have a lower biomass compared to those plants that were not contaminated by Pb. The DW of *P. pellucida* was significantly affected ($p>0.05$) by 500 mg/L of lead. The low biomass may be attributed to the relatively lower plant height, number of leaves and leaf area. In addition, the dry weight reduction relates to high Pb concentration, since plants may have to use energy to cope with the high Pb concentration in their tissues ([Karimi et al., 2012](#)).

Table 1. Lead tolerance of *P. pellucida* after 28 days of exposure.

Treatments	Dry weight (g)			Lead tolerance parameters	
	Roots	Shoots	Total	Survival rate (%)	Tolerance index (%)
Control (0 mg/L)	0.43±0.20 ^a	2.65±0.95 ^a	3.08±1.08 ^a	93.70	-
Pb-contaminated (500 mg/L)	0.21±0.10 ^b	1.15±0.37 ^b	1.35±0.46 ^b	71.80	43.40

Note: Each value is mean of four replications ± standard deviation. Mean of each column indexed with different small letters denote a significant difference of relative leaf number between absence and presence of Pb concentration (500 mg/L) as determined by paired t-test at $p\leq0.05$.

Higher survival rate was also observed in the control group with 93.70%, while only 71.80% survival rate was observed in Pb contaminated plants. Result also shows that plants exposed to 500 mg/L Pb had a tolerance index (TI) of 43.40% which is relatively low. [Herlina et al. \(2020\)](#) suggested that plants with TI values greater than 100% reflect a net increase in biomass and tolerance-acquisition of the plant, whereas, TI values lower than 100% indicate a net decrease in biomass and a stressed plant condition. However, it was suggested by [Zhivotovsky et al. \(2011\)](#) and [Wang et al. \(2014\)](#) that a 60% TI criterion value indicates ability of plants to tolerate heavy metals. The recorded TI value for *P. pellucida* (43.40%) was far below 100%, indicating that the plants have become stressed throughout the experiment as evident in the retardation of growth of the plants.

Different plant species develop different mechanisms to tolerate excess levels of metals ([Aini Syuhaida et al., 2014](#)). The earliest mechanism is a

synthesis of polysaccharide such as callose (β -1, 3 glucan) deposited on the outside of the cell membrane, thereby reducing the diffusion of heavy metal ions into the plant cell. In *in situ* applications and in soil experiments, plant roots secrete exudates into the soil matrix to chelate metals and to prevent their uptake inside the cells ([Furini, 2012](#); [Małachowska-Jutz and Gnida, 2015](#)). However, in a hydroponics experiment, this mechanism is hardly employed due to the roots being suspended in a liquid environment, thus preventing the roots from releasing the exudates and thereby reducing the resistance from lead uptake.

3.3 Lead accumulation and lead absorptive capacity of *P. pellucida*

[Table 2](#) presents the accumulation and absorptive capacity of *P. pellucida* after 28 days of exposure to 500 mg/L to Pb. This lead absorptive capacity was measured in terms of Pb uptake ($\mu\text{g/plant}$), bio-accumulation factor (BCF) and translocation factor (TF).

Table 2. Lead absorptive capacity of *P. pellucida* after 28 days of exposure.

	Pb-accumulation ($\mu\text{g/g}$)		Lead absorptive capacity parameters		
	Roots	Shoots	Lead uptake ($\mu\text{g/plant}$)	BCF	TF
Pb-contaminated (500 mg/L)	158.60	43.20	272.43	0.40	0.27

Results showed that there is an accumulation of Pb in the tissues of *P. pellucida* plants. The amount of Pb accumulated in the roots (158.6 $\mu\text{g/g}$) is greater than the amount accumulated in the shoots (43.2 $\mu\text{g/g}$). This result implies that the roots system of the *P. pellucida* has the ability to absorb Pb; however, translocation into the shoot system might have been restricted. According to Mleczek et al. (2019), mechanisms of metal uptake and accumulation in plants have demonstrated that plants have the ability to translocate selected elements in its tissues, with the roots being the most capable organ in taking up significant quantities of Pb whilst simultaneously restricting translocation to hypogean parts.

The Pb concentrations (158.6 $\mu\text{g/kg}$ in shoots, and 43.2 $\mu\text{g/kg}$ in roots) from this study were lower than Pb concentrations reported in shrubs; for example, *Chromolaena odorata* (L.) with Pb in shoots 1,721 mg/kg, and in roots 51,493 mg/kg (Niu et al., 2007). The results follow a similar trend as some other studies. The other common phenomenon is Pb accumulation in roots more than that in shoots and several previous studies, including this study, show the same pattern. Zhivotovsky et al. (2011) found that at the highest Pb concentration of 241 μM , *Salix lucida*, *Salix nigra*, and *Salix serissima* had higher Pb concentration in roots than in aerial tissue, such as wood, in shoot and in leaves. Liu et al. (2015) found that *Phyllostachys pubescens* grown in nutrient solution supplemented with 200 μM Pb contained higher Pb in the root (1,221 mg/kg) as compared to that in the stem (351 mg/kg) and in leaf (165 mg/kg).

The Pb uptake of *P. pellucida* plants was calculated to be 272.43 $\mu\text{g/plant}$. Meanwhile, BCF and TF values were recorded at 0.40 and 0.27, respectively. Ramana et al. (2021) stated that (BCF) and Translocation Factor (TF) are the defining parameter in phytoremediation by providing insight on metal uptake, mobilization and storage. Since, BCF and TF values are used to evaluate a plant's ability to accumulate and translocate heavy metals, and identify the suitability of plants for phytoextraction and phytostabilization (Niu et al., 2007; Wang et al., 2014), values >1 indicate that the plant has the potential for phytoextraction (Ali et al., 2013). With

BCF criterion, *P. pellucida* shows relatively low potential for bioaccumulation.

According to Napoli et al. (2020), a high value of TF ($\text{TF}>1$) signifies promising ability of a plant to translocate heavy metals from roots to aerial tissues. On the other hand, a low value ($\text{TF}<1$) indicates a limited capacity of a plant to translocate the metal to aerial tissues. In this study, *P. pellucida* recorded TF value <1 . This is indicative of *P. pellucida*'s low capacity to uptake high quantity of Pb, potentially classifying the plant as an excluder of Pb.

The uptake and translocation of a pollutant in plants depends on many factors: (1) the pollutant's concentration in the solution, (2) its efficiency to enter the root system, and (3) the rate of transpiration in the plants (Glime, 2017). Pepper elder plants are very reliant to the turgor pressure within their systems, and any disruption in this system might compromise the integrity of their structures and the plant in general.

In this study, *P. pellucida* was determined to have the capacity to accumulate and uptake lead in its tissues. On the other hand, the results showed values of phytoremediation parameters (SR, TI, BCF, TF) that are below the criterion for each respective parameter. This implies that, the plants were affected by the spiking of 500 mg/L of Pb. Despite this, the plants showed the capacity to uptake lead and still survive, which is promising considering that the concentration of lead used to spike the nutrient solution was relatively high. Nevertheless, it must still be taken into account that the experiment was conducted *ex situ* in a hydroponic setting with a single treatment. The present conditions might have affected the capacity of *P. pellucida* to survive, uptake and accumulate lead in its tissues, and different results may be obtained in a pot experiment.

4. CONCLUSION

Manifestations of toxicity became apparent as the plants were exposed longer to Pb. Prolonged exposure to Pb induced phytotoxicity symptoms and reduced biomass production, affecting plant height, leaf number and leaf area as implied in the curb of the respective growth parameters during the third week of exposure, which consequently caused retardation of

growth. Lead-adsorptive capacity parameters imply that the plant may be classified as a heavy metal excluder. Despite the manifestations of phytotoxicity, *P. pellucida* absorbed considerable amounts of lead within its tissues, especially its roots. This indicates that the plant may be further exploited for their capacity to absorb heavy metals. Only a limited number of studies and reports on bioaccumulation, phytoremediation potential and heavy metal uptake capacity of *P. pellucida* are available. Hence, this study may establish a framework for future studies to improve efficiency and ability of the plant in heavy metal accumulation.

ACKNOWLEDGEMENTS

The author would like to give special thanks to the faculty of the Department of Biological Sciences of Isabela State University for their assistance in carrying out this study.

REFERENCES

- Aini Syuhaida AW, Norkhadajah SIS, Praveena SM, Suriyani A. The comparison of phytoremediation abilities of water mimosa and water hyacinth. *ARPN Journal of Science and Technology* 2014;4:722-31.
- Ali H, Naseer M, Sajad MA. Phytoremediation of heavy metals by *Trifolium alexandrinum*. *International Journal of Environmental Science* 2013;2:1459-69.
- Anoliefo G, Ikhajiagbe B, Okonofua B, Diafe F. Eco-taxonomic distribution of plant species around motor mechanic workshops in Asaba and Benin City, Nigeria: Identification of oil tolerant plant species. *African Journal Of Biotechnology* 2006;5(19):1757-62.
- Arquion RD, Galanida CC, Villamor B, Aguilar HT. Ethnobotanical study of indigenous plants used by local people of Agusan del Sur, Philippines. *Asian Pacific Higher Education Journal* 2015;2(2):1-11.
- Atayese MO, Eigbadon AI, Oluwa KA, Adesodun JK. Heavy metal contamination of amaranthus grown along major highways in Lagos, Nigeria. *African Crop Science Journal* 2009;6:135-225.
- Belonias BS. Bioaccumulation of lead in the medicinal plant *Peperomia pellucida* (L.) Kunth. *Philippine Journal of Crop Science* 2009;34(1):115.
- Calawagan KM, Japitana JJ, Lapada JA, Alviator HB. Phytoremediation potentials of carabao grass (*Paspalum conjugatum*), talahib (*Saccharum spontaneum*), and ulasimang bato (*Peperomia pellucida*) in removing copper (Cu), lead (Pb), and manganese (Mn) in soils. *Proceedings of the PSSN 13th National Scientific Meeting; 2013 May 21-25; Cebu Business Hotel, Cebu City: Philippines; 2013.*
- De Guzman CC. Hydroponic culture of pansit-pansitan (*Peperomia pellucida*). *Proceedings of the 1998 Regional Research and Development Symposia, Philippine Council for Agriculture, Forestry and Natural Resources Research and Development; University of the Philippines Los Baños, Los Baños, Laguna: Philippines; 1999. p. 120.*
- Furini A. *Plants and Heavy Metals*. Dordrecht, Netherlands: Springer; 2012.
- Glime JM. Water relations: Conducting structures. In: Glime JM, editor. *Bryophyte Ecology (Volume 1)*. USA: Michigan Technological University and the International Association of Bryologists; 2017. p. 1-26.
- Gothberg A, Greger M, Holm K, Bengtsson BE. Influence of nutrient levels on uptake and effects of mercury, cadmium, and lead in water spinach. *Journal of Environmental Quality* 2004;33(4):1247-55.
- Herlina L, Widianarko B, Sunoko HR. Phytoremediation potential of *Cordyline fruticosa* for lead contaminated soil. *Jurnal Pendidikan IPA Indonesia* 2020;9(1):42-9.
- Jaja ET, Odoemena CSI. Effect of Pb, Cu, and Fe compounds on the germination and early seedling growth of tomato varieties. *Journal of Applied Sciences and Environmental Management* 2004;8(2):51-3.
- Karimi R, Fitzgerald TP, Fisher NS. A quantitative synthesis of mercury in commercial seafood and implications for exposure in the United States. *Environmental Health Perspective* 2012;120:1512-9.
- Kirk JL, Klirnomos JN, Lee H, Trevors JT. Phytotoxicity assay to assess plant species for phytoremediation of petroleum-contaminated soil. *Bioremediation Journal* 2002;6:57-63.
- Lado LR, Hengl T, Reuter HI. Heavy metals in European soils: A geostatistical analysis of the FOREGS Geochemical database. *Geoderma* 2008;148:189-99.
- Liu S, Xia X, Shen M, Liu R. Polycyclic aromatic hydrocarbons in urban soils of different land uses in Beijing, China: Distribution, sources and their correlation with the city's urbanization history. *Journal of Hazardous Materials* 2010;177:1085-92.
- Liu D, Li S, Islam E, Chen JR, Wu JS, Ye ZQ, et al. Lead accumulation and tolerance of Moso bamboo (*Phyllostachys pubescens*) seedlings: Applications of phytoremediation. *Journal of Zhejiang University Science B* 2015;16(2):123-30.
- Małachowska-Jutysz A, Gnida A. Mechanisms of stress avoidance and tolerance by plants used in phytoremediation of heavy metals. *Archives of Environmental Protection* 2015;41(4):96-103.
- Mandkini LL, Bandara NG, Gunawardana D. A Study on the phytoremediation potential of *Azolla pinnata* under laboratory conditions. *Journal of Tropical Forestry and Environment* 2016;6(1):36-49.
- McIntyre T. Phytoremediation of heavy metals from soils. *Advances in Biochemical Engineering/Biotechnology* 2003;78:97-123.
- Meeinkuirt W, Pokethitiyook P, Kruatrachue M, Tanhan P, Chaiyarat R. Phytostabilization of a Pb-contaminated mine tailing by various tree species in pot and field trial experiments. *International Journal of Phytoremediation* 2012;14:925-38.
- Mirsal IA. *Soil Pollution, Origin, Monitoring and Remediation*. Berlin, Heidelberg, Germany: Springer; 2004.
- Mleczek M, Rutkowski P, Kaniuczak J, Szostek M, Budka A, Magdziak Z, et al. The significance of selected tree species age in their efficiency in elements phytoextraction from wastes mixture. *International Journal of Environmental Science and Technology* 2019;16:3579-94.
- Mojiri A. The potential of corn (*Zea mays*) for phytoremediation of soil contaminated with cadmium and lead. *Journal of Biological and Environmental Science* 2011;5(13):17-22.

- Mosango DM. *Peperomia pellucida* (L.) Kunth. In: Schmelzer GH, Gurib-Fakim A, editors. *Prota 11(1): Medicinal Plants/Plantes médicinales 1*. Wageningen, Netherlands: PROTA; 2008.
- Napoli M, Cecchi S, Grassi C, Baldi A, Zanchi CA, Orlandini S. Phytoextraction of copper from a contaminated soil using arable and vegetable crops. *Chemosphere* 2020;219:122-9.
- Nas FS, Ali M. The effect of lead on plants in terms of growing and biochemical parameters: A review. *MOJ Ecology and Environmental Sciences* 2018;3(4):265-8.
- Niu ZX, Sun LN, Sun TH, Li YS, Hong W. Evaluation of phytoextracting cadmium and lead by sunflower, ricinus, alfalfa, and mustard in hydroponic culture. *Journal of Environmental Science* 2007;19:961-7.
- Ona LF, Alberto AP, Prudente JA, Sigua GC. Levels of lead in urban soils from selected cities in the rice-based region of the Philippines. *Environmental Science and Pollution Research* 2006;13(3):177-83.
- Padmavathiamma PK, Li LY. Phytoremediation technology: Hyperaccumulation metals in plants. *Water, Air and Soil Pollution* 2007;184:105-26.
- Putra RS, Novarita D, Cahyana F. Remediation of lead (Pb) and copper (Cu) using water hyacinth (*Eichornia crassipes* (Mart.) Solms) with electro-assisted phytoremediation (EAPR). *AIP Conference Proceedings* 2016;1744:020052.
- Raghavendra HL, Kekuda TRP. Ethnobotanical uses, phytochemistry and pharmacological activities of *Peperomia pellucida* (L.) Kunth (Piperaceae): A review. *International Journal of Pharmacy and Pharmaceutical Sciences* 2018; 10(2):1-8.
- Ramana S, Tripathi AK, Kumar A, Dey P, Saha JK, Patra AK. Phytoremediation of soils contaminated with cadmium by *Agave americana*. *Journal of Natural Fibers* 2021;In press:1-9.
- Salt DE, Smith RD, Raskin I. Phytoremediation. *Annual Review of Plant Physiology and Plant Molecular Biology* 1998;49:643-68.
- Santos PJA, Ocampo ETM. SNAP hydroponics: Development and potential for urban vegetable production. *Philippine Journal of Crop Science* 2005;30(2):3-11.
- Sharma P, Dubey RS. Lead toxicity in plants. *Brazilian Journal of Plant Physiology* 2005;17:1-19.
- Solidum JN, Dahilig VRA, Omran A. Lead levels of water sources in Manila, Philippines. *Annals of Faculty Engineering Hunedoara - International Journal of Engineering* 2010;8:111-8.
- Tablang JO, Campos RC, Jacob JS. Phytochemical screening and antibacterial properties of silverbush (*Peperomia pellucida*) against selected cultured bacteria. *Global Journal of Medicinal Plant Research* 2020;8(1):1-6.
- Tanhan P, Kruatrachue M, Pokethitiyook P, Chaiyarat R. Uptake and accumulation of cadmium, lead and zinc by Siam weed (*Chromolaena odorata* (L.) King and Robinson). *Chemosphere* 2007;68:323-9.
- Thayaparan M, Iqbal SS, Chathuranga PK, Iqbal MC. Rhizofiltration of Pb by *Azolla pinnata*. *International Journal of Environmental Sciences* 2013;3(6):1811-21.
- Tolentino RD, Tomas VCB, Travezonda JC, Magnaye BP. Herbal medicine utilization among Batangueños. *Asian Pacific Journal of Education, Arts and Sciences* 2019;6(1):9-22.
- United States of America Environmental Protection Agency (USEPA). *Selection of Control Technologies for Remediation of Lead Battery Recycling Sites: EPA/540/S-92/011*. Washington, DC: Office of Emergency and Remedial Response; 1992.
- United States of America Environmental Protection Agency (USEPA). *Method 7000B Flame Atomic Absorption Spectrophotometry*, United States of America Environmental Protection Agency. Washington, DC: Office of Emergency and Remedial Response; 2007.
- Vamerali T, Bandiera M, Mosca G. Field crops for phytoremediation of metal-contaminated land: A review. *Environmental Chemistry Letters* 2010;8:1-17.
- Wang Y, Yang X, Zhang X, Dong L, Zhang J, Wei Y, et al. Improved plant growth and Zn accumulation in grains of rice (*Oryza sativa* L.) by inoculation of endophytic microbes isolated from a Zn Hyperaccumulator, *Sedum alfredii* H. *Journal of Agricultural Food Chemistry* 2014;62:1783-91.
- Wilson B, Pyatt FN. Heavy metal bioaccumulation by the important food plant, *Olea europaea* L., in an ancient metalliferous polluted area of Cyprus. *Bulletin of Environmental Contamination and Toxicology* 2007;78:390-4.
- Yaowakhan P, Kruatrachue M, Pokethitiyook P, Soonthornsarathool V. Removal of lead using some aquatic macrophytes. *Bulletin of Environmental Contamination and Toxicology* 2005;75:723-30.
- Zhivotovsky O, Kuzovkina Y, Schulthess C, Morris CT, Pettinelli D. Lead uptake and translocation by willows in pot and field experiments. *International Journal of Phytoremediation* 2011; 13:731-49.

Effects of Campaign-Based Soil and Water Conservation Practice on Soil Properties: The Case of Workkamba Watershed, Debarik District, North Ethiopia

Muluneh Bogale^{1*}, Getnet Wondie¹, and Abdrahman Shafi²

¹Department of Natural Resource Management, Debarik University, College of Agriculture and Environmental Science (DKU CAES), P.O Box 90, Debarik, Ethiopia

²Department of Natural Resource Management, Wolkite University, College of Agriculture and Natural Resource Management, P.O Box 70, Wolkite, Ethiopia

ARTICLE INFO

Received: 6 Dec 2020
Received in revised: 5 Apr 2021
Accepted: 21 Apr 2021
Published online: 27 May 2021
DOI: 10.32526/enrj/19/2020256

Keywords:

Campaign soil and water conservation work/ Workkamba watershed/ Land degradation/ Soil erosion/ Soil and water conservation

* Corresponding author:

E-mail:
mulunehbogale241@gmail.com

ABSTRACT

Land degradation is a serious environmental problem in Ethiopia. To address the problem, soil and water conservation practices were implemented through campaign. This study was conducted at Workkamba watershed Debarik district, North Ethiopia to assess the effect of campaign soil and water conservation (SWC) practice on selected soil properties. Composite soil samples from 1.5 meters above the soil bunds, at the center and 1.5 meters below the soil bunds between the two consecutive structures were collected. The soil samples were analyzed following standard laboratory procedures. Results showed bulk density (BD), electrical conductivity (EC), calcium (Ca²⁺), and sodium (Na⁺) were not significantly affected by slope gradient and terrace position and their interaction. But pH was significantly influenced by the interaction effect. Cation exchange capacity (CEC), exchangeable potassium (K⁺), and clay content were significantly changed with both slope gradient and terrace position. Whereas, total nitrogen (TN), available phosphorus (Av-P), and magnesium (Mg²⁺), and soil organic carbon (SOC) were significantly affected with terrace position and slope gradient, respectively. Because of the conservation barrier, most soil properties were better at the bottom terrace position and gentle slope gradient.

1. INTRODUCTION

Land degradation is a loss of natural capital, the value to society of land, water, plant and animal resources and the direct detriment to primary production in the agricultural system and related industries (Hurni et al., 2010; Tesfa and Mekuriaw, 2014). Farming populations have experienced decline in real income due to demographic, economic, social and environmental changes (Esser et al., 2002). Land degradation has also become apparent in many different angles: vegetation becomes increasingly scarce; footpaths grow into gullies and soils become thin and stony. All of these manifestations have negative impacts on the environment (Berry, 2003; Temesgen et al., 2014).

Soil erosion is one of the main causes of land degradation and environmental change that affect the

physical and chemical properties of the soil and its productive potential (Esser et al., 2002). It is the primary and the most generalized problem in nearly all tropical mountain regions including Ethiopia (Nyssen et al., 2009; Demelash and Stahr, 2010). About 350 million (M) hectares or 20 to 25 percent of the total land area of sub-Saharan Africa is estimated to be severely damaged with about 100 million (M) hectares damaged from agricultural use (Zingore et al., 2015). In Ethiopia, loss of arable land is most common everywhere; the top-soil and even part of the sub-soil in some areas has been removed (Esser et al., 2002). In locations with the most intense population density, the area of greatest livestock density and the area of greatest land degradation, recorded measurements of soil loss range from 3.4 to 84.5 tons/ha/year with a mean of 32.0 tons/ha/year (Berry, 2003). Similarly,

Citation: Bogale M, Wondie G, Shafi A. Effects of campaign-based soil and water conservation practice on soil properties: The case of Workkamba Watershed, Debarik District, North Ethiopia. Environ. Nat. Resour. J. 2021;19(4):292-301. (<https://doi.org/10.32526/enrj/19/2020256>)

Dagneu et al. (2015) reported that soil erosion affects half of the agricultural land and results in an annual soil loss rate of 1.5 to 2 billion tons. (Amdemariam et al., 2011; Mekonnen and Michael, 2014) also explained that the extent and scale of the problem has dramatically increased. The issue is also critical in the highlands (greater than 1,500 m.a.s.l.) (Gebremedhin and Swinton, 2003; Demelash and Stahr, 2010).

However, considerable efforts have been made by the government of Ethiopia in collaboration with donor organizations since the 1980s. Rehabilitation of degraded environment, minimizing and stopping further degradation and enhancing soil fertility works were done to arrest the problem (Bewket, 2007; Nyssen et al., 2009; Amdihun et al., 2014; Temesgen et al., 2014; Dagneu et al., 2015). Additionally, afforestation and conservation practices; which include physical soil and water conservation structures like stone bund, hill-side terraces, soil bund, fanya juu, and other biological measures have been introduced at massive scale (Amsalu and Graaff, 2007). Despite these efforts, sustainable utilizations were not expected and the success has been uncertain and limited in addressing the problem (Bishaw, 2001; Amsalu and Graaff, 2007; Amdihun et al., 2014; Dagneu et al., 2015), because the emphasis has been on more of construction of mechanical soil and water conservation (SWC) structures and the conservation activities were applied through blanket recommendation, fundamental truth, and top-down approach (Bewket, 2001; Bewket and Sterk, 2002; Bewket, 2007; Mushir and Kedru, 2012; Amare et al., 2014). Blanket approach to conservation intervention could make the measures inconvenient to local conditions and eventually less accepted by technology users (Amsalu and Graaff, 2007). The practice also largely remained delivery oriented in which the farmers were forced to implement conservation measures designed for them by technical experts (Bewket, 2007). Similarly, it is highly claimed that the local farmers were eventually highly ignorant of land management and were not welcomed to judge on the introduced conservation options (Esser et al., 2002; Bewket 2007; Amdihun et al., 2014).

As shown by experiences of the previous works, these blanket and top-down conservation interventions cannot be expected to be effective (Bewket, 2007). In recognition of the truth on the ground, some efforts towards participatory and community-based

watershed management approaches (public campaign) have been made since 2012 (Haregeweyn et al., 2012; Dagneu et al., 2015). Increasing agricultural productivity with double digit trough maintaining the environment and improving natural resource conservation efforts was the main objective of the program (MoFED, 2010). Following the launch of the program the regional bureaus of agriculture, district agricultural offices, including Debark District and other local administrative bodies, mobilized the farmers to help with the construction of soil and water conservation (SWC) measures. Farmers massively and voluntarily implemented soil and water conservation measures on the farm lands at different watershed within an average of 40 to 50 working days (MoFED, 2013). Within a year, greater than 3,000 community watersheds were treated with mechanical and biological conservation techniques. Except food insecure areas, over 15 million peoples participated without any incentives and over 40,000 hectares of land were covered by different soil and water conservation (SWC) measures (Dagneu et al., 2015). However, beyond presenting a monitoring and evaluation report in terms of area coverage, no more meaningful study was conducted on the effect on selected soil properties. Since the practice is campaign-based, evaluating its effect on selected soil physical and chemical properties would be vital for enhancing and improving the conservation effort. Therefore, the objective of this study is intended to evaluate the effects of soil and water conservation (SWC) practice implemented through mass community mobilization on selected soil physico-chemical properties.

2. METHODOLOGY

2.1 Study area description

The study was carried out in Workamba watershed at Debark District North Gondar zone, Amhara national regional state Ethiopia. The study area is located at about 830 km North of Addis Ababa which is the capital city of Ethiopia (Figure 1). The district is geographically situated at 2,712 m to 3,122 m above sea level (m.a.s.l.) and located between latitude of 13°03' to 13.133°N and longitude of 37°54' to 37.900°E. The mean annual maximum and minimum temperatures are 20.7°C and 6.2°C, respectively and the mean annual rainfall varies between 900 and 1,400 mm.

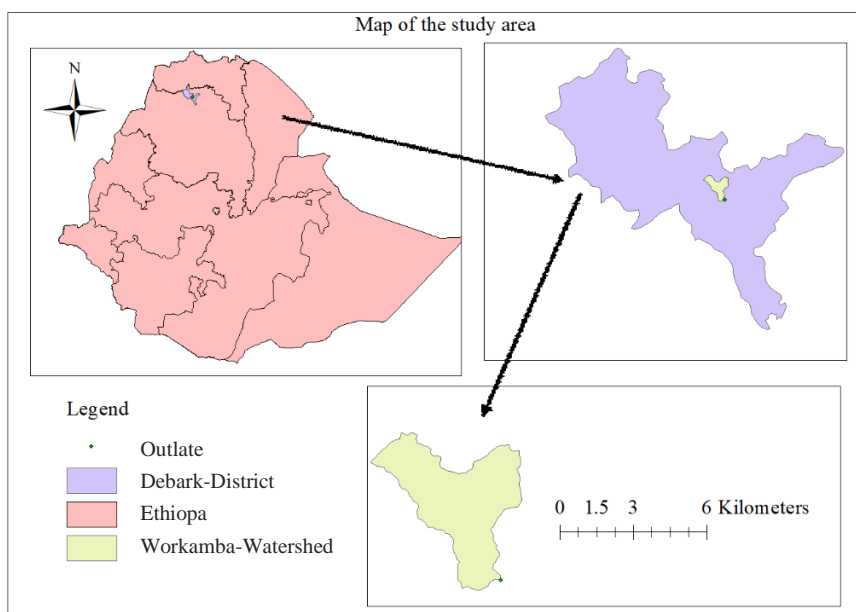


Figure 1. Study area map

The area is mostly mountainous and degraded. Most commonly shallow soil is predominant. The major soils types of the area are Andosols, Cambisols, Vertisols, Luvisols and Lithosols (FAO, 1986; Hurni, 1988). The natural vegetation is almost removed, but in some areas and around the Orthodox Church *Juniperus procera* is sparsely populated. Proportionally, the vegetation coverage of the area dominated by manmade plantation with eucalyptus.

The total human population of the district was estimated to be about 159,193, out of which 80,274 are male and 78,919 are female (CSA, 2007). The major farming systems of the people are subsistence farming practicing mixed crop and livestock agriculture. Among the annual crops, barley (*Hordeum vulgare*), wheat (*Triticum* spp.), fava bean (*Vicia faba*), pea (*Pisum sativum*) and flax (*Linum usitatissimum*) are the most common in the area (Tefera et al., 2014).

2.2 Methods of data collection

Before sampling, a visual field survey of the study area was made to identify appropriate sampling site. Based on the slope gradient, the study watershed was divided in to three slope classes (steep, moderate, and gentle). Composite soil samples were collected from crop lands found in each slope gradient (steep, moderate, and gentle) treated with campaign soil and water conservation practices at nine separate fields up to 20 cm depth using auger. Soil samples from the bottom spot (1.5 meter from the lower soil bunds or above the bunds), center spot (midpoints between the

two successive bunds), and upper spot (1.5 meter from the upper soil bunds or below the soil bunds) between the two consecutive soil and water conservation (SWC) structures were collected following Vancampenhout et al. (2006). A total of 27 composite soil samples 3 (slope class: gentle, moderate and steep) *3(terrace position: bottom spot, center spot or midpoint and upper spot) *3(replications) were collected for laboratory analysis. Additionally, undisturbed soils were collected using core sampler for soil bulk density determination.

2.2.1 Soil laboratory analysis

Soil physical and chemical properties analysis were conducted in the soil laboratory at the Srinka Regional Agricultural Research Institute (SRARI). Soil samples were air-dried, ground and passed through 2 mm sieve for analysis. The particle size distributions (texture) were determined using standard hydrometer methods. The soil bulk density also estimated by using a core sample method, after the soil dried in an oven at 105°C for 24 h.

The pH (pH-H₂O) of the suspension was read using a pH meter. The Total nitrogen (TN) was determined by macro-Kjeldahl digestion-distillation and titration procedures, available phosphorus (Av-P) by using Bray-II extraction method, and exchangeable bases (Ca²⁺, Mg²⁺, K⁺, and Na⁺) determined by ammonium acetate (NH₄OAc) at pH 7.0. Exchangeable Ca²⁺ and Mg²⁺ in the extracts were analyzed using atomic absorption spectrophotometer,

while Na^+ and K^+ were analyzed by flame photometer. The cation exchange capacity (CEC) was determined by extraction with ammonium acetate. Electrical conductivity (EC) was determined by EC-meter. Additionally, the soil organic carbon (SOC) was determined by the Walkley-Black oxidation wet digestion and titration method.

2.3 Methods of statistical analysis

The data were subjected to analysis using statistical package for social science (SPSS v.22) software. In order to evaluate the effect of campaign-based soil and water conservation (SWC) practices on selected soil properties, soil physical and chemical properties were subjected to two-way factorial analysis of variance (ANOVA) through the general linear model (GLM). Slope categories and terrace position/sampling spot considered as factor variables and the selected soil properties were dependent variables. Additionally, mean values were compared using Tukey's Honest Significant Difference test (Tukey-Kramer test) at ($p < 0.05$).

3. RESULTS AND DISCUSSION

3.1 Effects of soil and water conservation (SWC) practice on properties of soil

3.1.1 Soil texture

Based on the two-way factorial ANOVA test result (Table 1), the particle size distribution of the soil was not significantly ($p > 0.05$) influenced by the interaction effect of slope gradient by terrace position. However, it was significantly ($p < 0.05$) affected by the slope gradient and terrace position.

The highest percentages of clay (49.770% and 53.611%) (Significance $p < 0.05$) were observed in samples when the slope and terrace position were gentle and at bottom spot, respectively (Table 2). While, the slope and terrace position were steep and upper position, greater (32.278% and 34.639%) percentage of sand content were recorded respectively. The clay content showed an increasing trend as slope gradient decrease while sand content showed a decreasing trend (Aytenew, 2015). Similarly, Guadie et al. (2020) the overall mean of sand fraction was found to be higher in the upper slope and low in the lower slope positions.

Table 1. Interaction effect of slope gradient by terrace position on some physical properties of soil

Sources of variation	SS	Df	MS	F-value
Clay (%)				
Slope	439.014	2	219.507	4.761*
Terrace position	1444.264	2	722.132	15.662*
Slope*Terrace position	303.306	4	75.826	1.645 ^{Ns}
Silt (%)				
Slope	304.222	2	152.111	4.047*
Terrace position	550.125	2	275.062	7.317*
Slope*Terrace position	129.069	4	32.267	0.858 ^{Ns}
Sand (%)				
Slope	204.292	2	102.146	4.751*
Terrace position	527.764	2	263.882	12.274*
Slope*Terrace position	129.736	4	32.434	1.509 ^{Ns}
Bulk density (g/cm^3)				
Slope	0.083	2	0.041	0.522 ^{Ns}
Terrace position	0.258	2	0.129	1.624 ^{Ns}
Slope*Terrace position	0.087	4	0.022	0.273 ^{Ns}

^{Ns}=not-significant at $p > 0.05$; (*)=Significant at $p < 0.05$; Slope*Terrace=interaction effect

3.1.2 Soil bulk density (BD)

As shown in (Table 1), soil bulk density analysis was not significantly ($p > 0.05$) varied with either the change in slope gradient and terrace position or their interaction effect. Dagnachew et al. (2020) also determined that bulk density of the soil did not

show any significant variations with slope gradient and positions within the terraces as well as their interaction effects. Nevertheless, the significant different results of this study revealed that higher bulk density ($1.663 \text{ g}/\text{cm}^3$ and $1.729 \text{ g}/\text{cm}^3$) values were

observed in the steep slope gradient and upper terrace position, respectively (Table 2).

The lower bulk density (1.539 g/cm^3) from gentle slope gradient and (1.491 g/cm^3) bottom spot position is due to the presence of organic materials transported from the steeper slope. As the land slope gradient decreases, the runoff speed also decreases,

causing sediments and organic matter to settle. At the position of lower slope gradient, the presence of significantly greater organic matter evidently reduced the bulk density of the soil (Demelash and Stahr, 2010). Hailu et al. (2012) also reported that soil bulk density has a direct relationship with slope gradient.

Table 2. Some physical properties of soil in relation to slope gradient and terrace position

Soil properties	Slope gradient				Terraced position/sampling spot			
	Steep	Moderate	Gentle	F-value	Upper	Center	Bottom	F-value
Clay (%)	40.972 ^a	41.500 ^a	49.770 ^b	4.760*	35.833 ^a	42.806 ^a	53.611 ^b	15.662*
Silt (%)	26.750 ^a	31.972 ^{ab}	23.861 ^b	4.048*	29.528 ^a	31.778 ^a	21.278 ^b	7.317*
Sand (%)	32.278 ^a	26.528 ^b	26.361 ^b	4.751*	34.639 ^a	25.417 ^b	25.111 ^b	12.274*
Bulk density (g/cm^3)	1.663 ^a	1.649 ^a	1.539 ^a	0.522 ^{Ns}	1.729 ^a	1.631 ^a	1.491 ^a	1.624 ^{Ns}

Ns=not-significant at $p>0.05$; (*)=Significant at $p<0.05$; Rows having the same letters are not statistically significant at 0.05 significance level (Tukey-Kramer)

3.1.3 Soil reaction (pH)

Soil reaction was significantly ($p<0.05$) affected with slope gradient, terrace position and their interaction effect (Table 3). The result of this study is in-contrast with other findings. Vancampenhout et al. (2006) stated that pH values did not vary with respect to terrace position. Amare et al. (2014) also found a non-significant difference in soil pH value between the loss and depositional zone of the two consecutive soil and water conservation structures. Similarly, Challa et al. (2016) reported there was no significant difference in soil pH value between slope gradient. However, the result of this study is in line with a previous study done by Alemayehu and Fisseha (2018) who reported the soil pH significantly varied between slope gradient.

The highest pH (5.902 and 5.959) values were observed at gentle slope and bottom terrace position and the lowest (5.139 and 4.923) at steep and upper spot of the terrace position, respectively (Table 4). In line with this finding, Aytenuw (2015) reported the highest pH (6.8) value was obtained on gently sloping gradient soils. Based on the rating of Landon (1991), the overall mean pH value of the study soil was from 4 to 6, which is categorized as moderately acidic.

3.1.4 Soil electrical conductivity (EC)

According to Brady and Weil (2002), the electrical conductivity (EC) of a soil solution is an indirect measurement of salt content. The overall means of electrical conductivity of the sampled soils were not significantly ($p>0.05$) influenced by slope

gradient and terrace position, and their interaction effect (Table 3).

Even though, the statistical test showed no significant ($p>0.05$) difference, the mean value was slightly changed with slope gradient. Relatively higher electrical conductivity values (0.077 dS/m and 0.072 dS/m) were found at gentle and bottom terrace position. Whereas lower values (0.021 dS/m and 0.022 dS/m) were recorded at steep slope gradient and upper terrace position, respectively (Table 4). The results of this study are somewhat inconsistent with the study of Hailu et al. (2012), that found the electrical conductivity variations of the soil was significant with respect to the slope gradient. Based on Landon (1991) salinity range classification, the soil in the study area could be regarded as salt free.

3.1.5 Soil organic carbon (SOC)

The soil organic carbon contents in Table 3 were significantly ($p<0.05$) affected by the conserved land slope gradient. However, it was not significantly ($p>0.05$) influenced by terrace position and their interaction effect. The organic carbon content under steep slope gradient (1.554%) was significantly lower ($p<0.05$) than gentle (2.957%) and moderate (2.802%) slopes (Table 4). This might be due to accumulation of organic materials that are transported from the higher sloping due to the speed of running water.

The results of this study contradicted with the study conducted by Gadisa and Hailu (2020) who reported there was no significant difference between slope gradient in soil organic carbon content.

However, the result agreed with the finding of [Hailu et al. \(2012\)](#) who observed soil organic carbon content significantly varied with slope gradient. The results of this study are again consistent with [Aytenuw \(2015\)](#)

who found that the minimum soil organic carbon was recorded under soils of the strongly sloping area, whereas the maximum was recorded in soils of the gently sloping area.

Table 3. Interaction effect of slope gradient and terrace position on some chemical properties of soil

Sources of variation	SS	Df	MS	F-value
pH (H₂O)				
Slope	2.728	2	1.364	8.523*
Terrace position	4.893	2	2.446	15.286*
Slope*Terrace position	1.821	4	0.450	2.844*
Electrical conductivity (EC Ds/m)				
Slope	0.015	2	0.077	2.398 ^{Ns}
Terrace position	0.011	2	0.006	1.865 ^{Ns}
Slope*Terrace position	0.77	4	0.002	0.680 ^{Ns}
Soil organic carbon (SOC %)				
Slope	10.637	2	5.318	13.913*
Terrace position	1.434	2	0.717	1.876 ^{Ns}
Slope*Terrace position	0.784	4	0.196	0.513 ^{Ns}
Total nitrogen (TN %)				
Slope	0.380	2	0.190	2.775 ^{Ns}
Terrace position	1.5799	2	0.789	11.5838*
Slope*Terrace position	0.172	4	0.043	0.628 ^{Ns}
Available phosphorus (Av-P mg/kg)				
Slope	2.915	2	1.457	0.268 ^{Ns}
Terrace position	2.915	2	37.589	6.915*
Slope*Terrace position	75.17	4	5.497	1.011 ^{Ns}
Cation exchange capacity (CEC cmol/kg)				
Slope	113.790	2	56.895	4.171*
Terrace position	284.451	2	142.226	10.427*
Slope*Terrace position	24.707	4	6.177	0.453 ^{Ns}

Ns=not-significant at $p>0.05$; (*)=Significant at $p<0.05$; Slope*Terrace=interaction effect

3.1.6 Total nitrogen (TN)

Total nitrogen analysis [Table 3](#) revealed that there was a significant ($p<0.05$) difference between the three terrace positions. On the other hand, there was no significant variation ($p>0.05$) related with the topographic slope of the area. Similar trends were also observed in the interaction effect of slope gradient by terrace position. The result of this study is inconsistent with the result of [Dagnachew et al. \(2020\)](#) who reported total nitrogen was not significantly varied with terrace position, but statistically significant different with slope and the interactions effects.

Significantly ($p<0.05$) higher value (1.097%) of total nitrogen at the bottom spot position and slightly greater mean value (0.890%) at gentle slope gradient were recorded ([Table 4](#)). This indicated total nitrogen

content of the study soil showed decreasing trend towards the steep slope and upper terrace position. According to [Aytenuw \(2015\)](#), an increasing trend in the total nitrogen content of the soil of the study site from moderately steep to gently sloping gradient was observed. Similarly, [Guadie et al. \(2020\)](#) reported the highest total nitrogen was recorded in the lower slope gradient than in the higher slope gradients.

The reason might be due to the transportation of organic material and clay particles that hold some easily transportable plant nutrient inside the inter-structural terrace area. According to [Amdemariam et al. \(2011\)](#), terraced land where soils are actively eroded and deposited to the soil accumulation zone, forming spatial variability in nutrient availability within the inter-terrace space.

3.1.7. Available phosphorus (Av-P)

The available phosphorus of the sampled soils was not significantly varied ($p>0.05$) with respect to slope gradient and interaction effect. However, available phosphorus was significantly influenced ($p<0.05$) by terrace position (Table 3). Significantly greater value (10.321 mg/kg) was observed at the bottom terrace position as compared to upper and midpoint (Table 4). Alemayehu and Fisseha (2018) and Gadisa and Hailu (2020) also stated there were statistically significant differences in available phosphorus with respect to terrace position.

Significant accumulation of phosphorus at the bottom terrace position might be the inherent capacity of phosphorus to adhere with other soil materials and

easily transported by erosion effect and accumulate due to structural barriers of conservation practice. Vancampenhout et al. (2006) also reported higher values of available phosphorus in the accumulation zone was observed due to tillage and water erosion and formation of slow forming terraces.

In terms of slope gradient, slightly greater mean available phosphorus was found at the gentle slope gradient (8.4251 mg/kg) than the steep (7.703 mg/kg) and moderate slope (7.7561 mg/kg). According to the ratings following Olsen (1965), the overall means of available phosphorus was (5-9 mg/kg) which is low concentration in the study soils. This might be due to low availability of phosphorus in the low pH soil.

Table 4. Some chemical properties of soil in relation to slope gradient and terrace position

Soil properties	Slope gradient				Terraced position/sampling spot			
	Steep	Moderate	Gentle	F-value	Upper	Center	Bottom	F-value
pH (H ₂ O)	5.139 ^a	5.388 ^a	5.902 ^b	8.523 [*]	4.923 ^a	5.547 ^b	5.959 ^b	15.286 [*]
EC (Ds/m)	0.021 ^a	0.036 ^a	0.077 ^a	2.398 ^{Ns}	0.022 ^a	0.041 ^a	0.072 ^a	1.865 ^{Ns}
SOC (%)	1.554 ^a	2.802 ^b	2.957 ^b	13.913 [*]	2.191 ^a	2.376 ^a	2.746 ^a	1.876 ^{Ns}
TN (%)	0.605 ^a	0.798 ^a	0.890 ^a	2.775 ^{Ns}	0.529 ^a	0.666 ^a	1.097 ^b	11.533 [*]
Av-P (mg/kg)	7.703 ^a	7.756 ^a	8.425 ^a	0.268 ^{Ns}	6.759 ^a	6.802 ^a	10.321 ^b	6.915 [*]
CEC (cmol/kg)	41.896 ^a	43.828 ^{ab}	46.882 ^b	4.171 [*]	41.600 ^a	42.228 ^a	48.778 ^b	10.427 [*]

Ns=not-significant at $p>0.05$; (*)=Significant at $p<0.05$; Rows having the same letters are not statistically significant at 0.05 significant level (Tukey-Kramer); EC=Electrical conductivity; TN=Total nitrogen; Av-P=Available phosphorus; CEC=Cation Exchange Capacity

3.1.8 Cation exchange capacity of soil (CEC)

According to Table 3, the cation exchange capacity (CEC) of the study soil was significantly ($p<0.05$) affected by both slope gradient and terrace position; but the interaction of the two factors was not statistically significant ($p>0.05$).

Significantly ($p<0.05$) lower CEC values were measured at steep slope (41.896 cmol/kg) and upper terrace position (41.600 cmol/kg) and significantly ($p<0.05$) higher values were measured at gentle slope (46.882 cmol/kg) and bottom terrace position (48.778 cmol/kg) were observed (Table 4). This might be due to the fact that the high rainfall, coupled with a steep slope gradient, accelerates leaching of cations. The same holds true for Aytenuw (2015), which reported an increasing trend of exchangeable basic cations available from moderately steep to gently sloping gradient. This might be due to their loss through runoff erosivity and erosion in the high sloping areas and concentration in areas having lower slope gradient.

3.1.9 Exchangeable bases (K^+ , Na^+ , Ca^{2+} , and Mg^{2+})

The interaction of slope gradient by the terrace position were not significantly ($p>0.05$) affected the K^+ , Na^+ , Ca^{2+} , and Mg^{2+} values of the sampled soil properties. On the other hand, the exchangeable potassium (K^+) significantly ($p<0.05$) altered with both the slope gradient and the terrace position (Table 5). Likewise, exchangeable Mg^{2+} was significantly ($p<0.05$) influenced by terrace position. The results of this study are somewhat consistent with Amare et al. (2014). Regardless of soil depositional variation, the value of exchangeable bases i.e., Na^+ , K^+ , Ca^{2+} , and Mg^{2+} did not show significant change.

The highest mean values of exchangeable potassium (K^+) were measured at the gentle slope land (6.371 cmol/kg) and bottom terrace position (5.662 cmol/kg), and the lowest means were recorded at the steep slope gradient (3.455 cmol/kg) and upper terrace position (4.027 cmol/kg) (Table 6). Similarly,

exchangeable Na⁺ was also slightly higher under gentle slope gradient (4.342 cmol/kg) and bottom terrace position (4.299 cmol/kg) and moderately lower under steep slope (2.378 cmol/kg) and upper terrace position (2.651 cmol/kg).

Considering Table 6, statistically slightly different increments in the mean value of exchangeable magnesium at the gentle slope gradient

(2.305 cmol/kg) was observed as compared to steep (1.559 cmol/kg) and moderate slope (1.132 cmol/kg). Similarly, slightly higher mean values of exchangeable calcium were observed at the gentle slope gradient (7.526 cmol/kg) and bottom terrace position (7.788 cmol/kg) as compared to at the moderate slope (6.4267cmol/kg) and upper terrace position (6.148 cmol/kg).

Table 5. Interaction effect of slope gradient and terrace position on exchangeable bases

Sources of variation	SS	Df	MS	F-value
Ca²⁺ (cmol/kg)				
Slope	5.528	2	2.764	0.951 ^{Ns}
Terrace position	12.163	2	6.082	2.092 ^{Ns}
Slope*Terrace position	7.316	4	1.829	0.629 ^{Ns}
Mg²⁺ (cmol/kg)				
Slope	6.349	2	3.175	2.569 ^{Ns}
Terrace position	12.626	2	6.313	5.108*
Slope*Terrace position	1.758	4	0.440	0.356 ^{Ns}
K⁺ (cmol/kg)				
Slope	38.355	2	19.178	10.866*
Terrace position	12.704	2	6.352	3.599*
Slope*Terrace position	1.717	4	0.429	0.243 ^{Ns}
Na⁺ (cmol/kg)				
Slope	17.420	2	8.710	2.246 ^{Ns}
Terrace position	12.562	2	6.281	1.620 ^{Ns}
Slope*Terrace position	17.638	4	4.409	1.137 ^{Ns}

Ns=not-significant at p>0.05; (*)=Significant at p<0.05; Slope*Terrace=interaction effect

In general, regardless of the significant difference all the exchangeable bases showed increasing trend when the slope and terrace position go towards gentle and bottom (Table 6). The results of this study coincide with Ademe et al. (2017) who found average exchangeable K⁺ values of 5.70, 5.50

and 4.53 ppm from the bottom, middle and upper position of the field, respectively. The overall relative mean concentration of basic cations of the sampled soil was in the order of Ca²⁺>K⁺>Na⁺>Mg²⁺, which is different from the finding of (Miheretu and Yimer, 2018).

Table 6. Exchangeable bases of soil in relation to slope gradient and terrace position

Soil properties	Slope gradient				Terraced position/sampling spot			
	Steep	Moderate	Gentle	F-value	Upper	Center	Bottom	F-value
Ca ²⁺ (cmol/kg)	6.851 ^a	6.4267 ^a	7.526 ^a	0.951 ^{Ns}	6.148 ^a	6.868 ^a	7.788	2.092 ^{Ns}
Mg ²⁺ (cmol/kg)	1.559 ^a	1.132 ^a	2.305 ^a	2.569 ^{Ns}	0.931 ^a	1.488 ^{ab}	2.578 ^b	5.108*
K ⁺ (cmol/kg)	3.455 ^a	5.041 ^b	6.371 ^b	10.866*	4.027 ^a	5.179 ^{ab}	5.662 ^b	3.599*
Na ⁺ (cmol/kg)	2.378 ^a	3.466 ^a	4.342 ^a	2.246 ^{Ns}	2.651 ^a	3.236 ^a	4.299 ^a	1.620 ^{Ns}

Ns=not-significant at p>0.05; (*)=Significant at p<0.05; Rows having the same letters are not statistically significant at 0.05 significance level (Tukey-Kramer)

4. CONCLUSION

Land degradation is one of the major environmental problems that limit the productive capacity of agriculture lands in Ethiopia. Some efforts

towards a campaign for soil and water conservation practice were made to reduce the problem. Since the practices is a campaign, evaluation of its effect on selected soil properties were critical.

Soils analyzed in the study area indicated moderately acidic condition. The soil pH, texture, cation exchange capacity (CEC), and exchangeable potassium (K⁺) were changed with both slope gradient and terrace position, whereas, total nitrogen, available phosphorus, magnesium, and calcium were changed with terrace position. Soil organic carbon significantly varied only with slope gradient. Soil properties were significantly higher at gentle slope gradient and bottom terrace position than the steep and the upper terrace position between the two consecutive soil and water conservation structures. The observed soil property gradient is due to the effect of past soil erosion and inappropriate tillage implementation and conservation barrier. Integration of biological conservation practice, proper maintenance and appropriately following the contour line during tillage practice are important for soil property improvement.

ACKNOWLEDGEMENTS

The authors would like to thank Debark University for covering the research cost. We also would like to acknowledge Debark District agriculture office (Milligebssa kebele agriculture office) and Srinka Regional Agricultural Research Institute (SRARI) for their helps and assistances, during field data collection and soil laboratory analysis respectively. Lastly, our gratitude extends to the anonymous reviewers and editorial for their valuable comments which helps to improve the manuscript.

REFERENCES

- Ademe Y, Kebede T, Mullatu A, Shafi T. Evaluation of the effectiveness of soil and water conservation practices on improving selected soil properties in Wonago District, Southern Ethiopia. *Journal of Soil Science and Environmental Management* 2017;8(3):70-9.
- Alemayehu T, Fisseha G. Effects of soil and water conservation practices on selected soil physicochemical properties in Debre Yakob Micro-watershed, Northwest Ethiopia. *Ethiopian Journal of Science and Technology* 2018;11(1):29-38.
- Amare T, Zegeye AD, Yitafaru B, Steenhuis TS, Hurni H, Zeleke G. Combined effect of soil bund with biological soil and water conservation measures in the Northwestern Ethiopian highlands. *Ecology and Hydrobiology* 2014;14(3):192-9.
- Amdemariam T, Selassie YG, Haile M, Yamoh C. Effect of soil and water conservation measures on selected soil physical and chemical properties and barley (*Hordeum* spp.) yield. *Journal of Environmental Science and Engineering* 2011;5(11).
- Amdihun A, Gebremariam E, Rebelo LM, Zeleke G. Suitability and scenario modeling to support soil and water conservation interventions in the Blue Nile Basin, Ethiopia. *Environmental Systems Research* 2014;3(1):23.
- Amsalu A, De Graaff J. Determinants of adoption and continued use of stone terraces for soil and water conservation in an Ethiopian highland watershed. *Ecological Economics* 2007;61(2-3):294-302.
- Ayteneu M. Effect of slope gradient on selected soil physicochemical properties of in Dawja watershed in Enebe Sar Midir District, Amhara National Regional State. *American Journal of Scientific and Industrial Research* 2015;6(4):74-81.
- Berry L. Land Degradation in Ethiopia: Its Extent and Impact. World Bank; 2003. p. 2-7.
- Bewket W, Sterk G. Farmers' participation in soil and water conservation activities in the Chemoga watershed, Blue Nile basin, Ethiopia. *Land Degradation and Development* 2002;13(3):189-200.
- Bewket W. Soil and water conservation intervention with conventional technologies in northwestern highlands of Ethiopia: Acceptance and adoption by farmers. *Land Use Policy* 2007;24(2):404-16.
- Bewket W. The need for a participatory approach to soil and water conservation (SWC) in the Ethiopian highlands: A case study in Chemoga watershed, East Gojjam. *Eastern Africa Social Science Research Review* 2001;17(2):43-68.
- Bishaw B. Deforestation and land degradation in the Ethiopian highlands: A strategy for physical recovery. *Northeast African Studies* 2001;1:7-25.
- Brady NC, Weil RR. *The Nature and Properties of Soils*. 13th ed. New Jersey, USA: Prentice Hall; 2002. p. 249.
- Central Statistical Agency (CSA). *Statistical Reports of the Census for Amhara Region Population Size and Characteristics*. Addis Ababa, Ethiopia: Central Statistical Agency of Ethiopia; 2007.
- Challa A, Abdelkadir A, Mengistu T. Effects of graded stone bunds on selected soil properties in the central highlands of Ethiopia. *International Journal of Natural Resource Ecology and Management* 2016;1(2):42-50.
- Dagnachew M, Moges A, Kebede A, Abebe A. Effects of soil and water conservation measures on soil quality indicators: The case of Geshy sub-catchment, Gojeb river catchment, Ethiopia. *Applied and Environmental Soil Science* 2020; 2020:e1868792.
- Dagnaw DC, Guzman CD, Zegeye AD, Tibebe TY, Getaneh M, Abate S, et al. Impact of conservation practices on runoff and soil loss in the sub-humid Ethiopian highlands: The Debre Mawi watershed. *Journal of Hydrology and Hydromechanics* 2015;63(3):210-9.
- Demelash M, Stahr K. Assessment of integrated soil and water conservation measures on key soil properties in South Gonder, North-Western Highlands of Ethiopia. *Journal of Soil Science and Environmental Management* 2010;1(7):164-76.
- Esser K, Magen T, Tilahun Y, Haile M. *Soil conservation in Tigray, Ethiopia*. Noragric Report No. 5. Oslo, Norway: Agricultural University of Norway; 2002.
- Food and Agriculture Organization of the United Nations (FAO). *Ethiopian Funds in Trust: Ethiopian Highland Reclamation Study: Volume 1*. FAO; 1986.
- Gadisa S, Hailu L. Effect of level soil bund and fayna juu on soil physico-chemical properties, and farmers adoption towards the practice at Dale Wabera District, Western Ethiopia. *American Journal of Environmental Protection* 2020;9(5): 107-20.
- Gebremedhin B, Swinton SM. Investment in soil conservation in Northern Ethiopia: The role of land tenure security and public programs. *Agricultural Economics* 2003;29(1):69-84.

- Guadie M, Molla E, Mekonnen M, Cerdà A. Effects of soil bund and stone-faced soil bund on soil physico-chemical properties and crop yield under rain-fed conditions of Northwest Ethiopia. *Land* 2020;9(1):13.
- Hailu W, Moges A, Yimer F. The effects of 'fanya juu' soil conservation structure on selected soil physical and chemical properties: The case of Goromti watershed, Western Ethiopia. *Resources and Environment* 2012;2(4):132-40.
- Haregeweyn N, Berhe A, Tsunekawa A, Tsubo M, Meshesha DT. Integrated watershed management as an effective approach to curb land degradation: A case study of the Enabered watershed in Northern Ethiopia. *Environmental Management* 2012; 50(6):1219-33.
- Hurni H, Abate S, Bantider A, Debele B, Ludi E, Portner B, et al. Land degradation and sustainable land management in the highlands of Ethiopia. *Global Change and Sustainable Development* 2010;187-207.
- Hurni H. Degradation and conservation of the resources in the Ethiopian highlands: International mountain society. *Mountain Research and Development* 1988;8(2):123-30.
- Landon JR. *A Handbook for Soil Survey and Agricultural Land Evaluation in the Tropics and Subtropics*. Hong Kong: Longman Scientific and Technical Group Ltd; 1991.
- Mekonnen GT, Michael AG. Review on overall status of soil and water conservation system and its constraints in different agro-ecology of Southern Ethiopia. *Journal of Natural Sciences Research* 2014;4(7):59-69.
- Miheretu BA, Yimer AA. Spatial variability of selected soil properties in relation to land use and slope position in Gelana sub-watershed, Northern highlands of Ethiopia. *Physical Geography* 2018;39(3):230-45.
- Ministry of Finance and Economic Development (MoFED). Federal Democratic Republic of Ethiopia (FDRE): Growth and transformation plan of Ethiopia (GTP): Annual Progress Report for F.Y. MoFED; 2013.
- Ministry of Finance and Economic Development (MoFED). The Federal Democratic Republic of Ethiopia (FDRE): Growth and Transformation Plan of Ethiopia (GTP). MoFED; 2010.
- Mushir A, Kedru S. Soil and water conservation management through indigenous and traditional practices in Ethiopia: A case study. *Ethiopian Journal of Environmental Studies and Management* 2012;5(4):343-55.
- Nyssen J, Poesen J, Deckers J. Land degradation and soil and water conservation in tropical highlands. *Soil and Tillage Research* 2009;103(2):197-202.
- Olsen SR. Test of an ascorbic acid method for determining phosphorus in water and NaHCO₃ extracts from soil. *Soil Science Society of America Journal* 1965;29(6):677-8.
- Tefera B, Ruelle ML, Asfaw Z, Tsegay BA. Woody plant diversity in an Afromontane agricultural landscape (Debarq District, Northern Ethiopia). *Forests Trees and Livelihoods* 2014; 23(4):261-79.
- Temesgen G, Amare B, Silassie HG. Land degradation in Ethiopia: Causes, impacts and rehabilitation techniques. *Journal of Environment and Earth Science* 2014;4(9):98-104.
- Tesfa A, Mekuriaw S. The effect of land degradation on farm size dynamics and crop-livestock farming system in Ethiopia: A Review. *Open Journal of Soil Science* 2014;4(1):1-5.
- Vancampenhout K, Nyssen J, Gebremichael D, Deckers J, Poesen J, Haile M, et al. Stone bunds for soil conservation in the Northern Ethiopian highlands: Impacts on soil fertility and crop yield. *Soil and Tillage Research* 2006;90(1-2):1-5.
- Zingore S, Mutegi J, Agesa B, Tamene L, Kihara J. Soil degradation in sub-Saharan Africa and crop production options for soil rehabilitation. *Better Crops* 2015;99(1):24-6.

***In Vitro* Removal of Electronic and Electrical Wastes by Fungi Isolated from Soil at Annaba Area in Northeast of Algeria**

**Ghania Bourzama^{1*}, Nadjat Iratni², Nadjat Ennaghra³, Houria Ouled-Haddar⁴,
Boudjema Soumati¹, Khouloud Amour¹, and Khouloud Bechiri¹**

¹Laboratory of Biochemistry and Environmental Toxicology, Department of Biochemistry, Faculty of Sciences, University of Badji Mokhtar, Annaba 23000, Algeria

²Faculty of Sciences, University of Bordj Bou Arreridj, Bordj Bou Arreridj 3400, Algeria

³Deparement de SNV, Faculty of Sciences, 20 August University, Skikda 21000, Algeria

⁴University of Mohamed Seddik Benyahia, Laboratory of Molecular Toxicology, Jijel 18000, Algeria

ARTICLE INFO

Received: 28 Dec 2020

Received in revised: 17 Mar 2021

Accepted: 21 Apr 2021

Published online: 28 May 2021

DOI: 10.32526/enrj/19/2020294

Keywords:

Bioremediation/ Keratinolytic enzyme/ Fungi/ Electrical and electronic waste

*** Corresponding author:**

E-mail: gbourzama@yahoo.fr

ABSTRACT

Electronic and electrical wastes (EEW) have increased exponentially in recent years due to technological progress. The uncontrolled incineration of these wastes causes pollution of air, soil, and water that has dangerous effects on health of human beings and other living organisms. This work isolated fungi that are capable of degrading some of these electronic wastes. In this study, fungi isolated from soil polluted by EEW were grown on potatoes dextrose agar (PDA) medium. The estimation of the biodegradation was achieved by inoculation of both rechargeable batteries and printed circuit boards on a minimum solid and liquid medium with selected fungal strains. During the process of biodegradation on solid medium, microscopic observation was done, and on liquid medium the production of keratinolytic enzymes was evaluated using a colorimetric method after incubation with keratine powder. After 30 days, the obtained results showed that *Geotrichum candidum* is capable of degrading battery and circuit boards with rates of 23% and 71%, respectively, while *Rhizopus stolonifer* reduced battery weight by 7% and printed circuit boards by 60%. Microscopic observations showed no morphological modification in *Geotrichum candidum*, while there was sporocyst formation in *Rhizopus stolonifer*. The detection of enzymatic production indicated that there is a relation between the biodegradation process of electronic wastes and keratinolytic enzymes in *Geotrichum candidum*.

1. INTRODUCTION

The use of electrical and electronic equipment (EEE) is nowadays increasing rapidly and significantly in all fields, which has led to the accumulation of their wastes in the environment (Gavilán-García et al., 2009; Hall and Williams, 2007). EEW are rich in highly toxic metals such as Cd, Hg, Pb, As, Cr, Cu, Ni, and Zn (Huang et al., 2009; Sodhi and Reimer, 2001; Sum, 1991). These wastes are toxic due to their complexed primary substance, and their effect on the environment. The composition fully justifies the specific management of the wastes resulting from these equipments once used. Moreover, these wastes represent an interesting and a respectable source of raw materials (Cui and Zhang, 2008). Faced with this

situation, chemical processes have been used for the bioremediation and recovery of metals from EEW, but the residues from these processes are highly polluting and corrosive and also consume large amounts of energy (Cui and Zhang, 2008; Weidenhamer and Clement, 2007).

Recently, microorganisms provide new pathways for eliminating the accumulated electronic wastes. In view of the environmental problems caused by these metal extraction processes, a very limited amount of research have been realized about the microorganisms, including filamentous fungi, for the biodegradation of EEW and the recovery of metals from these wastes by several methods. This limited research focuses on species of the genera of *Aspergillus*,

Citation: Bourzama G, Iratni N, Ennaghra N, Ouled-Haddar H, Soumati B, Amour K, Bechiri K. *In Vitro* removal of electronic and electrical wastes by fungi isolated from soil at Annaba Area in Northeast of Algeria. Environ. Nat. Resour. J. 2021;19(4):302-309. (<https://doi.org/10.32526/enrj/19/2020294>)

Penicillium and *Rhizopus* and their ability to recover metals from these wastes. These fungal strains are able to perform several mechanisms to biodegrade and remove these wastes. Hydrolysis as the first stage is defined as the reaction with water where the water molecules lead to cleavage of chemical bonds within a material followed by the esterification, dehydrogenation, hydroxylation, and dioxygenation in order to obtain simple molecules that are easy to use by fungal cells and other cells (Brandl et al., 2001).

In absence of sufficient research on this subject, the objective of this work is to isolate potential filamentous fungi from polluted soil that are able to biologically degrade EEW without any risk to the environment, and to estimate the production of certain enzymes during this process, since filamentous fungi are the preferred source of industrial enzymes due to their excellent capacity to produce extracellular proteins (Kubicek et al., 2009; Schaffner and Toledo, 1991). Because of their consistent morphology and versatile metabolic ability, fungi play crucial roles as degraders and symbionts in the environment as a whole, including soil and aquatic habitats (Tomer et al., 2020). The use of fungi isolated from natural sources that are able to remediate these wastes is more effective and safer as they do not harm the environment, and the research can be expanded and applied in all areas to eliminate these wastes which are harmful to humans in short and long term.

2. METHODOLOGY

2.1 Isolation and identification of fungal strains

The fungal strains were isolated and screened from a soil rich in electronic and electrical wastes located at the Wilaya of Annaba in Algeria, in this site, EEW have accumulated for more than 20 years. After, 5 cm of the surface layer of the soil is removed using a sterile spatula, 100-150 g of soil were collected in a sterile flask and transported to the laboratory at 4°C (Pochon and Tardieux, 1962).

A 10 g aliquot of soil was diluted in 90 mL of sterile normal saline, then decimal dilutions were prepared until 10^{-6} (Clark et al., 1983). The isolation was carried out on PDA with gentamicin antibiotic in order to inhibit the growth of bacteria (Botton et al., 1990). PDA was prepared using extracts of 200 g of Potatoes, 20 g of Dextrose and 15 g of Agar in 1 L of distilled water then autoclaved at 120°C for 20 min. Surface, 1 mL of each dilution was inoculated onto the PDA medium, plates were incubated at 25°C for 7 days (Botton et al., 1990).

For purification of the isolated fungi, a small piece of agar was taken where the hyphal end is located and transfer to another agar plate.

Fungi were identified by their morphology in culture and their mycelium and spores under the optical microscope with magnification of 40X and 60X.

2.2 Screening of the isolated fungal strains

The isolated and identified fungi were transferred to PDA medium with electronic and electrical wastes. The diameter of the isolated fungal mycelium were measured in order to screen the fungal strain for the biodegradation test.

2.3 Preservation of the screened strains

The most common method for preserving fungal strains consists of seeding the strains into PDA slants agar, these cultures were kept for one week at 25°C, then they are stored at 4°C to promote their viability and limit the possibility of variations (Botton et al., 1990).

2.4 Preparation of EEW

EEW namely, rechargeable batteries (Sony) and printed circuit boards (Sony) have been cut into small pieces with a known weight (0.3 g); they were then disinfected separately with ethanol (Figure 1).

2.5 Test of biodegradation

2.5.1 In liquid medium

In this method, a piece of EEW was placed in a 1 L flask containing 800 mL of the basal medium which consists of (g/mL): K_2HPO_4 (6.4), KH_2PO_4 (0.8), $(NH_4)_2SO_4$ (0.4), $MgSO_4$ (0.16), NaCl (0.08), $FeSO_4 \cdot 7H_2O$ (0.016), $CuSO_4$ (0.0004), $ZnSO_4$, $CaCO_3$ (0.4) with pH=7 (Nakajima-Kambe et al., 1999). EEW pieces were added to an erlenmeyer flask (250 mL) containing 100 mL of the basal medium described above. Agar disks with fungal mycelium (7 mm diameter) were then used to inoculate each fungal strain, a control was also prepared which was free of EEW pieces, after inoculation, the media were incubated in a shaker incubator (100 rpm) at 27°C for 1 month. The weight of EEW was measured before and after to evaluate the weight variation.

2.5.2 On solid medium

The pieces of EEW with equal weights were put on the surface of Petri plates, then the basal solid medium supplemented with Tween 80 (0.6 mL/L) was

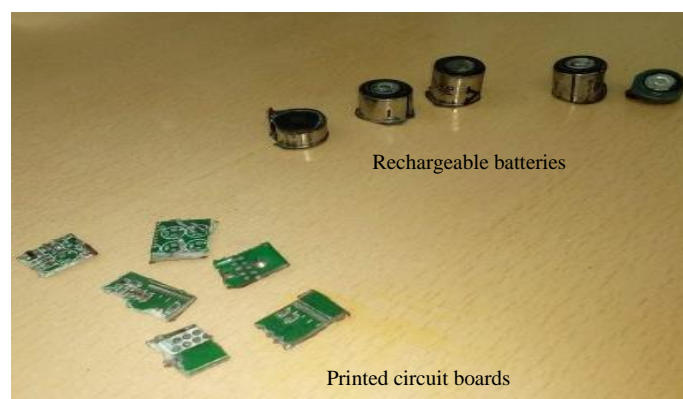


Figure 1. Preparation of EEW

added (Brunner et al., 2018). Agar disks with fungal mycelium were inoculated into the solid medium. The plates were incubated at 27°C for one month.

2.6 Microscopic observation

This part was carried out since the growth of fungal strains on unconventional carbon sources could modify the mycelium morphology, these modifications are observable with a light microscope (Bourzama et al., 2019). The mycelium parts were spread out on a glass slide with sterile normal saline, and observed under a light microscope in order to observe the modifications shown on hyphal tips in comparison with the observation of the same fungal strain on conventional carbon source (grown on PDA).

2.7 Keratinolytic activity

For keratinolytic activity determination, keratin powder (20 mg) was incubated with 3.0 mL of phosphate buffer (pH 7.8) and 2.0 mL of the culture filtrate for 1 h at 37°C in a shaking water-bath at 160 rev/min. 2.0 mL of 10% trichloroacetic acid (TCA) was added to stop the enzyme reaction. Samples were stored on a refrigerator at 4°C for 30 min. They were then centrifuged for 15 min at 10,000 g in a cooled

centrifuge. The absorbance of the supernatant fluid at 280 nm was measured using a UV-Visible spectrophotometer (Takiuchi et al., 1982). During the biodegradation process, keratinolytic activity of the screened strains was tested and compared to a control, i.e., the fungal strain growing on a conventional source of carbon (PDA).

3. RESULTS

3.1 Isolation and strain identification

Four fungal strains were isolated and identified to be *Aspergillus niger*, *Geotrichum candidum*, *Penicillium italicum*, and *Rhizopus stolonifer*. The fungal morphology was studied macroscopically by observing the colony characteristics (color, shape, size, and hyphae), and microscopically by a microscope with a digital camera (Table 1) (Gaddeyya et al., 2012).

3.2 Screening of the EEW-degrading fungal strains

Among the four identified fungal strains, only two (*Geotrichum candidum* and *Rhizopus stolonifer*) were selected because their growth was faster when compared to the others based on their mycelium diameter (Table 2).

Table 1. The characteristics of isolated fungal strains

Fungal strain	Macroscopic characteristics	Microscopic characteristics
<i>Aspergillus niger</i>	The conidial heads to be globose and dark brown in color that have been shown to divide into a number of columns.	The carbon black/dark brown color of the spores from their conidial heads (biserite). Hyphae are septate.
<i>Geotrichum candidum</i>	Flat, white to cream, dry and finely suede-like with no reverse pigment.	Hyphae are hyaline, septate, branched and break up into chains subglobose to cylindrical arthroconidia.
<i>Penicillium italicum</i>	Small colonies, greens dark to yellow	Very abundant conidia produced in a chain at the end of the phialids on penicilles larges, triverticillé.
<i>Rhizopus stolonifer</i>	A grayish fluffy mass, a body unbranching sporangiophores.	Black spores and are similar to cotton candy are also visible.

Table 2. Diameter of the isolated fungal mycelium on PDA at 27°C for 7 days

Fangual strain	Diameter (mm)
<i>Aspergillus niger</i>	15
<i>Geotrichum candidum</i>	63
<i>Penicillium italicum</i>	31
<i>Rhizopus stolonifer</i>	74

3.3 Test of biodegradation

3.3.1 In liquid medium

After the first 10 days, *Geotrichum candidum* caused a decrease in the weight of battery pieces while the weight of the boards remained constant. After 30 days, the weight of battery continued to decrease (23%) and the weight of board was highly reduced (71%) (Figure 2(a)).

After 10 days, *Rhizopus stolonifer* gave a

decrease in the weights of both EEW types. In addition, at day 30, the weight of the battery and the board decreased to 7% and 60%, respectively (Figure 2(b)).

3.3.2 On solid medium

The results of this test showed that the tested strain *Geotrichum candidum* grew on the minimum medium containing a piece of EEW with a diameter of 2 cm after 30 days. While *Rhizopus stolonifer* grew on the same medium with a diameter of 7.1 cm after 30 days (Table 3). This growth on a minimum medium that does not contain any carbon source except two electronic wastes (EEW) could be explained by the ability of both strains to degrade all wastes into simple carbon compounds and use their carbon content for continuing their vegetative development but without the production of CO₂.

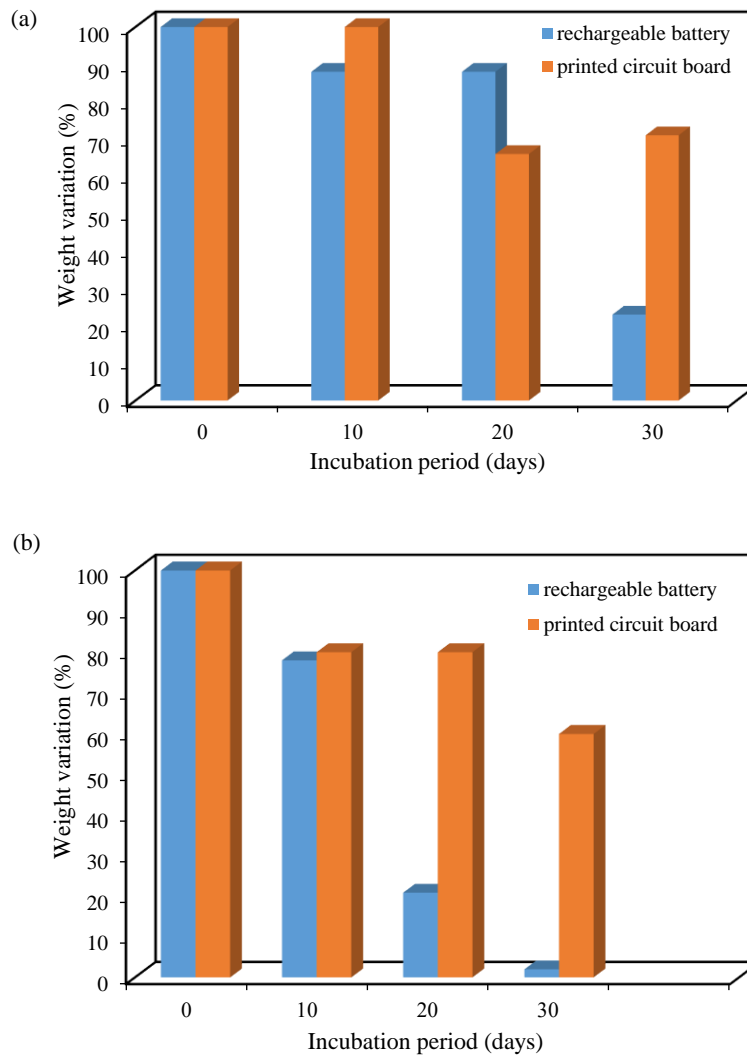


Figure 2. Weight variation of EEW during the incubation period (30 days), (a)=in presence of *Geotrichum candidum*, (b)=in presence of *Rhizopus stolonifera*

Table 3. Growth of *Geotrichum candidum* and *Rhizopus stolonifer* on a minimum solid medium with the parts of EEW after 30 days

Fungal strain	Diameter with rechargeable batteries (mm)	Diameter with printed circuit boards (mm)
<i>Geotrichum candidum</i>	20	19
<i>Rhizopus stolonifer</i>	68	71

3.4 Microscopic observation

The following Figure 3(a) showed that there is no difference in microscopic observation between the fungal strain *Geotrichum candidum* after 30 days incubation on a minimum medium, and that on the conventional carbon source (PDA). While in *Rhizopus stolonifer* with EEW parts, sporocyst formation was observed at the tip which gives the black color which is darker than the normal and bursts to release a higher

number of spores, also the formation of spherical vesicles (Figure 3(a) and (b)) compared to the control on a conventional carbon source (on PDA) was noticed.

3.5 Keratinolytic activity

As shown in Figure 4(a), the highest values of enzyme secretion were obtained after 10 days of incubation and it decreased following the same pattern of the control. This may be explained by the presence of a relation between this enzyme secretion and the biodegradation process.

The same note was observed with *Rhizopus stolonifer* (Figure 4(b)) but after 20 days, keratinolytic activity was not detected. This means that there no relation between this enzyme and EEW biodegradation.

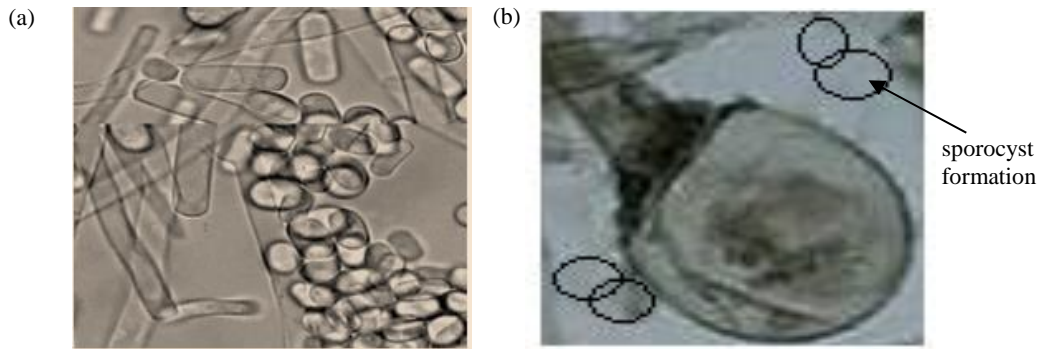


Figure 3. Microscopic observation of the screened strains, (a) *Geotrichum candidum*, (b) *Rhizopus stolonifer* after 30 days of incubation on a basal medium solid with EEW (60X).

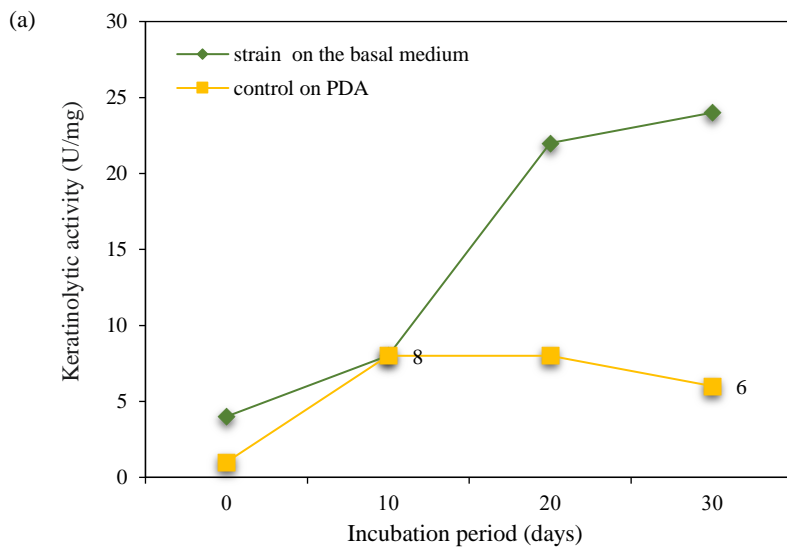


Figure 4. Relation between the keratinolytic activity (U/mg) and the degradation of EEW during the incubation period (days) in comparison with the control grown on a conventional source of carbon (PDA) for each screened strain, (a)=*Geotrichum candidum*, (b)=*Rhizopus stolonifer*.

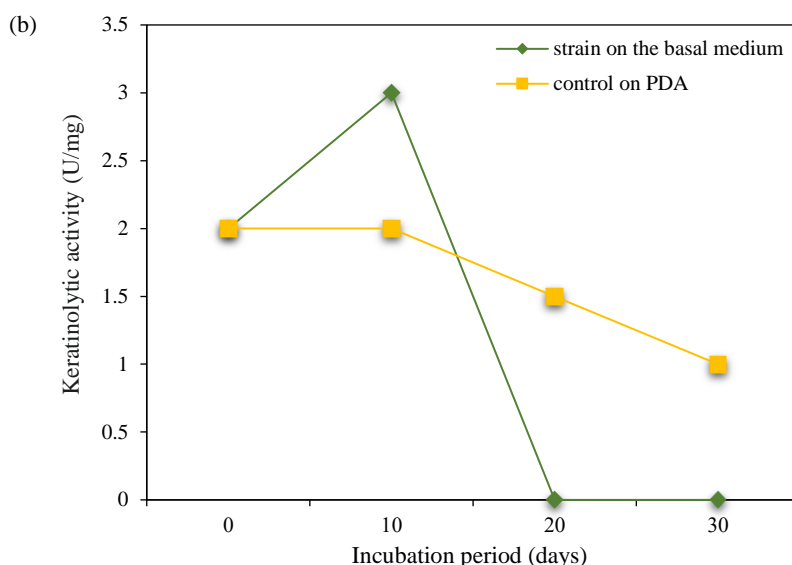


Figure 4. Relation between the keratinolytic activity (U/mg) and the degradation of EEW during the incubation period (days) in comparison with the control grown on a conventional source of carbon (PDA) for each screened strain, (a)=*Geotrichum candidum*, (b)=*Rhizopus stolonifera*. (cont.)

4. DISCUSSION

Recent chemical research aiming to recycle some components of EEW have been carried out to eliminate these dangerous wastes (Mozos et al., 2020). Thus, the aim of the current study is to safely remove some types of EEW using microorganisms. Tomer et al. (2020) exposed several mechanisms for biodegradation in fungi. Microorganisms achieve this process directly by the cells or indirectly by the extracellular enzymes (Muthu, 2014). Fungi have a large exo-enzymatic arsenal capable of degrading organic macromolecules that are unable to bio-assimilate due to their high molecular weight (Internship report IUT, 2013), like in *Geotrichum candidum* in our study. Many fungi excrete enzymes into the environment and can be used as producers of keratinolytic enzymes. A specific class of proteolytic enzymes includes the keratinases which catalyse the hydrolysis of keratins. The microorganisms responsible for biodegradation are different from each other and they have their own optimal growth conditions. The biodegradation is generally considered to be enzyme-catalyzed hydrolysis and non-enzymatic hydrolysis (Wackett and Hershberger, 2001).

EEW are rich mainly in metals and heavy metals: Cu, Fe, Cd, Cr, Pb, etc., and with lower rate, plastic substances (Huang et al., 2009; Sodhi and Reimer, 2001; Sum, 1991). In our study, we used printed circuit boards (PCBs) which are flat bases generally made of phenolic resin reinforced with glass fibre that functions as an electrical insulator. These boards are made up mainly of metallic and non-

metallic parts and organic compounds (Szałatkiewicz et al., 2014). The metallic parts include 13% Cu, 5% Fe, and 2% Al (Hall and Williams, 2007). Rechargeable lithium-ion batteries have also been used, consisting of lithium, Mn, Ni, Cd, Zn, and Cu. This leads us to the fact that *Geotrichum candidum* and *Rhizopus stolonifera* are also able to absorb/adsorb heavy metals from rechargeable batteries.

However, only few studies have been carried out on the use of fungi in the biodegradation of EEW. Some studies focused on the biodegradation of EEW by two species of fungi, *Aspergillus niger* and *Penicillium* sp. to extract lithium and cobalt from spent batteries by the production of organic acids (oxalic acid and citric acid). These acids have the effect of leaching and extracting up to 85% of lithium and 48% of cobalt from the cathodes of the batteries (Cunningham and Harwood, 2016). Similarly, Navaneethakrishnan et al. (2020) used fungi, namely, *Ustilago trichophora* and *Aspergillus niger*, for recycling lithium ion batteries. The acids change the status of several metals such as copper in EEW (Brandl et al., 2001). Citric acid produced by *A. niger* is the main leaching agent for PCB heavy metals (Aung and Ting, 2005). Because of the lack of reports on other species of fungi, we have chosen to extrapolate our study on other species which are *Rhizopus* sp. and *Geotrichum* sp.

The fungi are non-chlorophyllous, therefore they are incapable of performing photosynthesis. They need to find their carbon in organic compounds. In spite of the use of a minimum medium that is free of organic matter for biodegrading EEW with our fungal

strains, they were still alive. This suggests that they have used some of the components of the EEW as a source of carbon.

The growth of the fungal strains supplemented with the EEW was very fast because the tested fungi already contained the biodegradation enzymes, as they were isolated from a soil rich with these class of wastes.

Rhizopus sp. produces several organic acids (De Reu et al., 1995). However, in PCB biodegradation, the produced acids facilitate the elimination of the metallic components of PCBs via solubilization (Dave et al., 2018). The acids induce leaching of metals from PCB wastes through acidolysis and complexolysis mechanisms (Ceci et al., 2015). After extensive research, only a few studies were found on the ability of *Geotrichum candidum* to biodegrade the EEW. Therefore, the current study will be a first step in this field. This work is only a preliminary step and further studies are intended regarding the application of these fungal strains in EEW removal and the role of keratinolytic enzymes in the biodegradation process as well as to understand the nature of sporocyst formation in *Rhizopus stolonifer*. This application can be by insertion of nonspecific extracellular enzymes such as keratinolytic enzymes directly in the natural environments for providing degradation of EEW, or by formation of fungal biofilm mainly in the aquatic media.

5. CONCLUSION

The results of this research are very encouraging, considering that the isolated fungal strains *Geotrichum candidum* and *Rhizopus stolonifer* showed a significant capacity to biodegrade EEW, which was more remarkable with *Geotrichum candidum*. This study also affirmed a role of the keratinolytic enzymes in *Geotrichum candidum* and sporocyst formation in *Rhizopus stolonifer* during the biodegradation process of electronic wastes.

ACKNOWLEDGEMENTS

This study was funded by Department of Biochemistry, Faculty of Sciences, University of Annaba, Badji Mokhtar. The authors would like to thank the head of the Department of Biochemistry; Branes Zidane for all facilities provided.

REFERENCES

Aung KMM, Ting YP. Bioleaching of spent fluid catalytic cracking catalyst using *Aspergillus niger*. Journal of Biotechnology 2005;116(2):159-70.

- Botton B, Breton A, Fevre M, Gauthier S, Guy P, Larpent JP. Useful and Harmful Mold: Importance Industrial (Moisissure Utiles et Nuisibles: Importance industrielle). Paris, France: Elsevier Masson; 1990. p. 11-190.
- Bourzama G, Ennaghra N, Soumati B, Benoune S, Atriche N. Effect of zinc metal at high concentration on secondary metabolic pathways in *Penicillium chrysogenum* strain. Journal of Microbiology, Biotechnology and Food Sciences 2019;9(2):307-13.
- Brandl H, Bosshard R, Wegmann M. Computer-munching microbes: Metal leaching from electronic scrap by bacteria and fungi. Hydrometallurgy 2001;59:319-26.
- Brunner I, Fischer M, Ruthi J, Stierli B, Frey B. Ability of fungi isolated from plastic debris floating in the shoreline of a lake to degrade plastics. PLOS ONE 2018;13(8):e0202047.
- Ceci A, Kierans M, Hillier S, Persiani AM, Gadd GM. Fungal bioweathering of mimetite and a general geomycological model for lead apatite mineral biotransformations. Applied and Environmental Microbiology 2015;81:4955-64.
- Clark EM, White JF, Patterson RM. Improved histochemical techniques for the detection of *Acremonium coenophialum* in tall fescue and methods of in vitro culture of the fungus. Journal of Microbiology Methods 1983;1:149-55.
- Cui J, Zhang L. Metallurgical recovery of metals from electronic waste: A review. Journal of Hazardous Materials 2008;58: 228-56.
- Cunningham JA, Harwood V. Fungi recycle rechargeable lithium-ion batteries. American Chemical Society [Internet]. 2016 [cited 2020 Aug 21]. Available from: <https://www.sciencedaily.com/releases/2016/08/160821093037.htm>.
- Dave SR, Sodha AB, Tipre DR. Microbial technology for metal recovery from e-waste printed circuit boards. Journal of Bacteriology and Mycology 2018;6(4):241-7.
- De Reu JC, Rombouts FM, Nout MJR. Influence of acidity and initial substrate temperature on germination of *Rhizopus oligosporus* sporangiospores in tempe fermentation. Journal of Applied Bacteriology 1995;78:200-8.
- Gaddeyya G, Niharika PS, Bharathi P, Kumar PKR. Isolation and identification of soil mycoflora in different crop fields at Salur Mandal. Advances in Applied Science Research 2012;3:2020-6.
- Gavilán-García A, Román-Moguel A, Almada-Calvo F, Aburto-Mejía S. Electronic waste generation and technology for an appropriate management in México. Boletín de la Sociedad Química de México 2009;3(2):85-92.
- Hall WJ, Williams PT. Processing waste printed circuit boards for material recovery. Circuit World 2007;33:43-50.
- Huang K, Guo J, Xu Z. Recycling of waste printed circuit boards: A review of current technologies and treatment status in China. Journal of Hazardous Materials 2009;164:399-408.
- Kubicek CP, Mikus M, Schuster A, Schmoll M, Seiboth B. Metabolic engineering strategies for the improvement of cellulose production by *Hypocrea jecorina*. Biotechnology Biofuels 2009;2:19.
- Mozos EA, Bilbao AR, Díaz-Martín F. WEEE Recycling and circular economy assisted by collaborative robots. Applied Science 2020;10(14):4800.
- Muthu SS. Roadmap to Sustainable Textiles and Clothing: Environmental and Social Aspects of Textiles and Clothing Supply Chain. New York, USA: Springer Singapore; 2014.
- Nakajima-Kambe T, Shigeno-Akutsu Y, Nomura N, Onuma F, Nakahara T. Microbial degradation of polyurethane, polyester

- polyurethanes and polyether polyurethanes. *Applied Microbiology and Biotechnology* 1999;51(2):134-40.
- Navaneethakrishnan V, Pavithra K, Vanitha V. Recycling of lithium ion batteries using fungi based organic acids. *Materials Science and Engineering* 2020;872:12-3.
- Internship report IUT. Nîmes on Study of the biodegradation of biodegradable polymers (Etude de la biodégradation de polymères biodégradables). Paris, France: Ecole des Mines d'Alès; 2013.
- Pochon J, Tardieux P. Soil microbiology analysis technique (Technique d'analyse en microbiologie du sol). Edition of Tourtourielle. France: Saint-Mandé; 1962.
- Schaffner DW, Toledo RT. Cellulase production by *Trichoderma reesei* when cultured on xylose-based media supplemented with sorbose. *Biotechnology and Bioengineering* 1991;37:12-6.
- Sodhi MS, Reimer B. Models for recycling electronics end-of-life products. *OR Spektrum* 2001;23:97-115.
- Sum E. The recovery of metals from electronic scrap. *Journal of Metallurgy* 1991;43:53-61.
- Szałatkiewicz J, Szewczyk R, Budny E, Missala T, Winiarski W. Measurement and control system of the Plasmatron Plasma reactor for recovery of metals from printed circuit board waste. *Advanced Intelligent* 2014;267:687-95.
- Takiuchi I, Higuchi D, Sei Y, Koga M. Isolation of an extracellular proteinase (keratinase) from *Microsporum canis*. *Sabouraudia* 1982;20:281-8.
- Tomer A, Singh R, Singh SK, Dwivedi SA, Reddy CU, Keloth MRA, et al. Role of Fungi in Bioremediation and Environmental Sustainability. Switzerland: Springer Nature; 2020. p.1-20.
- Wackett LP, Hershberger CD. Biocatalysis and Biodegradation: the Microbial Transformation of Organic Compounds. Washington, USA: ASM Press; 2001.
- Weidenhamer JD, Clement ML. Leaded electronic waste is a possible source material for lead-contaminated jewelry. *Chemosphere* 2007;7:1111-5.

Environmental and Microbial Influences on Corrosion of Selected Types of Petroleum Industry Steel

Anwuli U. Osadebe*, Dorcas C. Olorondu, and Gideon C. Okpokwasili

Department of Microbiology, Faculty of Science, University of Port Harcourt, P.M.B. 5323, Choba, Nigeria

ARTICLE INFO

Received: 22 Jan 2021
Received in revised: 13 Apr 2021
Accepted: 23 Apr 2021
Published online: 1 Jun 2021
DOI: 10.32526/enrj/19/2021004

Keywords:

Corrosion/ Environment/ Iron bacteria/ Steel/ Sulphate reducing bacteria/ Petroleum industry

* Corresponding author:

E-mail: anwuli.osadebe@gmail.com

ABSTRACT

This study explored the influence of brackish water sediment, mangrove swamp sediment, clayey/lateritic soil, and river water (freshwater) sediment on the corrosion rates of carbon, mild, and stainless steels and the species of sulphate reducing bacteria (SRB) and iron bacteria associated with the process. The material loss following burial of the steel samples for a 9-month period was assessed. Standard and specialised microbiological techniques were employed in the characterisation of the bacterial species. Qualitative assessment for corrosion was done via optical microscopy and macroscopy. Corrosion was highest on steel buried in brackish water sediment and lowest in that from river water sediment. Carbon steel was the most susceptible to corrosion while stainless steel was the most resistant. Sulphite, sulphide, nitrate and phosphate concentrations had a strong impact on corrosion rates. *Thiobacillus*, *Leptothrix* and *Gallionella* dominated amongst the iron bacteria while *Desulfobacter* and *Desulfovibrio* dominated amongst the SRB. There were significant differences in corrosion rates and bacterial abundance from one environment to the other. Iron bacteria showed greater abundance than SRB across the different environments and steel types. Iron bacteria counts, however, did not correlate positively with corrosion rates. The findings suggest that oil industry facilities in brackish water environments are more liable to corrosion than those located in fresh water ecosystems.

1. INTRODUCTION

Corrosion is a naturally occurring electrochemical process driven by physical, chemical or biological processes working in synergy. Environmental stimuli around the metal are the most common triggers of physicochemical corrosion. Properties like characteristics of the metal, chloride and SO₂ deposition rates, temperature, humidity, pH, salinity and length of exposure are key initiators of physical and chemical corrosion in steel installations (Yan et al., 2020). Biological corrosion, more commonly tagged microbially influenced corrosion (MIC), is the irreversible deterioration of metal by the activities of microorganisms. It is also termed biocorrosion. MIC results from the combined action of microbial cells, their cellular metabolites, the metal surface and environmental factors (Maluckov, 2012). Groups of microorganisms will often adhere to surfaces via biofilms; MIC then ensues beneath these

biofilms via mechanisms like direct electron transfer, cathodic depolarization, build-up of a concentration gradient or galvanic cell formation (Akpan and Iliyasu, 2015; Da Silva et al., 2019). Microbial involvement has been reported to speed up corrosion rates by up to ten times (Liu and Cheng, 2018).

Steel is the material of choice for oil and gas and marine installations. It is used for the construction of platforms and transportation infrastructure for the conveyance of petroleum and water amongst other uses. Most pipelines are constructed with carbon steel. Although highly prone to corrosion and attack by microbes, carbon steel is preferred as it succumbs easily to welding, endures bending well and is less liable to cracking under stress. Furthermore, it is considered durable and of relatively low cost. Mild steel and stainless steel, though not as popular as carbon steel, are also used. Stainless steel is considered expensive and less malleable. The

Citation: Osadebe AU, Olorondu DC, Okpokwasili GC. Environmental and microbial influences on corrosion of selected types of petroleum industry steel. Environ. Nat. Resour. J. 2021;19(4):310-319. (<https://doi.org/10.32526/enrj/19/2021004>)

susceptibility of steel to corrosion is a chief concern in oil and gas plants as the maintenance of failed pipelines and fittings is often not only expensive but challenging. This is especially true of sub-surface instalments. Mechanical failure with regards to pipelines is usually corrosion-related in form of rupture from loss of wall thickness or fracturing (Hou et al., 2016; Valencia-Cantero and Peña-Cabriales, 2014). Corrosion of carbon steel was reported to be about 6 times greater when SRB are involved with the corrosion pit depth 7.7 times deeper than without SRB (Liu et al., 2019).

Research establishes a 4% and 20% reduction in national Gross Domestic Product (GDP) in developing and developed countries respectively due to corrosion in industry (Kruger, 2011; Hou et al., 2017; Fayomi et al., 2019). Arena-Ortiz et al. (2019) place the global corrosion cost including management measures at \$4 trillion. In 2011, corrosion accounted for \$13.4 billion in annual expenses in the US petroleum industry with biocorrosion consuming \$2 billion of the sum (Bermont-Bouis et al., 2007). Corrosion has been implicated in most cases of pipeline failure in the Gulf of Mexico (Arena-Ortiz et al., 2019). In the global oil and gas sector it is estimated that for 50% of buried installations and about 40% of internal pipelines, MIC accounts for the observed corrosion. For anaerobic environments, the total value for both is lower at about 20% (Bano and Qazi, 2011; Rasheed et al., 2019).

Sulphate Reducing Bacteria (SRB), Sulphate Oxidising Bacteria (SOB), Iron Oxidising Bacteria (IOB), Iron Reducing Bacteria (IRB), manganese-oxidisers and acid-producing bacteria are the main microbial groups involved in MIC (Beech and Gaylarde, 1999; Bano and Qazi, 2011; Akpan and Iliyasu, 2015). Khouzani et al. (2019) opine that SRB are the main culprits in severe biodeterioration and rupture of buried pipelines. SRB are anaerobic and so where oxygen is present, they tend to occur underneath deposits of soil, sediment or rust on the pipeline or even beneath an already formed biofilm creating the oxygen-deficient microenvironment they require (Liu et al., 2019). Iron bacteria are a group of aerobic bacteria that generate energy by oxidation of ferrous ions as a key part of their metabolism (Bryce et al., 2018). They are the main culprits of rust deposits on metals and are known to cause corrosion by creating an oxygen gradient which splits the metal surface to which the biofilm is attached into small anodic sites surrounded by larger cathodic areas. They are more

commonly associated with the crevice type of corrosion (Beimeng et al., 2015). SRB and iron bacteria often co-exist on buried metal infrastructure and tend to exert a more aggressive corrosive effect as a team than as individual colonisers of the metal surface (Valencia-Cantero and Peña-Cabriales, 2014).

An understanding of the varying influences on the rate of corrosion of steel is essential to predicting its longevity and suitability for purpose. In this study, corrosion of three types of steel used in the petroleum industry was analysed using microscopic assessment and weight loss to establish corrosion rates relative to environmental conditions. Furthermore, the species of autochthonous SRB and iron bacteria associated with the observed corrosion were determined.

2. METHODOLOGY

2.1 Sample sites

The sediment/ soil for this study were mangrove swamp sediment, brackish water sediment, fresh (river) water sediment and clayey/lateritic soil. All the mangrove swamp and brackish water sediment samples were collected from Eagle Island in Nkpolu area of Port Harcourt, Rivers State. The freshwater sediment samples were obtained from the New Calabar River, Choba, Nigeria. The sampling site for the ochre-coloured clayey/lateritic soil was the Postgraduate Hall of Abuja campus, University of Port Harcourt.

2.2 Study design

The study was field based. The steel samples were placed in fabricated wide-mesh plastic baskets before being buried to a depth of 1 m, similar to the minimum depth for pipelines, for a period of 9 months. The baskets were for ease of location and retrieval while allowing the bars to be in complete contact with the environment on all sides. Sediment or soil samples from the area around the metal bars were taken before and during retrieval for physicochemical and microbiological analysis. Sampling was done in triplicates.

2.3 Sample collection

2.3.1 Steel samples

Three types of structural grade customised steel bars were used to monitor the rate of corrosion in the environment-carbon steel ASTM A36, mild steel ASTM A283 and stainless steel ASTM A316L. The samples were supplied by Sirpi AluSteel Construction

Ltd., Trans-Amadi Industrial layout, Port Harcourt, Nigeria. The bars measured 80 mm × 25 mm × 6 mm. The minimum recommended pipeline thickness is

6.35 mm (0.25 in). The mechanical properties of the steel bars used are described in [Table 1](#).

Table 1. Mechanical Properties of the Metal Samples

Sample	CS ASTM A36	MS ASTM A283	SS ASTM A316L
Type	Structural quality carbon	Structural quality carbon	Austenite
Condition of steel	AS Rolled	AS Rolled	Annealed
Tensile strength (KSI)	58-80	55-60	75 minimum
Yield strength (KSI)	36 minimum	30 minimum	30
% Elongation in "2"	23	25	60 minimum
% Elongation in "8"	20	22	65
Approx. Brinell hardness	137	133	180
Carbon content (%)	0.26-0.29	0.24	0.03

CS=Carbon steel; MS=Mild steel; SS=Stainless steel

The steel bars of known weight were first degreased using analytical grade acetone and then rinsed with distilled water. This was followed by sterilisation by immersion in ethanol for 30 sec. They were then dried and kept desiccated ([Rasheed et al., 2019](#)). The final weights of the steel bars in the desiccator were determined prior to burial.

2.3.2 Soil/sediment sample collection

Samples of soil and sediment were collected for analyses prior to burial of the steel bars and after their retrieval. The soil samples were collected for analyses using a hand trowel and put in heat resistant plastic bottles. Sediment samples were obtained using a sediment grab. Water samples were collected using a 1 L clean plastic container. All the samples were appropriately labelled with date, time and place of collection.

2.4 Determination of physicochemical parameters

The physicochemical parameters were measured in the environments before burial and at retrieval. Salinity was determined using a digital salinometer (Hanna Instruments), while for pH, a pH meter (Wintab digital pH meter, Germany) was used. The sulphate (SO_4^{2-}), sulphite (SO_3^{2-}) and sulphide (S^{2-}) concentrations were determined using the method of [Fogg and Wilkinson \(1952\)](#). The ferric ion (Fe^{3+}) concentration was measured using the ferrozine assay. Electrical conductivity was determined using a benchtop combination meter. The nitrite (NO_2^-) and nitrate ion (NO_3^-) content was measured using the spectrophotometric method described by [Narayana and Sunil \(2009\)](#). The combined modified methods of spectroscopy and molybdenum blue phosphorus

method of [Kharat and Pagar \(2019\)](#) was used for analysis of phosphate ion (PO_4^{3-}) content.

2.5 Determination of loss in material and corrosion analysis

The outer debris on the steel bars was carefully rinsed off with distilled water. Following removal of any attached biological material via probe sonication and drying in an oven (ThermoFisher Scientific PR305225M, USA) at 70°C for 15 min, the dimensions of the bars were determined using calipers and a ruler. The weights of the steel bars were measured as well using an analytical balance (Mettler Toledo New Classic ML204T, Switzerland). The Area was calculated. The volume of the bars was determined using the modified water displacement technique of [Hargens et al. \(2014\)](#).

Corrosion analysis was via the weight loss technique. Assuming uniform corrosion over the entire surface of the bars, the corrosion rate in millimetre per year was determined using the formula from [Daille et al. \(2020\)](#):

$$CR = \frac{KW}{ATD}$$

Where; CR=corrosion Rate, K is a constant (8.76×10^4), W=weight loss in grams, A=area in cm^2 , T=time of exposure in hours, and D=density in g/cm^3 .

2.6 Qualitative analysis of steel bars

The cleaned corroded surfaces of the retrieved bars were observed under the x400 magnification of the optical microscope. Visible (non-microscopic) changes were also recorded.

2.7 Enumeration and characterisation of micro-organisms from biofilms

The biofilms formed on the retrieved metal samples were scrapped off using sterile surgical blade. Any possible remaining biological material was extracted by sonification. The scrapings were collected in sterile bottles containing about 5 mL phosphate buffered saline at pH 7. Following four-fold serial dilution, 1 mL aliquots were plated out on specialised media in triplicates using the pour plate technique. Discrete colonies were purified by streaking unto fresh media. Pure cultures were preserved on relevant media slants for further investigation.

The iron bacteria medium described by APHA (2012) at pH 5.0 was used for the isolation of iron bacteria. Incubation was at room temperature for 7-14 days. Postgate B medium was used for the isolation of the sulphate reducing bacteria, SRB. Inoculation was done via the tube method. After inoculation, the tubes were rapidly cooled with screw caps to seal the tubes to prevent aeration and dehydration of the medium. The cultures were incubated at room temperature in an anaerobic jar containing Gas Pak for about 4 weeks with regular observation for the black colonies representative of sulphate reducing bacteria (SRB).

The abundance of the SRB and iron bacteria isolates was determined in colony forming units per

gram (CFU/g) using an automated colony counter. Identification of the isolates was on the basis of cell morphology and cultural and biochemical characteristics. Apart from the microscopic observation of the cells and observation of colony characteristics, several standard biochemical tests were employed in the characterisation of the isolates; some of the tests include Gram's staining, urease production, lysine utilisation, nitrate reduction, hydrogen sulphide production, citrate utilisation, motility, methyl red, Voges Proskauer reaction, ornithine utilisation, gelatine liquefaction, triple sugar iron test, phenylamine deamination, indole production, starch utilisation, catalase reaction, oxidase production, ONPG and utilisation of 10 simple and complex sugars.

2.8 Statistical analysis

The relationship between corrosion rates and SRB and iron bacteria counts and physicochemical parameters from one environment to the other was assessed using Microsoft Excel 2016.

3. RESULTS AND DISCUSSION

3.1 Physicochemical influences

The changes in the physicochemical properties of the different environments studied before burial of the bars and at retrieval are shown in Table 2.

Table 2. Observed variation physicochemical characteristics during the study

Parameters	Brackish water sediment		Mangrove swamp		Clayey/lateritic soil		River water sediment	
	At burial	At retrieval ^a	At burial	At retrieval ^a	At burial	At retrieval ^a	At burial	At retrieval ^a
pH	7.65	7.10	3.72	6.88	6.27	6.84	6.14	6.05
Salinity (ppt)	15.303	13.000	13.100	10.327	0.011	0.010	0.002	0.001
Conductivity (µS/m)	738	1011	1724	814	212	484	388	548
PO ₄ ³⁻ (mg/kg)	0.149	1.40	0.0002	0.05	0.0121	0.50	0.0086	0.70
NO ₃ ⁻ (mg/kg)	1.00	93.60	1.10	112.20	1.20	835.70	1.40	54.90
S ²⁻ (mg/kg)	30.40	41.20	29.30	53.60	17.00	32.28	13.30	5.59
SO ₄ ²⁻ (mg/kg)	0.10	8.29	0.25	3.39	0.25	0.077	0.15	0.219
SO ₃ ²⁻ (mg/kg)	0.10	7.50	0.25	12.50	0.25	11.00	0.15	11.00
Fe ³⁺ (mg/kg)	0.07	7.97	0.02	5.37	0.03	5.54	0.06	34.94
NO ₂ ⁻ (mg/kg)	0.00	2.20	0.20	0.16	0.20	0.70	0.30	0.59

a=month 9-peak of wet season

A study on biocorrosion by SRB in the Yucatan Peninsula concluded that physicochemical properties have a strong influence on corrosion rates (Arenas-Ortiz et al., 2019). In the same vein, Obuekwe et al. (1987) demonstrated extensive pitting of mild steel when ferrous and sulphide ions were being formed

concurrently. When only sulphide was produced, corrosion rates first increased and then declined due to the formation of a protective iron sulphide (FeS) film. Gubner and Andersson (2007) and Agarry et al. (2015) both linked corrosion rates to pH levels. It has been found that pH exerts a stronger impact on corrosion

rates than salinity or nitrate concentration with the more acidic pH levels encouraging faster corrosion rates. The observed pH in this current study generally revolved around neutral except in the mangrove swamp sediment where more acidic values were originally observed.

3.2 Observed corrosion, corrosion rates, and environmental influences

The steel samples from brackish water sediment and Mangrove swamp sediment demonstrated the greatest loss in material and the highest corrosion rates. Stainless steel samples fared best having the lowest material loss while carbon steel showed relatively high material loss. Table 3 outlines the mean

percentage material loss in thickness, area, volume and weight observed.

Table 4 highlights the physical changes observed in the different steel samples following retrieval while Figure 1 provides a comparison of corrosion rates across the four environments studied. Carbon steel showed the greatest corrosion rates across the board followed by mild steel. Corrosion rates ranged from 0.07214-0.76505 mm/year, 0.0668-0.55143 mm/year, 0.00991-0.23851 mm/year and 0.00762-0.23038 mm/year for brackish water sediment, mangrove swamp sediment, lateritic soil, and river water sediment, respectively, from stainless steel (lowest observed values) to carbon steel (highest values).

Table 3. Mean percentage material loss in the steel samples

Sample	% Loss in area	% Loss in thickness	% Loss in volume	% Loss in weight
CS E ₁	5.63	6.86	12.10	2.66
CS E ₂	5.60	20.59	25.04	2.35
CS E ₃	1.15	6.13	7.20	1.32
CS E ₄	0.72	4.68	5.37	0.82
MS E ₁	1.71	1.12	2.81	1.41
MS E ₂	2.53	3.66	6.10	0.86
MS E ₃	0.58	2.84	3.40	0.48
MS E ₄	0.69	2.22	4.57	0.27
SS E ₁	0.39	0.004	0.78	0.41
SS E ₂	0.69	1.69	2.38	0.34
SS E ₃	1.80	0.00	0.00	0.05
SS E ₄	0.002	0.20	0.20	0.005

CS=Carbon steel; MS= Mild steel SS=Stainless steel

E1= Brackish water sediment E2=Mangrove swamp bottom sediment; E3=Clayey/lateritic soil; E4=River Water sediment

Table 4. Qualitative assessment of the retrieved steel bars

Sample	Corrosion-related observations after retrieval
Carbon Steel ASTM A36	
CS E ₁	Generalised corrosion (iron oxide). Very heavy pitting on most of the surfaces. Presence of crevices. Severe edge corrosion. Presence of sulphide coatings
CS E ₂	Extensive corrosion. Crevice corrosion and surface corrosion. Deposition of iron oxide as well as sulphide coatings. Pitting significantly present.
CS E ₃	Generalised surface corrosion. Sulphide coating on one side of the slab surface. Scanty blister formations. Localised deep pitting on one side of the slab surface. Scaling effect along the edges.
CS E ₄	Generalised surface corrosion with deposition of iron oxide. No pitting or sulphide coating seen. Scaling effect not too severe.
Mild Steel ASTM A283	
MS E ₁	Generalised corrosion (iron oxide). Deep pitting, sulphide coating, scaling along the edges.
MS E ₂	Extensive corrosion. Heavy pitting and skinning effects concentrated around the edges. Presence of sulphide cover.
MS E ₃	Generalised corrosion. Less pitting and skinning effect. Sulphide cover on one side of the slab. No crevices observed
MS E ₄	Generalised corrosion, no pitting or skinning

CS=Carbon steel; MS= Mild steel SS=Stainless steel

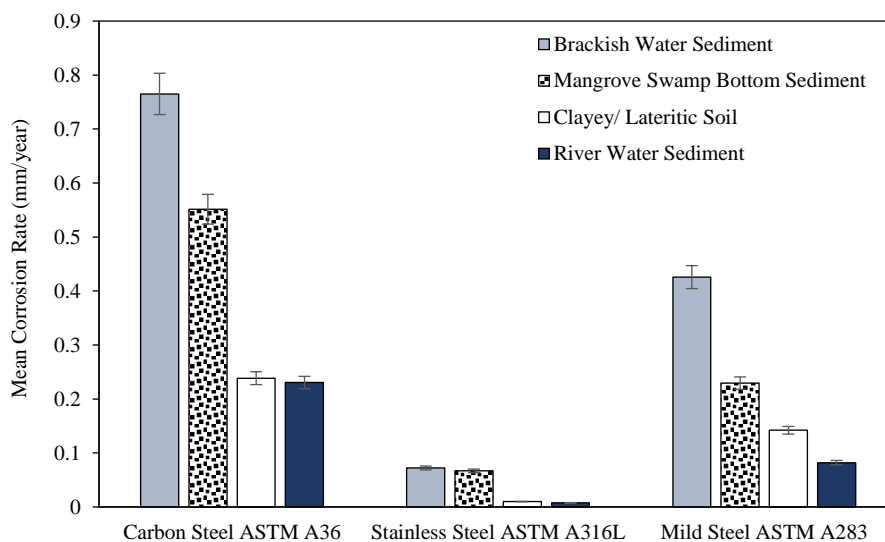
E1= Brackish water sediment E2=Mangrove swamp bottom sediment; E3=Clayey/lateritic soil; E4=River Water sediment

Table 4. Qualitative assessment of the retrieved steel bars

Sample	Corrosion-related observations after retrieval
Stainless Steel ASTM A316L	
SS E ₁	Only slight corrosion observed on both surfaces of the slab, localised pitting observed.
SS E ₂	Localised pitting and blackening on both surfaces of the slab and along edges. Concentrated deposition of iron oxide along the edges where blackening was observed.
SS E ₃	Localised fine pitting on a small area of only one surface
SS E ₄	Two separate pitting portions with formation of iron oxide on only one surface. Fine localised pitting observed.

CS=Carbon steel; MS= Mild steel SS=Stainless steel

E1= Brackish water sediment E2=Mangrove swamp bottom sediment; E3=Clayey/lateritic soil; E4=River Water sediment

**Figure 1.** Mean corrosion rates of the different steel types

Pure iron is innately reactive and so naturally corrodes quite rapidly. The addition of carbon makes iron more stable; this stability is informed by both the concentrations of incorporated carbon and the presence of other alloying elements. The greatest mean material loss and highest corrosion rate was seen with the carbon steel bars most likely because it is the steel with the highest percentage of incorporated carbon (0.26-0.29%) in the absence of other alloying metals. The mild steel bars (0.24% carbon) from the results come next in mean material loss and corrosion rates. Stainless steel (0.03% carbon) demonstrated a stronger resistance to MIC than the other steel types having the lowest mean material loss and corrosion rate. Apart from its low carbon content, this resistance could be further attributed to the presence of certain alloying elements like chromium and nickel. Its chromium content (10.5-11.0%) particularly, results in the formation of an oxidation-inhibiting chromium oxide layer in oxygenated systems.

Average percentage weight loss (APWL) values under microbial influence, in one study, were found to be 2.8% and 5.4% for MS in sandy soil and water-

logged soil, respectively, and 3.6% and 4.5% for CS in sandy soil and water-logged soil, respectively. For the SS, APWL was 0.12% and 0.08% for the water-logged soil and the sandy soil, respectively (Oparaodu and Okpokwasili, 2014). While this corroborates the finding in this study that MIC proceeds at faster rates in anaerobic or low oxygen environments, the APWL values in the present study are lower than those recorded.

The higher corrosion rates observed in the mangrove swamp and brackish water sediment corresponds with conclusions from a study on the biocorrosion of stainless steel in varying tidal cycles in a coastal region that high salinity tends to be associated with increased corrosion rates (Daille et al., 2020). Several studies report similar microorganism-induced corrosion rates as recorded in the current study. An assessment of microbial biofilms on carbon steel found comparable corrosion rates of 0.45 ± 0.01 - 0.12 ± 0.01 mm/year dependent on environmental conditions (De Melo et al., 2011). Pratikno and Titah (2016) observed corrosion rates of 0.5797-0.6173 mm/year in steel during a ten-day study in saline and

seawater environments. With the introduction of microorganisms, these rates reached levels 2-3 times greater. In the presence of *Thiobacillus ferroxidans*, this value increased to 1.253-1.3212 mm/year. Other studies, however, recorded corrosion rates much greater than this study. Corrosion rates in a study in Nigeria were 3.51 mm/year, 5.58 mm/year, and 0.32 mm/year for CS, MS and SS, respectively, in water-logged soil and 3.67 mm/year, 3.18 mm/year, and 0.19 mm/year, respectively, in sandy soil (Oparaodu and Okpokwasili, 2014). Maximum biocorrosion rates of

4 mm/year on carbon steel were found in a study on corrosion of linepipe steel, while *Acidophilis ferroxidans* on carbon steel was found to achieve MIC rates of about 8 mm/year at pH 2 (Al-Abbas et al., 2013; Zlatev et al., 2013).

3.3 Microbial influences

The isolates obtained from the biofilms and their occurrence are illustrated in Figure 2. For iron bacteria, 5 genera from 17 isolates were observed, while SRB had 7 genera from 48 isolates.

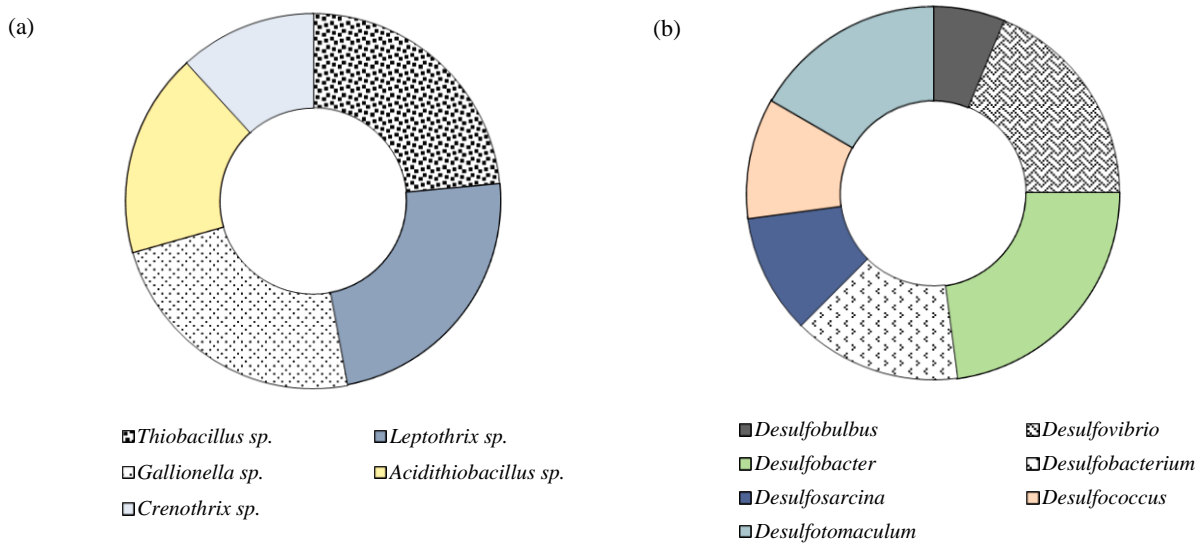


Figure 2. Distribution of Iron Bacteria (A) and SRB (B) Genera Isolated

The mean counts observed for iron bacteria and SRB across the different environments before and after retrieval of the steel bars is summarised in Table 5. SRB generally showed lower counts than iron bacteria but had the higher mean percentage increase in counts compared to the control; 82.14-1081.48% increase in SRB abundance compared to the 79.88-147.94% increase seen in iron bacteria counts. The greatest SRB counts were seen in brackish water sediment for CS and MS and mangrove swamp sediment for CS. Iron bacteria showed the highest abundance in clayey/lateritic soil and river water sediment. The highest abundance of iron bacteria counts was seen with carbon steel in clayey/lateritic soil.

The enhanced abundance of SRB and iron bacteria after retrieval of the steel bars is considered confirmation that the observed corrosion is microbially influenced (Beech et al., 2000). The number of SRBs decreased as one moved from E1-E4 possibly because of the change in environment from anaerobic to fairly aerobic. Aerobic because soil and

river water samples are not water-logged and where inundated still allow the diffusion of oxygen as the inhibiting salt molecules found in anaerobic environments are absent. The mostly anaerobic and halophytic nature of the mangrove swamp aids in the expulsion of oxygen (Knight et al., 2013). Iron bacteria counts, in contrast, increased as one moved from E₁-E₄. Iron bacteria show a proclivity for more acidic environments so the observed counts tended to increase as their iron precipitating activity makes the environment more acidic further encouraging their growth. This corresponds with the findings of Agarry et al. (2015) that pitting corrosion (commonly associated with the iron bacteria) of mild steel in an acidic environment was more severe. The lack of a sulphide coating on the steel samples from the river water sediment found in the current study, tallies with the low SRB counts observed in the river water sediment (Table 4). It would mean that MIC in the more aerated systems is dominated by iron bacteria over the SRB.

Table 5. Mean abundance of SRB and iron bacteria

Sample	Sulphate reducing bacteria $\times 10^2$ (CFU/g)		Iron bacteria $\times 10^2$ (CFU/g)	
	Before burial	At retrieval	Before burial	At retrieval
Brackish water sediment	4.65	8.50	6.80	9.11
CS E ₁	-	12.05	-	14.10
MS E ₁	-	11.50	-	14.01
SS E ₁	-	8.53	-	13.65
Control	4.65	4.03	6.80	7.23
Mangrove swamp sediment	1.75	6.30	8.30	8.56
CS E ₂	-	11.35	-	15.49
MS E ₂	-	9.40	-	15.22
SS E ₂	-	5.10	-	14.93
Control	1.75	2.89	8.30	8.52
Clayey/lateritic soil	0.40	2.90	13.04	18.80
CS E ₃	-	4.20	-	24.99
MS E ₃	-	3.19	-	24.46
SS E ₃	-	1.02	-	23.71
Control	0.40	0.33	13.04	12.99
River water sediment	0.49	1.20	8.97	17.41
CS E ₄	-	1.70	-	22.24
MS E ₄	-	1.15	-	22.05
SS E ₄	-	0.75	-	21.10
Control	0.49	0.40	8.97	9.04

E₁=Brackish Water Sediment; E₂=Mangrove Swamp Bottom Sediment; E₃=Clayey/Lateritic Soil; E₄=River Water Sediment

The presence of substantial numbers of iron oxidising bacteria, iron reducing bacteria and sulphate reducing bacteria has been recorded in biofilms from carbon steel associated with diesel and biodiesel mixtures (De Melo et al., 2011). SRB counts in soils around corroded pipelines ranged from 2.5×10^3 CFU/g - 6.50×10^4 CFU/g. The microbial community analysis in an offshore oil production facility indicated that, like in the current study, *Desulfovibrio* species, dominated in the biofilms (Vigneron et al., 2016). The species of SRB identified in biofilms of corroded oil pipelines in Rivers state, Nigeria were *Desulfuromonas acetoxidans*, *Desulfobulbus propionicus*, and *Desulfosarcina variabilis*, while *Desulfobulbus* sp. and *Desulfobacterium* sp. dominated in a study on a drinking water reservoir in Eastern China (Akpan and Iliyasu, 2015; Yang et al., 2015). Akin to the current study where abundance varied but diversity was relatively the same from one environment to the other, a study on four different environments in Mexico concluded that the distribution of SRB genera was relatively consistent across the different environment but the abundance differed. The SRB group implicated in corrosion of steel out of 37 isolates were *Desulfatibacillum*, *Desulfatitalea*, *Desulfobacula*, *Desulfobulbus*,

Desulfotignum, *Desulfotomaculum*, *Desulfovibrio*, and *Sulfurospirillum*. *Desulfatibacillum* was more abundant in the lagoon and the sea while *Desulfovibrio* were more abundant in the freshwater environment. In the wetlands, *Desulfotignum*, *Desulfovibrio*, and *Desulfatibacillum* had the highest counts. *Desulfotomaculum* was spread across the sampling sites (Arena-Ortiz et al., 2019).

It has been noted that SRB and IR work in tandem, the product of one being the antecedent for the other's growth. SRB oxidise sulphides back to sulphates in oxygenated soils producing gypsum if calcium is present in the soil or sulphuric acid in the absence of calcium with a resultant reduction in pH to around 2-3. This drop in pH restricts the growth of SRB but supports the proliferation of iron bacteria. A lack of correlation between the degree of corrosion and the counts of attached microbial cells in a biofilm layer was reported by Beech et al. (2000). This observation is corroborated by a number of researchers who state that the metabolic by-products of microorganisms have a stronger influence on MIC rates than abundance. Certain researchers maintain that mean corrosion rates generally correlate with soil moisture content (Wan et al., 2013; Oparaodu and Okpokwasili, 2014). This seems to contradict certain findings in the current study

as corrosion rates in clayey/lateritic soil were greater than in river water sediment.

3.4 Statistical analyses

There were statistically significant differences in corrosion rates of MS, CS, and SS from one environment to the other and within each different environment. While iron bacteria counts differed from one environment to the other, SRB counts did not. SRB counts differed significantly from iron bacteria counts across board. A strong positive correlation was observed between corrosion rates for the three types of steel and SO_3^{2-} ($r=0.850$, mean value) and S^{2-} ($r=0.876$, mean value) concentrations, but a weak positive correlation between corrosion rates and SO_4^{2-} concentration ($r=0.266$, mean value) and SRB counts ($r=0.147$, mean value) was seen for CS and SS. For MS, a strong positive correlation ($r=0.710$) was recorded with regards to SO_4^{2-} concentration. This relationship is confirmed by Carbini et al. (2018) who confirmed that sulphite ions increase the corrosion rate of steel. Generally, sulphide formation drives corrosion rates by promoting the establishment of pits in the metal. These pits provide microenvironments for SRB where their activities eventually lead to stress corrosion cracking or hydrogen blistering. Iron bacteria counts, however, did not correlate positively with corrosion rates. A weak negative correlation ($r=-0.181$, mean value) was observed.

The increase in ferric ion (Fe^{3+}) concentration is indicative of the oxidation of iron, an occurrence fundamental to the corrosion process. Some researchers also maintain that it points to the activities of iron bacteria. Iron bacteria are known to precipitate Fe^{3+} which impedes corrosion unlike Fe^{2+} or $\text{Fe}(\text{SO}_4)_3$ that fuels the corrosion process. Iron bacteria hardly instigate corrosion but often facilitate the process using the by-products formed. An alternative influence of Fe^{2+} ions on corrosion rates lies in their proven capacity for enzyme regulation. Cheung and Beech (1996) established the regulatory action of ferrous ion (Fe^{2+}) on hydrogenase enzyme activity in *Desulfovibrio vulgaris*. The presence of Fe^{3+} ion did not have the same effect. A strong negative correlation ($r=-0.598$, mean value) was observed between NO_3^- concentrations and corrosion rates. This could be due to the ability of some SRB species to metabolise NO_3^- under low SO_4^{2-} concentrations. There was a greater build-up of nitrate ions (NO_3^-) than nitrites (NO_2^-) as corrosion proceeded. No relationship was observed between nitrite (NO_2^-) concentrations and corrosion

rate. The results for phosphate (PO_4^{3-}) indicated that an increase in phosphate concentration would precipitate a resultant increase in corrosion rates as a strong positive correlation was found between phosphate concentration and corrosion rates.

4. CONCLUSION

The study suggests that environmental conditions and the presence of SRB and iron bacteria play a significant role in the corrosion rate of steel. The findings showed that the more saline environments of the mangrove swamp and brackish water sediment had a stronger influence on corrosion rates. Sulphite, sulphide, nitrate and phosphate concentrations had a strong impact on observed corrosion rates. SRB showed greater influence in the more anaerobic mangrove swamp sediment and brackish water sediment, while iron bacteria had greater impact in the relatively aerobic lateritic soil and river water sediment. The different metals in order of resistance to corrosion and microbial attack were Stainless steel>Mild steel>Carbon steel. Stainless steel is, therefore, recommended for oil and gas installations where feasible.

CONFLICT OF INTEREST STATEMENT

The authors declare that there are no conflicts of interest regarding the publication of this manuscript.

REFERENCES

- Agarry SE, Salam KK, Arinkoola AO, Soremekun IO. Microbiologically influenced corrosion of mild steel in crude oil environment. European Journal of Engineering and Technology 2015;3(6):40-52.
- Akpan GU, Iliyasu M. Biocidal effects of ozone, sodium hypochlorite and formaldehyde, on sulphate reducing bacteria isolated from biofilms of corroded oil pipelines in the Niger Delta, Nigeria. Donnish Journal of Microbiology and Biotechnology Research 2015;2(2):8-14.
- Al-Abbas FM, Bhola SM, Spear JR, Olson DL, Mishra B. The shielding effect of wild type iron reducing bacterial flora on the corrosion of linepipe steel. Engineering Failure Analysis 2013;33:222-35.
- American Public Health Association (APHA). Standard Methods for the Examination of Water and Wastewater. 22nd ed, Washington D.C., USA: APHA; 2012.
- Arena-Ortiz LM, Muhilan M, Reyes-Sosa M, Ortiz-Alcantara J. Bio-corrosion, sulfate-reducing bacteria in the Yucatan Peninsula. Journal of Marine Biology and Oceanography 2019;8(1):1000202.
- Bano AS, Qazi JI. Soil buried mild steel corrosion by *Bacillus cereus*-SNB4 and its inhibition by *Bacillus thuringiensis*-SN8. Pakistan Journal of Zoology 2011;43(3):555-62.
- Beech IB, Gaylarde CC. Recent advances in the study of biocorrosion: An overview. Revista de Microbiologia 1999;30(3):177-90.

- Beech I, Bergel A, Mollica A, Flemming H, Scotto V, Sand, W. Simple methods for the investigation of the role of biofilms in corrosion. In: Microbially Influenced Corrosion of Industrial Materials. Brite-Euram III Thematic Network No. ERB BRRT-CT98-5084. Biocorrosion Network; 2000.
- Beimeng QI, Chongwei C, Yixing Y. Effects of Iron bacteria on cast iron pipe corrosion and water quality in water distribution systems. *International Journal of Electrochemical Science* 2015;10:545-58.
- Bermont-Bouis D, Janvier M, Grimont PAD, Dupont I, Vallaeys T. Both SRB and Enterobacteriaceae take part in marine biocorrosion of carbon steel. *Journal of Applied Microbiology* 2007;102:161-8.
- Bryce C, Blackwell N, Schmidt C, Otte J, Huang Y, Kleindienst S, et al. Microbial anaerobic Fe(II) oxidation-ecology, mechanisms and environmental implications. *Environmental Microbiology* 2018;20(10):3462-83.
- Carbini M, Lorenzi S, Pastore T. Effects of thiosulphates and sulphite ions on steel corrosion. *Corrosion Science* 2018; 135:158-66.
- Cheung CWS, Beech IB. The use of biocides to control sulphate reducing bacteria in biofilms on mild steel surfaces. *Biofouling* 1996;9:231-49.
- Daille LK, Aguirre J, Fischer D, Galarce C, Armijo F, Pizarro GE, et al. Effect of tidal cycles on bacterial biofilm formation and biocorrosion of stainless steel AISI 316L. *Journal of Marine Science and Engineering* 2020;8:124.
- Da Silva PS, de Senna FL, Goncalves MMM, do Lago DCB. Microbiologically-influenced corrosion of 1020 carbon steel in artificial seawater using garlic oil as natural biocide. *Materials Research* 2019;22(4):e20180401.
- De Melo IR, Filho SLU, Oliveira FJS, de França FP. Formation of biofilms and biocorrosion on AISI-1020 carbon steel exposed to aqueous systems containing different concentrations of a diesel/biodiesel mixture. *International Journal of Corrosion* 2011;2011:415920.
- Fayomi OSI, Akande IG, Odigie S. Economic impact of corrosion in oil sectors and prevention: An overview. *Journal of Physics: Conference Series* 2019;1378:022037.
- Fogg DN, Wilkinson NT. The determination of sulphur, sulphide, thiosulphate, sulphite and sulphate in commercial calcium chloride. *Journal of Applied Chemistry* 1952;2(7):357-67.
- Gubner R, Andersson U. Corrosion Resistance of Copper Canister Weld Material. Technical Report TR-07-07. Stockholm, Sweden: Swedish Nuclear Fuel and Waste Management Co; 2007.
- Hargens AR, Kim JM, Cao P. Accuracy of water displacement hand volumetry using ethanol and water mixture. *Aviation, Space and Environmental Medicine* 2014;85(2):187-90.
- Hou Y, Lei D, Li S, Yang W, Li C. Experimental investigation on corrosion effect on mechanical properties of buried metal pipes. *International Journal of Corrosion* 2016;5808372.
- Hou B, Li X, Ma X, Du C, Zhang D. The cost of corrosion in China. *Npj Materials Degradation* 2017;1:1-10.
- Kharat SJ, Pagar SD. Determination of phosphate in water samples of Nashik District (Maharashtra State, India) rivers by UV-Spectroscopy. *Journal of Chemistry* 2019;6(1):515-21.
- Khouzani MK, Bahrami A, Hosseini-Abari A, Khandouzi M, Taheri P. Microbiologically influenced corrosion of a pipeline in a petrochemical plant. *Metals* 2019;9:459.
- Kruger J. Cost of Metallic Corrosion: Uhlig's Corrosion Handbook. 3rd ed. Hoboken, NJ, USA: Wiley; 2011.
- Knight JM, Griffin L, Dale PER, Sheaves M. Short-term dissolved oxygen patterns in sub-tropical mangroves. *Estuarine, Coastal and Shelf Science* 2013;131:290-6.
- Liu H, Cheng YF. Microbial corrosion of X52 pipeline steel under soil with varied thicknesses soaked with a simulated soil solution containing sulfate-reducing bacteria and the associated galvanic coupling. *Electrochimica Acta* 2018; 266:312-25.
- Liu H, Meng G, Li W, Gu T, Liu H. Microbially influenced corrosion of carbon steel beneath a deposit of CO₂-saturated formation water containing *Desulfotomaculum nigrificans*. *Frontiers in Microbiology* 2019;10:1298.
- Maluckov BS. Corrosion of steels induced by microorganisms. *Metallurgical and Materials Engineering* 2012;18:223-31.
- Narayana B, Sunil K. A Spectrophotometric method for the determination of nitrite and nitrate. *Eurasian Journal of Analytical Chemistry* 2009;4(2):204-14.
- Obuekwe CO, Westlake JA, Plamebek JA. Bacterial corrosion of mild steel under the condition of simultaneous formation of ferrous and sulphide ions. *Applied Microbiology Technology* 1987;26(3):294-8.
- Oparaodu KO, Okpokwasili GC. Comparison of percentage weight loss and corrosion rate trends in different metal coupons from two soil environments. *International Journal of Environmental Bioremediation and Biodegradation* 2014; 2(5):243-9.
- Pratikno H, Titah HS. Biocorrosion of steel structure (ASTM A106 and A53) in marine environment. *Asian Journal of Applied Sciences* 2016;9:120-5.
- Rasheed PA, Jabar KA, Rasool K, Panday RP, Sliem MH, Helal M, et al. Controlling the biocorrosion of sulfate-reducing bacteria (SRB) on carbon steel using ZnO/chitosan nanocomposite as an eco-friendly biocide. *Corrosion Science* 2019;148:397-406.
- Valencia-Cantero E, Peña-Cabriales JJ. Effects of iron reducing bacteria on carbon steel corrosion induced by thermophilic sulphate reducing consortia. *Journal of Microbiology and Biotechnology* 2014;24(2):280-6.
- Vigneron A, Alsop EB, Chambers B, Lomans BP, Head IM, Tsesmetzis N. Complementary microorganisms in highly corrosive biofilms from an offshore oil production facility. *Applied Environmental Microbiology* 2016;82:2545-54.
- Wan Y, Ding L, Wang X, Li Y, Sun H, Wang Q. Corrosion behaviours of Q235 steel in indoor soil. *International Journal of Electrochemical Science* 2013;8:12531-42.
- Yan L, Diao Y, Laang Z, Gao K. Corrosion rate prediction and influencing factors evaluation of low-alloy steels in marine atmosphere using machine learning approach. *Journal of Science and Technology of Advanced Materials* 2020; 21(1):359-70.
- Yang X, Huang TL, Guo L, Xia C, Zhang HH, Zhou SL. Abundance and diversity of sulfate-reducing bacteria in the sediment of the Zhou Cun drinking water reservoir in Eastern China. *Genetics and Molecular Research* 2015;14(2):5830-44.
- Zlatev R, Stoycheva M, Kiyota S, Ovalle M, Valdez B, Ramos R. Microbially induced corrosion rate determination applying Clark amperometric sensor. *International Journal of Electrochemical Science* 2013;8:1079-94.

Characterization and Application of Mangosteen Peel Activated Carbon for Ammonia Gas Removal

Zarah Arwieny Hanami* and Puji Lestari

Faculty of Civil and Environmental Engineering, Bandung Institute of Technology, Bandung 40132, Indonesia

ARTICLE INFO

Received: 9 Jan 2021
Received in revised: 3 May 2021
Accepted: 21 May 2021
Published online: 10 Jun 2021
DOI:10.32526/enrj/19/2020298

Keywords:

Activated carbon/ Adsorption/
Ammonia/ Mangosteen peel

* Corresponding author:

E-mail:
zaraharwienyhanami@gmail.com

ABSTRACT

Mangosteen peel can be used as an activated carbon precursor because of its high lignin content and hardness. In this study, mangosteen peel activated carbon (MP-AC) was prepared by a physical activation method using CO₂ at 850°C. The Brunauer-Emmett-Teller (BET) analysis was used to assess the optimal activation time to identify the largest surface area. The properties of MP-AC were characterized by the SEM-EDS and FTIR analyses. The results showed that MP-AC obtained from the 120-minute activation time had the largest BET specific surface area of 588.41 m²/g and was selected as an adsorbent in the dynamic adsorption of ammonia gas. The values of moisture content, ash content, and iodine number of MP-AC were 6.07%, 9.8%, and 1153.69 mg/g, respectively. Breakthrough curve indicated that with lower inlet concentration and higher adsorbent mass, longer breakthrough time is reached. Equilibrium data was best fitted to the Langmuir isotherm, while the pseudo-first order kinetic model favorably described the adsorption kinetics. The results revealed a potential to utilize MP-AC as an adsorbent for ammonia gas removal with average NH₃ adsorption capacity of 0.41 mg/g.

1. INTRODUCTION

Ammonia (NH₃) is a colorless gas with pungent odor which is emitted from agriculture, fertilizer industry, fossil fuel combustion, and some chemical industries (Vohra, 2020). The typical NH₃ concentrations emitted from the industrial process can range from 5 to 60 ppm (Chung et al., 2001) and ammonia from agricultural activities comprises approximately 80%-90% of total anthropogenic ammonia emissions (Xu et al., 2019). Ammonia is a threat to the environment due to its contribution to aerosol (PM_{2.5}) formation that could adversely affect respiratory and cardiovascular systems, and its deposition leads to eutrophication, acidification, and loss of biodiversity (Xu et al., 2019).

Adsorption using activated carbon is a simple and low-cost method (Guo et al., 2005) to purify NH₃. Many reports have described the adsorption of ammonia gas by activated carbon (Domingo-Garcia et al., 2002; Ro et al., 2015; Vohra, 2020). This adsorption process depends on some factors such as the pore size, area, and surface chemistry (Bernal et al., 2018). Lignocellulosic agricultural wastes with

their abundant availability, biodegradability, and non-toxic nature (Crini and Lichtfouse, 2018) can be used as an ideal precursor to produce activated carbon due to its high carbon content from the lignin composition (Nor et al., 2013). Several studies that used fruit peels for activated carbon productions such as durian peel (Chandra et al., 2009), rambutan peel (Ahmad and Alrozi, 2011), orange peel (Fernandez et al., 2014), and mangosteen peel (Nasrullah et al., 2019) have been conducted, and mangosteen peel has the highest lignin content of 48.63% (Devi et al., 2012).

Mangosteen (*Garcinia mangostana* L.) is a fruit largely found in Indonesia. The production in 2018 reached 228,155 tons which increased 41.05% from the previous year (Statistics Indonesia, 2019). This mass production leads to the peel waste increase (Rattanapan et al., 2014) where, according to Foo and Hameed (2012) and this study, about 60-70% of 1 kg of mangosteen fruit is the peel. Mangosteen peel can be used as an activated carbon precursor because it hardens when exposed to air thus making it suitable for granular activated carbon productions, has high lignin content (Devi et al., 2012) and low volatile

Citation: Hanami ZA, Lestari P. Characterization and application of mangosteen peel activated carbon for ammonia gas removal. Environ. Nat. Resour. J. 2021;19(4):320-329. (<https://doi.org/10.32526/enrj/19/2020298>)

substances, and it has porous properties comparable to commercial activated carbon (Chen et al., 2011).

Physical activation using carbon dioxide (CO₂) has advantages such as creating narrower pores, being easy to control, inexpensive, and environmentally safe (Ahmad et al., 2013; Rangabhashiyam and Balasubramanian, 2019). However, the use of CO₂ activation for mangosteen peel activated carbon (MP-AC) is rarely reported. Mukti et al. (2015) was using steam activation, while other studies were using chemical activation (Rattanapan et al., 2014; Nasrullah et al., 2019). Although the effectiveness of mangosteen peel as an adsorbent in CO₂ and ethylene gas adsorption (Giraldo and Moreno-Piraján, 2017; Mukti et al., 2015) is accepted, none has assessed the MP-AC for the NH₃ adsorption. This study aims to characterize MP-AC prepared by CO₂ activation for NH₃ gas removal. Dynamic adsorption was used to illustrate the real conditions in the environment (Meneghetti et al., 2010; Patel, 2019) where emitted gas moves continuously through the bed. The adsorption capacities, kinetics, and isotherm were also investigated in this study. The results may provide necessary theoretical guidance of this material using physical activation method and implementation in the gas-phase dynamic adsorption.

2. METHODOLOGY

2.1 Adsorbent preparation

Mangosteen peels collected from the market were washed with distilled water and then dried at 105°C for 24 h (Li et al., 2018) before they were crushed using roll crushing machine and mortar grinder RM 200, and sieved into 10-20 mesh size. The carbonization was conducted in a tube furnace, Carbolite Gero HST 12/600 + 301 Controller, with a temperature of 700°C for 3 h under the flow of nitrogen (N₂) gas. The process continued with CO₂ activation under N₂ atmosphere at 850°C for 15, 120, and 180 min. The ramping rate for carbonization and activation process was 10°C/min. The purity of CO₂ and N₂ gases used in this study was industrial grade ≥99% from PT. Aneka Gas Industri.

2.2 Activated carbon characterization

The Brunauer-Emmett-Teller (BET) analysis (Quantachrome Nova Ver 11.0) carried out to determine the surface area through nitrogen adsorption experiment at the temperature of 77 K (-196.15°C). Scanning Electron Microscope-Energy Dispersive Spectroscopy (SEM-EDS, Analytical SEM JEOL

JSM-6510A) was used to determine the morphological and elemental composition of MP-AC. The surface functional group was also determined using FTIR spectroscopy (IRPrestige-21 Shimadzu) at the wave interval of 4,000 and 340 cm⁻¹.

Moisture content, ash content, and iodine adsorption were determined according to the Indonesian standard, SNI 06-3730-1995 (Hastuti et al., 2015). The moisture content test was done by drying 1 g of the MP-AC at 105°C until the constant mass. The MP-AC was heated in the furnace at 600°C for 4 h to determine the ash content. Meanwhile, the iodine number test was performed by mixing 0.5 g of MP-AC with 50 mL of 0.1 N of iodine solution for 15 min. The filtrate (10 mL) was then titrated with 0.1 N of sodium thiosulfate solution and starch as an indicator. The equations used were as follows:

$$\% \text{Moisture content} = \frac{a-b}{a} \times 100\% \quad (1)$$

$$\% \text{Ash content} = \frac{b}{a} \times 100\% \quad (2)$$

$$\text{Iodine number} \left(\frac{\text{mg}}{\text{g}} \right) = \frac{(V_1 N_1 - V_2 N_2) \times 126.93 \times fp}{W} \quad (3)$$

Where; a and b are initial and final mass of activated carbon (g) respectively; V₁ is the analyzed iodine volume (mL); V₂ is the volume of Na₂S₂O₃ used (mL); W is activated carbon weight (g); N₁ and N₂ are the iodine and Na₂S₂O₃ normality (N) respectively; fp is the dilution factor; and 126.93 is the iodine amount corresponding to 1 mL of Na₂S₂O₃ solution.

2.2 Adsorbate preparation

An analytical grade stock solution of ammonia (NH₄OH) was prepared in this study to make artificial gas by aerating dilute ammonia solution (Yani et al., 2013) with an air flow of 880 mL/min for 30 min. The NH₃ gas was produced and collected in a polyethylene bag with a volume capacity of 120 L.

2.3 Adsorption experiment

Dynamic adsorption experiments were conducted in the laboratory using the Duran glass column (diameter=1.2 cm, height=40 cm). The NH₃ gas was injected into the column at a flow rate of 1.1 L/min. The outlet gas was measured by a gas sensor SKY2000-M2 at intervals of one reading per minute. The test was carried out continuously until the adsorbent reached saturated condition. The schematic diagram for the adsorption test is presented in Figure 1.

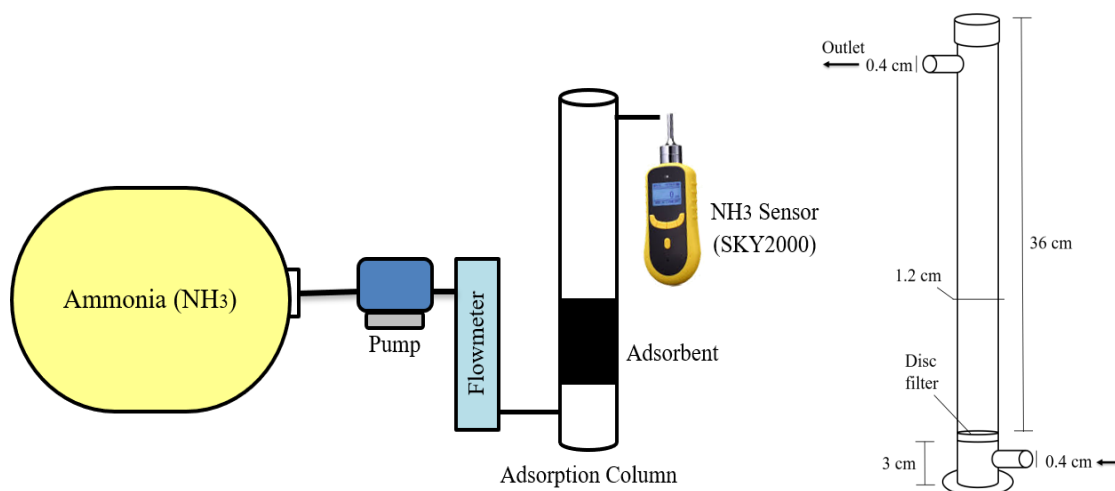


Figure 1. Illustration of the adsorption system test

The variations used in NH_3 adsorption process were adsorbent mass (1, 3, and 5 g) and initial NH_3 concentrations (10 ± 1 , 20 ± 1 , and 40 ± 1 ppm). Data were collected twice for each variation and the adsorption capacity was calculated using equation 4 (Choo et al., 2013):

$$q \left(\frac{\text{mg}}{\text{g}} \right) = \frac{(C_0 - C_t) \text{ mg/L} \times \text{Flowrate (L/min)} \times t \text{ (min)}}{\text{Adsorbent mass (g)}} \quad (4)$$

Where; t is the equilibrium time, C_0 and C_t are the gas inlet and outlet concentrations.

Activated carbon used in this study were disposed to the waste management and treatment facility by following applicable rules or can be regenerated using thermal, steam, and chemical processes (Reza et al., 2020).

3. RESULTS AND DISCUSSION

3.1 BET analysis and activation time selection

Microporosities and surface area are important properties that characterize carbon adsorbents (Saputro et al., 2020). The results of BET analysis at various activation times are shown in Figure 2.

Figure 2 shows that the surface area increased from $39.06 \text{ m}^2/\text{g}$ to $588.41 \text{ m}^2/\text{g}$ with activation times of 15 and 120 min, respectively, and then decreased to $535.62 \text{ m}^2/\text{g}$ with longer activation time (180 min). In the activation process, superheated CO_2 diffuses into the inner precursor which burns the blockage of the byproducts, expands the pore, and increases the surface area (Lan et al., 2019; Yuliusman et al., 2017). The activation reaction can be seen below (Cheremisinoff dan Ellerbusch, 1978).

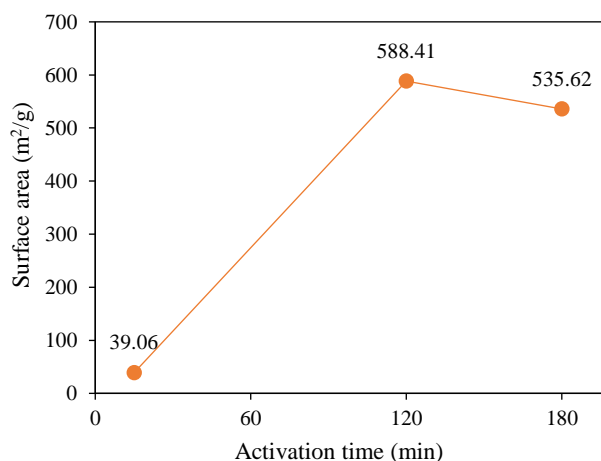
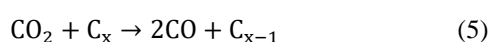


Figure 2. MP-AC surface area at various activation times.

According to Yang and Lua (2003), the increase in activation time increases the BET surface area. However, it can also result in the excessive carbon- CO_2 reaction, thus causing the expansion of the pores and some pore walls to collapse. Therefore, the surface area decreases in 180 min, and 120 min was chosen as the optimum activation time used in this study. The surface area obtained is smaller compared to the previous MP-AC studies using steam and chemical activation (Mukti et al., 2015; Nasrullah et al., 2019), probably due to the temperature and activating agent being used (Gebreegziabher et al., 2019). However, the surface area of activated carbon usually ranges $300\text{--}2,000 \text{ m}^2/\text{g}$ (Saputro et al., 2020), meaning that the result is still in the suitable range.

The isotherm graph obtained (Figure 3) showed the BET type 1 according to IUPAC classification, which usually indicates that the material is micro-shaped (Ambroz et al., 2018) with a relatively broad range of pore size distributions including wider and

narrower micropores (<~2.5 nm) (Giraldo and Moreno-Pirajan, 2018).

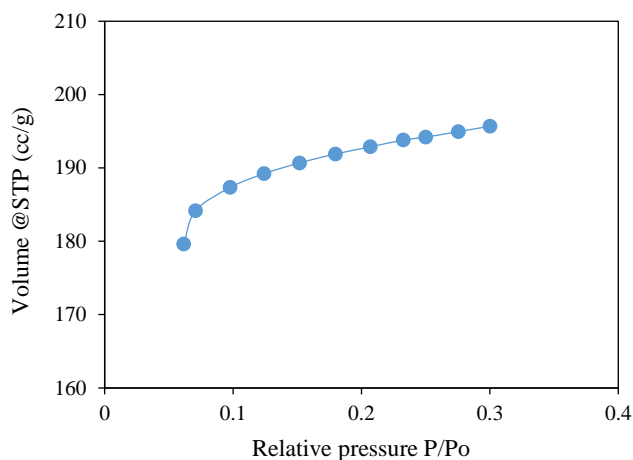


Figure 3. BET isotherm graph

3.2 Characterization of mangosteen peel activated carbon

The results of moisture, ash content, and iodine number compared to other studies are shown in Table 1.

Based on Table 1, the moisture content (6.07%) is higher than other studies' which use chemical activation, and lower than that of using physicochemical activation. This content indicates the hygroscopic nature which can affect the adsorption capacity (Hastuti et al., 2015). Meanwhile, the ash content which indicates the mineral content in activated carbon (Hastuti et al., 2015) has the highest value (9.8%) of all. According to Rangabhashiyam and Balasubramanian (2019), it can be influenced by the pyrolysis temperature and the activation method. The physical activation has a lower efficiency in reducing the mineral content than chemical activation, so the ash content becomes relatively higher.

Table 1. Characterization of MP-AC

Activation/temperature (°C)	Moisture content (%)	Ash content (%)	Iodine number (mg/g)	References
Physical CO ₂ /850	6.07	9.8	1153.69	This research
Chemical ZnCl ₂ 600	4.8	1.45	N/A	Nasrullah et al. (2019)
Chemical ZnCl ₂	1.07	5.68	820	Rattanapan et al. (2014)
Physicochemical KOH-CO ₂ /828	9.08	1.63	N/A	Ahmad and Alrozi (2010)

The iodine number obtained is 1153.69 mg/g, higher than that of Rattanapan et al. (2014). This iodine number shows adsorption ability, illustrates the porosity of activated carbon, and its higher value attributed to the presence of micropores as already proven in the BET isotherm graph. The result is also

included in the range of suitable activated carbon (500-1,200 mg/g) (Saka, 2012).

3.3 FTIR and SEM-EDS analyses

The surface functional group of MP-AC is characterized using FTIR as seen in Figure 4.

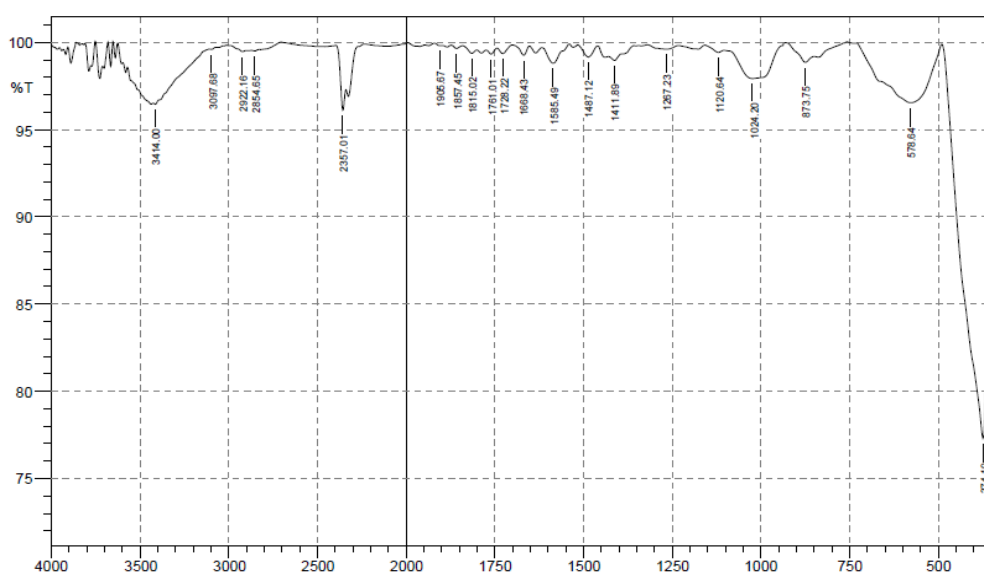


Figure 4. FTIR characterization spectrum of MP-AC

The FTIR result (Figure 4) shows many peaks which representing the complex nature of MP-AC (Nasrullah et al., 2019). The broad peak in 3,600-3,200 cm^{-1} indicates the presence of hydroxyl (O-H) group influenced by CO_2 as an activating agent, and the peak in 2,400-2,300 cm^{-1} shows a formation of nitrile ($\text{C}\equiv\text{N}$) (Ahmad et al., 2013). The small peak that occurs in 1,267.23 cm^{-1} and 1,120.64 cm^{-1} indicates the MP-AC contains a lack of C-O stretching as oxygen

functional group in lactonic groups, alcoholic groups, and carboxylate moieties (Chen et al., 2011; Nasrullah et al., 2019). Moreover, the peaks in range of 1,620-1,400 cm^{-1} , 1,760-1,690 cm^{-1} , 3,100-2,850 cm^{-1} , and <900 cm^{-1} , indicates C=C stretching, carbonyl group C=O, hydrocarbons C-H, and aromatic bond C-H, respectively (Ahmad et al., 2013).

The results of SEM analysis before and after the adsorption process can be seen in Figure 5 as follows

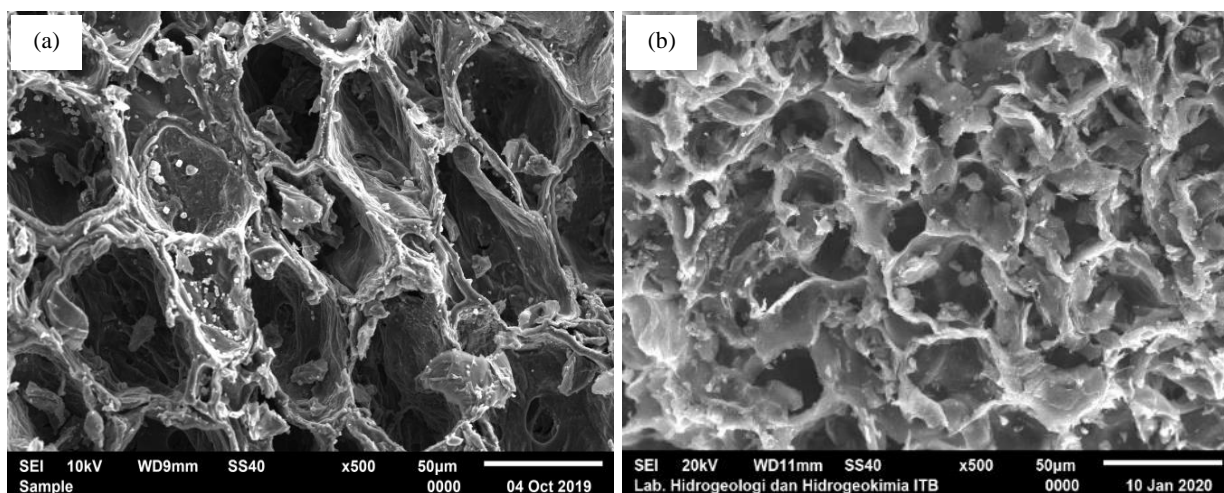


Figure 5. SEM image (a) before; (b) after NH_3 adsorption

Before adsorption (Figure 5(a)), morphology shows presence of circular pores in different size and crevices after the carbonization and CO_2 activation. It is shown that the MP-AC has porous nature that might affect the adsorption process (Nasrullah et al., 2019). After the adsorption (Figure 5(b)) there is an increase of impurities on MP-AC surface compared to the initial sample. This is because the adsorbate moves into the carbon pores during adsorption and results in the pore blockage (Basrur and Bhat, 2018). The surface elements of MP-AC determined using EDS is presented in Table 2.

Table 2. EDS analysis result of MP-AC before and after NH_3 adsorption

Sample	% mass			
	C	N	O	Other compounds
Before adsorption	71.84	16.07	8.77	3.32
After adsorption	70.62	16.94	9.43	3.01

Based on Table 2, the major compounds of MP-AC surface are carbon (71.84%), nitrogen (16.07%), and oxygen (8.77%). The N value of activated carbon

is higher than dried mangosteen peel (1-2.67%) (Devi et al., 2014; Giraldo and Moreno-Pirajan, 2018; Nasrullah et al., 2019), probably due to the use of N_2 as the inert atmosphere during the pyrolysis and cooling processes (Ahmad et al., 2013). Meanwhile, after the adsorption, there is no significant difference to these three major compounds.

3.4 Adsorption of NH_3

3.4.1 Effect of adsorbent mass and adsorbate concentration

The breakthrough curves of NH_3 adsorption at different adsorbent mass and adsorbate inlet concentration are presented in Figure 6.

Based on Figure 6, initially, NH_3 is fully adsorbed and adsorption process decreases with approaching equilibrium and gradually becomes constant. Figure 6(a) shows that for adsorbent mass of 1, 3, and 5 g, the equilibrium time was 16, 23, and 25 minutes respectively, indicating that saturation time becomes longer with the addition of adsorbent mass. This is due to the increasing surface area and available adsorption sites (Patel, 2019). Meanwhile, shown in Figure 6(b), smaller inlet concentrations produce the

longer breakthrough curves. According to [Ding and Liu \(2020\)](#) the decreasing inlet concentration

decreases the amount of gas molecule passing the adsorbent, so the active sites are exhausted slowly.

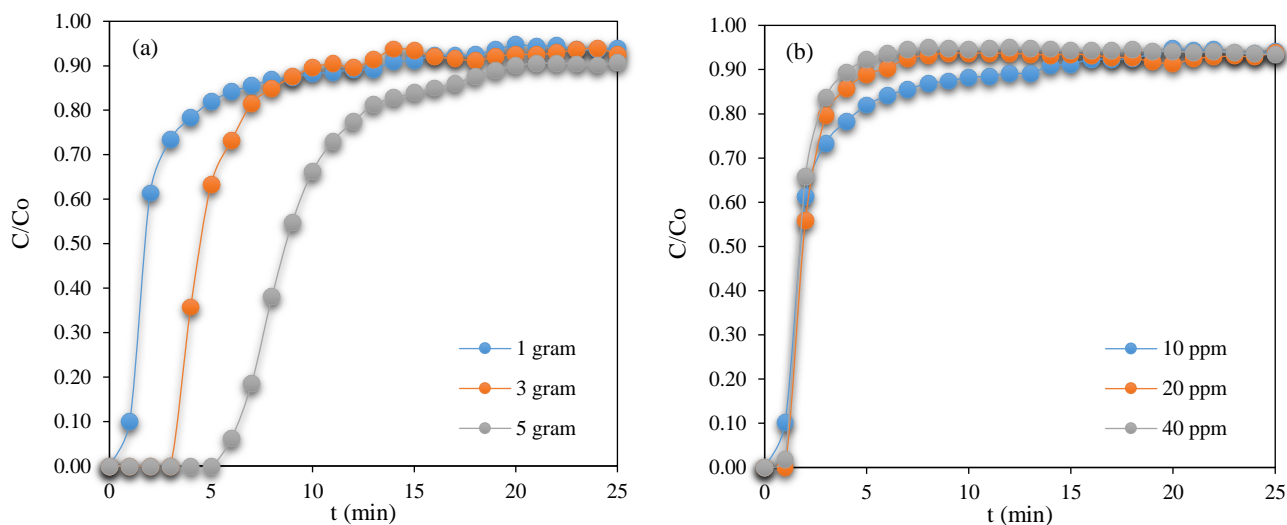


Figure 6. NH₃ breakthrough curve at different (a) adsorbent mass (10 ppm inlet concentration), and (b) different inlet concentration (adsorbent dosage 1 g/27.5 L)

3.4.2 Adsorption capacity

The adsorption capacity value is obtained from the breakthrough graph ([Figure 6](#)) which is calculated using Equation 4. The average NH₃ adsorption capacity on MP-AC is 0.41 mg/g. The value is lower compared to commercial activated carbon which ranges from 0.6 to 4.7 mg/g ([Ro et al., 2015](#)). This result correlates with the EDS result that the N compounds after and before adsorption do not show significant differences. The NH₃ adsorption may be affected by several factors such as surface functional group, pore size and structure, and surface area ([Kang et al., 2020](#); [Yeom and Kim, 2017](#)). Suspected in this study, acidic oxygen functional groups such as –OH, –NH, –C=O, –COOH, and metal ions is the main factor affecting adsorption capacity ([Ro et al., 2015](#); [Kang et al., 2020](#)). According to the FTIR result, some of acidic surface oxygen groups are present such as –OH and –C=O. However, the nitrile group is also found, thus increasing the basic nature of the activated carbon, as supported from the EDS result that the %mass of nitrogen can increase the basicity of the activated carbon ([Ahmad et al., 2013](#)). This finding might indicate that the surface of MP-AC is less acidic in nature due to the use of physical activation method ([Nowicki et al., 2015](#)) thus affecting the adsorption capacity. Additionally, further research is needed to enhance the NH₃ adsorption capacity and the use in numerous environmental applications.

3.4.3 Adsorption kinetics

Lagergren pseudo-first and pseudo-second order kinetic models are evaluated to describe the mechanism of NH₃ adsorption due to their good applicability in most cases ([Ghasemi et al., 2014](#)). The equations of pseudo-first order and pseudo-second order can be expressed as follows ([Lagergren, 1898](#); [Ho and McKay, 1999](#));

$$q_t = q_e [1 - e^{(-kt)}] \quad (6)$$

$$q_t = \frac{k_2 q_e^2 t}{1 + k_2 q_e^2 t} \quad (7)$$

Where; q_e and q_t (mg/g) are the adsorption capacity at equilibrium and time t , respectively; k and k_2 is the pseudo first and second order rate constant, respectively.

The results of kinetic parameters for each kinetic model are presented in [Table 3](#).

For determining the appropriate kinetic model, calculated q_e and R^2 values should be taken into account ([Unugul and Nigiz, 2020](#)). According to the results in [Table 3](#) and [Figure 7](#), both pseudo-first order and pseudo-second order kinetic models show high and good R^2 values. However, from the calculated q_e value, the pseudo-first order kinetic model is close to the experiment data. This indicates that the pseudo-first order kinetic model is more suitable to describe the adsorption mechanism where NH₃ adsorption is

physically controlled. The physisorption occurs due to the Van der Waals forces (Guo et al., 2005) and in the

pore surfaces which contain hydroxyl group as a preferred site to bind NH₃ (Yeom and Kim, 2017).

Table 3. Kinetics parameter of NH₃ adsorption on MP-AC

Mass (g)	Co (ppm)	qe exp (mg/g)	Pseudo-first order			Pseudo-second order		
			k ₁ (min ⁻¹)	qe ₁ (mg/g)	R ²	k ₂ (g/min.mg ⁻¹)	qe ₂ (mg/g)	R ²
1	10	0.413	0.205	0.404	0.971	0.394	0.516	0.986
	20	0.303	0.565	0.290	0.991	1.909	0.347	0.999
	40	0.316	0.793	0.309	0.996	2.507	0.370	1.000
3	10	0.363	0.231	0.345	0.988	0.619	0.417	0.992
	20	0.450	0.201	0.475	0.996	0.259	0.650	0.992
	40	0.448	0.306	0.474	0.993	0.415	0.637	0.987
5	10	0.427	0.134	0.441	0.994	0.204	0.586	0.986
	20	0.493	0.124	0.581	0.989	0.106	0.857	0.983
	40	0.515	0.169	0.612	0.989	0.135	0.908	0.984

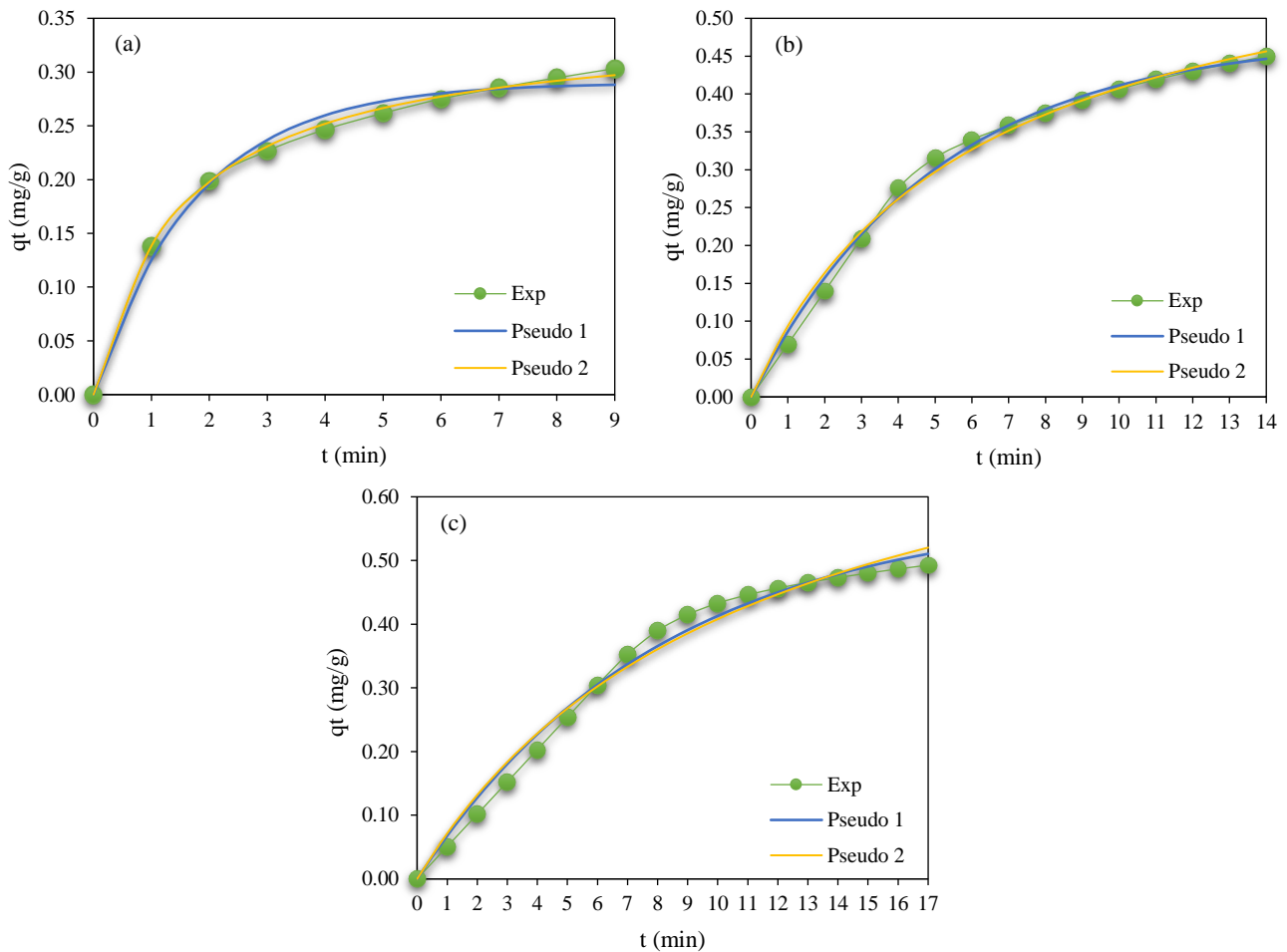


Figure 7. Adsorption kinetics of NH₃ on MP-AC at 20 ppm inlet concentration and adsorbent mass of (a) 1 g, (b) 3 g, and (c) 5 g

3.4.4 Adsorption isotherm

In this study, to describe the interaction between adsorbate and adsorbent at the equilibrium, the Freundlich and Langmuir isotherm were investigated. The linear equation of Freundlich and Langmuir isotherm model is shown in Equation 8 and 9

respectively as follows (Freundlich, 1906; Langmuir, 1917):

$$\log q_e = \log K_F + \frac{1}{n} \log C_e \tag{8}$$

$$\frac{C_e}{q_e} = \frac{C_e}{q} + \frac{1}{qK_L} \tag{9}$$

$$R_L = \frac{1}{1+K_L \cdot C_e} \quad (10)$$

Where; q_e is the adsorption capacity at equilibrium (mg/g adsorbent), K_F is the Freundlich constant, K_L is the Langmuir constant (L/mg), n is the constant related to the adsorption energy of

heterogeneity adsorbent site, C_e is the concentration of contaminants in equilibrium (mg/L), and R_L is equilibrium parameter.

The values of isotherm parameters for both Freundlich and Langmuir isotherm models are presented in Table 4.

Table 4. Isotherm parameters of NH_3 adsorption on MP-AC

Mass	Freundlich				Langmuir			
	1/n	N	K_f (mg/g)(L/mg) ^{1/n}	R ²	q (mg/g)	K_L (L/mg)	R_L	R ²
1 g	0.195	5.1	0.15	0.615	0.297	820.63	0.09	0.992
3 g	0.153	6.5	1.22	0.644	0.481	611.00	0.12	0.994
5 g	0.146	6.8	1.10	0.877	0.557	544.21	0.13	0.999

Based on determination coefficient (R^2) from Table 4, the Langmuir isotherm is more suitable to describe the NH_3 adsorption process with the R^2 of 0.999. The similar result has also been reported in previous studies for Methylene Blue adsorption (Foo and Hameed, 2012; Nasrullah et al., 2019), and in the NH_3 adsorption on corncob activated carbon (Gebreegziabher et al., 2019). Langmuir isotherms indicates the monolayer adsorption where there is no interaction in adsorbate molecules (El maguana et al., 2020), and the carbon surfaces have homogeneous structures and identical active sites (Kutluay et al., 2019). Moreover, the equilibrium parameter (R_L) value is in the range of $0 < R_L < 1$, suggesting that the NH_3 adsorption using MP-AC is favorable (Hamzaoui et al., 2018).

4. CONCLUSION

MP-AC prepared from physical activation using CO_2 at 850°C for 120 min shows good porosity with surface area of $588.41 \text{ m}^2/\text{g}$, 6.07% moisture content, 9.8% ash content, and iodine number of 1153.69 mg/g . MP-AC can be used as an adsorbent material to remove NH_3 with adsorption capacity of 0.41 mg/g which is lower than commercial activated carbon ($0.6\text{--}4.7 \text{ mg/g}$). The pseudo-first order kinetic and the Langmuir isotherm are best fitted to the experimental data. Consequently, mangosteen peel may be potentially used as an activated carbon precursor with further modification for NH_3 adsorption and various environmental applications.

ACKNOWLEDGEMENTS

The authors would like to acknowledge Research Center for Nanoscience and Nano-

technology ITB for providing facilities in this research.

REFERENCES

- Ahmad F, Daud WMAW, Ahmad MA, Radzi R, Azmi AA. The effects of CO_2 activation, on porosity and surface functional group of cocoa (*Theobroma cacao*): Shell based activation carbon. Journal of Environmental Chemical Engineering 2013;1:378-88.
- Ahmad MA, Alrozi R. Optimization of preparation conditions for mangosteen peel-based activated carbons for the removal of Remazol Brilliant Blue R using response surface methodology. Chemical Engineering Journal 2010;165:883-90.
- Ahmad MA, Alrozi R. Removal of malachite green dye from aqueous solution using rambutan peel-based activated carbon: Equilibrium, kinetic, and thermodynamic studies. Chemical Engineering Journal 2011;171:510-6.
- Ambroz F, Macdonald TJ, Martis V, Parkin IP. Evaluation of the BET theory for the characterization of meso and microporous MOFs. Small Methods 2018;2:1800173.
- Basrur D, Bhat J. Preparation of activated carbon from mustard seed and its adsorption efficiency towards dye and acid. Journal of Urban and Environmental Engineering 2018; 12:266-76.
- Bernal V, Giraldo L, Moreno-Piraján J. Physicochemical properties of activated carbon: Their effect on the adsorption of pharmaceutical compounds and adsorbate-adsorbent interactions. Journal of Carbon Research 2018;4:62.
- Chandra TC, Mirna MM, Sunarso J, Sudaryanto Y, Ismadji S. Activated carbon from durian shell: Preparation and characterization. Journal of the Taiwan Institute of Chemical Engineering 2009;40:457-62.
- Chen Y, Huang B, Huang M, Cai B. On the preparation and characterization of activated carbon from mangosteen shell. Journal of the Taiwan Institute of Chemical Engineers 2011;42:837-42.
- Cheremisinoff PN, Ellerbusch F. Carbon Adsorption Handbook. Michigan, USA: Ann Arbor Science Publishers; 1978.
- Choo HS, Lau LC, Mohamed AR, Lee KT. Hydrogen sulfide adsorption by alkaline impregnated coconut shell activated carbon. Journal of Engineering Science and Technology 2013;8:741-53.

- Chung Y, Huang C, Liu CH, Bai H. Biotreatment of hydrogen sulfide- and ammonia-containing waste gases by fluidized bed bioreactor. *Journal of the Air and Waste Management Association* 2001;51:163-72.
- Crini G, Lichtfouse E. *Green adsorbents for Pollutant Removal: Innovative material*. Heidelberg, Germany: Springer; 2018.
- Devi AS, Latif PA, Tham YJ, Taufiq-Yap YH. Physical characterization of activated carbon derived from mangosteen peel. *Asian Journal of Chemistry* 2012;24:579-83.
- Ding S, Liu Y. Adsorption of CO₂ from flue gas by novel seaweed-based KOH-activated porous biochars. *Fuel* 2020;260:116382.
- Domingo-Garcia M, Groszek AJ, Lopez-Garzon FJ, Perez-Mendoza M. Dynamic adsorption of ammonia on activated carbons measured by flow microcalorimetry. *Applied Catalysis A: General* 2002;233:141-50.
- El maguana Y, Elhadiri N, Benchanaa M, Chikri R. Adsorption thermodynamic and kinetic studies of methyl orange onto sugar scum powder as a low-cost inorganic adsorbent. *Journal of Chemistry* 2020;2020:1-10.
- Foo KY, Hameed BH. Factors affecting the carbon yield and adsorption capability of the mangosteen peel activated carbon prepared by microwave assisted K₂CO₃ activation. *Chemical Engineering Journal* 2012;180:66-74.
- Fernandez ME, Nunell GV, Bonelli PR, Cukierman AL. Activated carbon developed from orange peels: Batch and dynamic competitive adsorption of basic dyes. *Industrial Crops and Products* 2014;62:437-45.
- Freundlich H. Over the adsorption in solution. *Journal of Physics Chemistry* 1906;57:385-470.
- Gebreegziabher TB, Wang S, Nam H. Adsorption of H₂S, NH₃, and TMA from indoor air using porous corncob activated carbon: Isotherm and kinetic study. *Journal of Environmental Chemical Engineering* 2019;7:103234.
- Ghasemi M, Ghasemi N, Zahedi G, Alwi SRW, Goodarzi M, Javadian H. Kinetic and equilibrium study of Ni(II) sorption from aqueous solutions onto *Peganum harmala*-L. *International Journal of Environmental Science and Technology* 2014;11:1835-44.
- Giraldo L, Moreno-Piraján JC. CO₂ adsorption on activated carbon prepared from mangosteen peel. *Journal of Thermal Analysis and Calorimetry* 2017;133:337-54.
- Guo J, Xu WS, Chen YL, Lua AC. Adsorption of NH₃ onto activated carbon prepared from palm shells impregnated with H₂SO₄. *Journal of Colloid and Interface Science* 2005; 281:285-90.
- Hamzaoui M, Bestani B, Benderdouche N. The use of linear and nonlinear methods for adsorption isotherm optimization of basic green 4-dye onto sawdust-based activated carbon. *Journal of Materials and Environmental Sciences* 2018; 9:1110-8.
- Hastuti N, Pari G, Setiawan D, Mahpudin M, Godang DM. Acidity and alkalinity level of Mayan bamboo activated charcoal (MBAC) on saturated vapor of acid chloride and sodium hydroxide. *Widyariset* 2015;1:41-50.
- Ho YS, McKay G. Pseudo-second order model for sorption processes. *Process Biochemistry* 1999;34:451-65.
- Kang DW, Ju SE, Kim DW, Kang M, Kim H, Hong CS. Emerging porous materials and their composites for NH₃ gas removal. *Advanced Science* 2020;7:2002142.
- Kutluay S, Baytar O, Şahin Ö. Equilibrium, kinetic and thermodynamic studies for dynamic adsorption of benzene in gas phase onto activated carbon produced from *Elaeagnus angustifolia* seeds. *Journal of Environmental Chemical Engineering* 2019;7:102947.
- Lagergren S. About the theory of so-called adsorption of soluble substances. *Kungliga Svenska Vetenskapsakademiens Handlingar* 1898;24:1-39.
- Lan X, Jiang X, Song Y, Jing X, Xing X. The effect of activation temperature on structure and properties of blue coke-based activated carbon by CO₂ activation. *Green Processing and Synthesis* 2019;8:837-45.
- Langmuir I. The constitution and fundamental properties of solids and liquids. II. Liquids. *Journal of the American Chemical Society* 1917;3:1848-906.
- Li Y, Wang X, Cao M. Three-dimensional porous carbon frameworks derived from mangosteen peel waste as promising materials for CO₂ capture and supercapacitors. *Journal of CO₂ Utilization* 2018;27:204-16.
- Meneghetti E, Baroni P, Vieira RS, Da Silva MGC, Beppu MM. Dynamic adsorption of chromium ions onto natural and crosslinked chitosan membranes for wastewater treatment. *Material Research* 2010;13:89-94.
- Mukti NIF, Prasetyo I, Mindaryani A. Preparation of ethylene adsorbent by pyrolysis of mangosteen peels. *Proceeding of Indonesian National Seminar on Chemical Engineering 2015 Sustainable Energy and Mineral Processing for National Competitiveness*; 2015 Oct 12-13; Gajah Mada University Club Hotel, Yogyakarta: Indonesia; 2015.
- Nasrullah A, Saad B, Bhat AH, Khan AS, Danish M, Isa MH, et al. Mangosteen peel waste as a sustainable precursor for high surface area mesoporous activated carbon: Characterization and application for methylene blue removal. *Journal of Cleaner Production* 2019;211:1190-200.
- Nor NM, Lau LC, Lee KT, Mohamed AR. Synthesis of activated carbon from lignocellulosic biomass and its applications in air pollution control: A review. *Journal of Environmental Chemical Engineering* 2013;1:658-66.
- Nowicki P, Kazmierczak J, Pietrzak R. Comparison of physicochemical and sorption properties of activated carbons prepared by physical and chemical activation of cherry stones. *Powder Technology* 2015;269:312-9.
- Patel H. Fixed bed column adsorption study: A comprehensive review. *Applied Water Science* 2019;9:1-17.
- Rangabhashiyam S, Balasubramanian P. The potential of lignocellulosic biomass precursors for biochar production: Performance, mechanism, and wastewater application. *Industrial Crops and Products* 2019;128:405-23.
- Rattanapan S, Pengjam P, Kongsune P. Preparation and characterization of mangosteen peel activated carbon. *Thaksin University Journal* 2014;17:13-21.
- Reza MS, Yun CS, Afroze S, Radenahmad N, Bakar MSA, Saidur R, et al. Preparation of activated carbon from biomass and its applications in water and gas purification: A review. *Arab Journal of Basic and Applied Sciences* 2020;27:208-38.
- Ro KS, Lima IM, Reddy GB, Jackson MA, Gao B. Removing gaseous NH₃ using biochar as an adsorbent. *Agriculture* 2015;5:991-1002.
- Saka C. BET, TG-DTG, FT-IR, SEM, iodine number analysis and preparation of activated carbon from acorn shell by chemical activation with ZnCl₂. *Journal of Analytical and Applied Pyrolysis* 2012;95:21-4.
- Saputro EA, Wulan VDR, Winata BY, Yogaswara RR, Erliyanti NK. The process of activated carbon from coconut shells

- through chemical activation. *Journal of Science and Technology* 2020;9:23-9.
- Statistics Indonesia (BPS). *Statistics of Annual Fruit and Vegetable Plants Indonesia 2018*. Jakarta, Indonesia: BPS-Statistics Indonesia; 2019.
- Unugul T, Nigiz FU. Preparation and characterization an active carbon adsorbent from waste mandarin peel and determination of adsorption behavior on removal of synthetic dye solutions. *Water, Air and Soil Pollution* 2020;231:538.
- Xu R, Tian H, Pan S, Prior SA, Feng Y, Batchelor WD, et al. Global ammonia emissions from synthetic nitrogen fertilizer applications in agricultural systems: Empirical and process-based estimates and uncertainty. *Global Change Biology* 2019;25:314-26.
- Vohra M. Treatment of gaseous ammonia emissions using date palm pits based granular activated carbon. *International Journal of Environmental Research and Public Health* 2020;17:1519.
- Yang T, Lua AC. Characteristics of activated carbons prepared from pistachio-nut shells by physical activation. *Journal of Colloid and Interface Science* 2003;267:408-17.
- Yani M, Nurcahyani PR, Rahayuningsih M. Ammonia removal by biofilter technique packed with coral and granulated activated carbon (GAC) inoculated with enriched nitrifying bacteria. *Journal of Agroindustrial Technology* 2013;23:22-9.
- Yeom C, Kim Y. Adsorption of ammonia using mesoporous alumina prepared by a templating method. *Environmental Engineering Research* 2017;22:401-6.
- Yuliusman, Nasruddin, Afdhol MK, Haris F, Amiliana RA, Hanafi A, et al. Production of activated carbon from coffee grounds using chemical and physical activation method. *Advanced Science Letters* 2017;23:5751-5.

Removal of Iron from Groundwater by Ozonation: The Response Surface Methodology for Parameter Optimization

Apiradee Sukmilin¹ and Ratsamee Sangsirimongkolying^{2*}

¹Environmental Science and Technology Program, Faculty of Science and Technology, Phranakorn Rajabhat University, Bangkok 10220, Thailand

²Chemistry Program, Faculty of Science and Technology, Phranakorn Rajabhat University, Bangkok 10220, Thailand

ARTICLE INFO

Received: 11 Jan 2021
Received in revised: 21 Apr 2021
Accepted: 24 Apr 2021
Published online: 14 Jun 2021
DOI: 10.32526/enrj/19/2020286

Keywords:

Box-Behnken experiment design/
Groundwater/ Iron/ Ozonation/
Response surface methodology

* Corresponding author:

E-mail: ratsamee@gmail.com

ABSTRACT

This research studied the possibility of using ozone to remove iron from groundwater. The optimum conditions were investigated using a Box-Behnken experiment design with statistical analysis by response surface technique. The three parameters investigated, pH (6.0-8.0), hardness (300-500 mg/L as CaCO₃) and removal time (10 to 60 min) were independent parameters of iron removal. Data was examined for optimal conditions and included main effects and their interactions. Analysis of variance indicated that the proposed quadratic model successfully interpreted the experimental data with a coefficient of determination (R²) of 98.83% and adjusted R² of 96.72%. Through this model, it could predict the iron removal efficiency under variable conditions. Furthermore, the optimum conditions were pH 6.99, hardness of 300 mg/L as CaCO₃, and 10 min of reaction time. The predicted iron removal efficiency obtained from the model under the optimum conditions was 99.00%. The experiment confirmed that the optimum condition which validated the model's accuracy of iron removal efficiency was 98.45%. The results showed that ozone can remove iron from groundwater.

1. INTRODUCTION

Iron, the fifth most abundant element of the Earth's crust, easily contaminates groundwater (Das et al., 2007). Iron is an essential mineral for humans; however, its presence in groundwater above a certain level makes water unusable, mainly for aesthetic considerations such as giving reddish color, metallic taste, odor, and turbidity. Iron oxides which are formed in reservoirs upon aerial oxidation of dissolved iron can promote the growth of micro-organisms in water. Therefore, the World Health Organization (WHO) has set a guideline value of 0.3 ppm of iron in drinking water (WHO, 1984; Chaturvedi and Dave, 2012).

There are many conventional methods for the detection and removal of iron from water such as adsorption, complexation, ion exchange, water softening, and electrocoagulation (Das and Nandi, 2019; Thaweechai and Kaewvilai, 2019). These methods are expensive for domestic applications (Choothong et al., 2013; Das and Nandi, 2019). Another effective water treatment is the oxidation

method, which involves the transfer of electrons from iron(II) to iron(III). The most common chemical oxidants in water treatment are chlorine and potassium permanganate. Chlorination is widely used for oxidation of divalent iron. However, the formation of trihalomethane (THMs) in highly colored water can create a problem (Ellis et al., 2000). In contrast, potassium permanganate is normally more expensive than chlorine and must be carefully controlled. Furthermore, the former can form precipitates that cause mudball formations on filters that are difficult to remove and compromise filter performance. Alternatively, a low-cost method of providing oxidation by adding oxygen and reducing the use of chemicals and operating attention is often used. However, this method is not effective for iron in water with complex humic materials or other large organic molecules due to its inability to break strong complexes formed between iron and large organic molecules (Chaturvedi and Dave, 2012).

Citation: Sukmilin A, Sangsirimongkolying R. Removal of iron from groundwater by ozonation: The response surface methodology for parameter optimization. Environ. Nat. Resour. J. 2021;19(4):330-336. (<https://doi.org/10.32526/enrj/19/2020286>)

Ozone may provide a suitable catalyst for iron oxidation and leaves no environmentally harmful residues. The parameters that affect iron removal by ozone are time, pH, and hardness. Iron(II) can be easily oxidized by ozone, which is shown in Equation 1 (Araby et al., 2009).



In many studies, the optimization parameters are still based on trial and error, such as changing one factor at a time. This is an experimental technique based on varying a single factor while fixing the remaining parameters at a certain set of conditions. However, the single-dimensional factor of the experiment is a time-consuming technique and the attained optimum conditions are not accurate due to the neglect of the interaction between the operating variables (Tayeb et al., 2018). To solve this problem, the response surface methodology (RSM) has been suggested to define the effects of individual parameters.

RSM is an assortment of statistical and mathematical tools that have proven valuable for multifactor optimization of various processes. (Aljundi, 2011) Box Behnken design (BBD) is a widely exploited form of RSM, particularly tailored for three levels (-1, 0, and +1). BBD is more efficient than other factorial designs including Central Composite Design (CCD) and requires fewer experiments (Kumar et al., 2016). Recently, RSM has been extensively used in the optimization of operating parameters in combined systems (Qiu et al., 2014).

For this reason, the objective of this study was to investigate the optimum condition of iron removal from groundwater with ozonation by using RSM. Factors affecting ozonation including pH, time and hardness were studied. The results from this research, which exhibit achievements of the utilization of ozonation, can be applied to the oxidation of iron present in groundwater.

2. METHODOLOGY

2.1 Materials

All reagents used in this experiment, including sodium hydroxide (NaOH), sodium thiosulfate ($\text{Na}_2\text{S}_2\text{O}_3$), potassium iodide (KI), nitric acid (HNO_3) and sulfuric acid (H_2SO_4) were analytical grades. Sodium thiosulfate ($\text{Na}_2\text{S}_2\text{O}_3$) was used to quench residual ozone. Potassium iodide (KI) was used to

determine ozone concentration and to trap unreacted ozone. Groundwater was derived from a groundwater well with a depth of approximately 80 meters. The groundwater had a reddish color, an odor, and an initial pH of 7.5. The groundwater sample was preserved by adding 6 M of nitric acid until the pH was 2 in order to stabilize the metal in solution form and prevent precipitation (Rice et al., 2017).

2.2 Groundwater characterization, ozonation, and analysis

Iron concentration in groundwater was analyzed by inductively coupled plasma optical emission spectrophotometer (ICP-OES, Perkin model optima 2100 DV). Hardness was analyzed by following standard methods for water and wastewater treatment (Rice et al., 2017). The ozone generation rate measured by iodometric method was 0.57 mg/min. Ozonation experiments were carried out in batch mode using a cylindrical reactor. Ozone was generated by a laboratory ozone generator (ZON027) using oxygen from an air pump (CS-51). The ozone flow was introduced into the reactor via air diffusers. Aliquot samples of 50 mL were collected at the specified time. Ozone concentration was measured by standard iodometry (Rice et al., 2017). A few drops of sodium thiosulfate solution were added to quench the residual ozone. All experiments were performed in triplicates.

Ozone generation rate was measured with the iodometric method using 2% KI solution in the absorption of ozone gas, then subsequently titrated against sodium thiosulfate titrant. The total iron concentration and pH of groundwater before and after ozonation was analyzed by ICP-OES (Perkin model optima 2100 DV) and pH meter (Eutech Model CyberScan pH1100). The detection limit of ICP-OES was 0.1 $\mu\text{g/L}$. The instrument was calibrated by standard solutions for obtaining a curve with regression coefficient $R^2=0.9999$. Deionized water was used as a blank. The efficiency of iron removal was calculated and analyzed by using BBD and statistical analysis.

2.3 Box-Behnken design and statistical analysis

To analyse the problem and to achieve a model, the researcher used BBD, a RSM which is a collection of mathematical and statistical techniques. To investigate the optimum of the response, this study focused on three significant independent variables: (1) Time; (2) pH; and (3) Hardness as shown in Table 1.

Table 1. Levels of each factor for Box-Behnken design

Parameters	Code levels		
	-1	0	1
Time (min)	10	30	60
pH	6	7	8
Hardness (mg/L as CaCO ₃)	300	400	500

Each variable was manipulated independently over three levels between -1 and +1, at the determined ranges, based on a set of preliminary experiments. To reduced possible bias, experimental order was randomized. Considering that there are only three levels for each factor, the appropriate model was identified as the quadratic model as shown in Equation 2.

$$y = \beta_0 + \sum_{j=1}^k \beta_j x_j + \sum_{j=1}^k \beta_{jj} x_j^2 + \sum_i x_i \sum_{<j=2}^k \beta_{ij} x_i x_j + e_i \quad (2)$$

Where; y is the response; x_i and x_j are the variables; β is the regression coefficient; k is the number of factors studied and optimized in the experiment; and e is the random error. The optimum condition for iron removal was analyzed by RSM with different variable combinations according to the BBD.

3. RESULTS AND DISCUSSION

3.1 Groundwater characterization, ozonation, and analysis

The groundwater sample had a reddish color and odor. The chemical properties of groundwater were examined as shown in Table 2.

Table 3. Statistical summary for each model

Model	S	R ² (%)	R ² (adj) (%)
Linear	2.04572	85.49	81.54
Linear + square	1.07718	97.07	94.88
Linear + interaction	2.24922	87.25	77.68
Full quadratic	0.86253	98.83	96.72

Note: S is standard deviation; R² is coefficient of determination; R² (adj) is adjusted coefficient of determination

According to Table 3, the quadratic model had the lowest standard error (0.8625) and the highest adjusted decision coefficient R² (adj) (96.72 %). This shows that the Quadratic model is the most suitable to explain the results when it is compared to all the others. It might be indicated that the quadratic model was fit to data which explained that some parameters

Iron found in the groundwater was 109 mg/L, which was higher than the permissible concentration standard for iron in drinking water (0.3 mg/L) (Araby et al., 2009). The groundwater sample was considered very hard water with a hardness of 304 mg/L as CaCO₃. The most common sources of iron in groundwater occur naturally from weathering of iron-bearing minerals and rocks. Water hardness in natural water can be up to 100 mg/L as CaCO₃, depending on the associated sources. The concentration of iron and hardness in the groundwater was high due to minerals leached from surrounding soil releasing their constituents, including iron, calcium or magnesium carbonate into the source well (Pentamwa et al., 2011). The high iron and hardness of the groundwater sample not only effects health but also contributed to inefficient and costly operation resulting from scale deposition in the distribution system.

Table 2. Chemical properties of groundwater

Chemical properties	
Iron (mg/L)	109
pH	7.5
Hardness (mg/L as CaCO ₃)	304

3.2 Box-Behnken design and statistical analysis

A model suitability analysis was performed to explain the change in the efficiency of iron removal, resulting from ozonation at different lengths of time (min). The initial pH and hardness of the groundwater were analyzed using four models: (1) Linear model; (2) Linear + square model; (3) Linear + interaction model; and (4) Quadratic model as shown in Table 3.

are twice as effective for iron removal with ozone. On the other hand, the linear models did not provide suitable data of iron removal (high standard error with low R²) with ozone due to results that showed the y parameter did not change equally to the x parameter in the equation.

Table 4. Estimated coefficients and analysis of variance with coded units suggesting a quadratic model for removal of iron by ozone

Term	Coef	SE Coef	t	p
Constant	33.3286	26.9029	1.239	0.270
pH	29.6853	6.5518	4.531	0.006
Hardness	-0.2046	0.0474	-4.316	0.008
Time	-0.3900	0.1484	-2.628	0.057
pH × pH	-1.8513	0.4489	-4.124	0.009
Hardness × hardness	0.0002	0.0000	5.171	0.004
Time × time	0.0011	0.0007	1.512	0.191
pH × hardness	-0.0049	0.0043	-1.148	0.303
pH × time	0.0401	0.0173	2.325	0.068
Hardness × time	0.0002	0.0002	0.870	0.424

Note: Coef is coefficients; SE Coef is the standard error of the coefficients; t is t-value; p is p-value

According to [Table 4](#), regression coefficient, initial pH and hardness showed t significant factors in the removal of iron. The efficiency of iron removal at 95% confidence level with the p-value was less than the significance level ($p < 0.05$). The p-value of time was not significant because it was greater than the p-value ($p > 0.05$), indicating that the initial pH, groundwater and hardness significantly influenced iron removal efficiency at 95% confidence level. Considering the second influence (square terms) in [Table 4](#), which was pH × pH (pH^2), hardness × hardness (hardness^2) and time × time (time^2), the possibility of the square terms was $p = 0.005$. It can be interpreted that at least one independent variable influenced the efficiency of iron removal. The p-value of pH^2 and hardness^2 was less than 95%. This implied that these factors had a significant effect on iron removal efficiency at 95% confidence level. However, the fact that the p-value of time^2 was significantly greater than the p-value > 0.05 indicates that time^2 had no effect on the removal efficiency. When examining the interaction terms in [Table 4](#), it was found that pH × hardness had a p-value of 0.303 and pH × time had a p-value of 0.068, which were greater than the significance level ($p > 0.05$). Meanwhile hardness × time had a p-value of 0.424, which was greater than the significance level ($p > 0.05$). In other words, the change in time has no influence on iron removal in the groundwater.

The equations for predicting the iron removal efficiency in groundwater obtained from statistical analysis using RSM from the Quadratic model, showed the relationships among the independent variables (pH, hardness, and removal time) with iron

removal efficiency, which can be shown as Equation 3.

$$\begin{aligned} \text{Remove efficiency (\%)} & \quad (3) \\ & = 33.3286 + 29.6853 - 0.2046 \text{ hardness} - 0.3900 \text{ time} - \\ & \quad 1.8513 \text{ pH} \times \text{pH} + 0.0002 \text{ hardness} \times \text{hardness} + 0.0011 \\ & \quad \text{time} \times \text{time} - 0.0049 \text{ pH} \times \text{hardness} + 0.0401 \text{ pH} \times \text{time} \\ & \quad + 0.0002 \text{ hardness} \times \text{time} \end{aligned}$$

According to Equation 3, iron removal efficiency could be predicted by inserting values of hardness, pH and time. However, the range of each factor was limited (pH 6-8, hardness 300-500 mg/L, time 5-60 min). For this reason, Equation 3 may provide unexpected results for data outside these ranges.

3.3 Response surface optimization of iron ozonation

The determination of the optimum condition for iron removal was performed according to the BBD featuring different variable combinations. To determine the optimum level of independent variables, three-dimensional surface plots were constructed as shown in [Figure 1](#).

The effect of time and pH on iron removal at a fixed hardness at 300 mg/L as CaCO_3 clearly showed that iron removal favored high pH. According to previous studies, under alkaline pH conditions, iron(II) oxidized to iron(III) and subsequent formation of ferric hydroxide ([Abraham et al., 2020](#)). In the ozonation process, high pH is attributed to the decomposition of ozone and consequently the generation of the hydroxyl radicals (OH^\bullet), which was a very powerful radical and reacted with iron ([Sukmilin et al., 2019](#)). For these reasons, at pH 8 with ozone applied to oxidized iron from the groundwater, the removal efficiency of iron was almost 100 %.

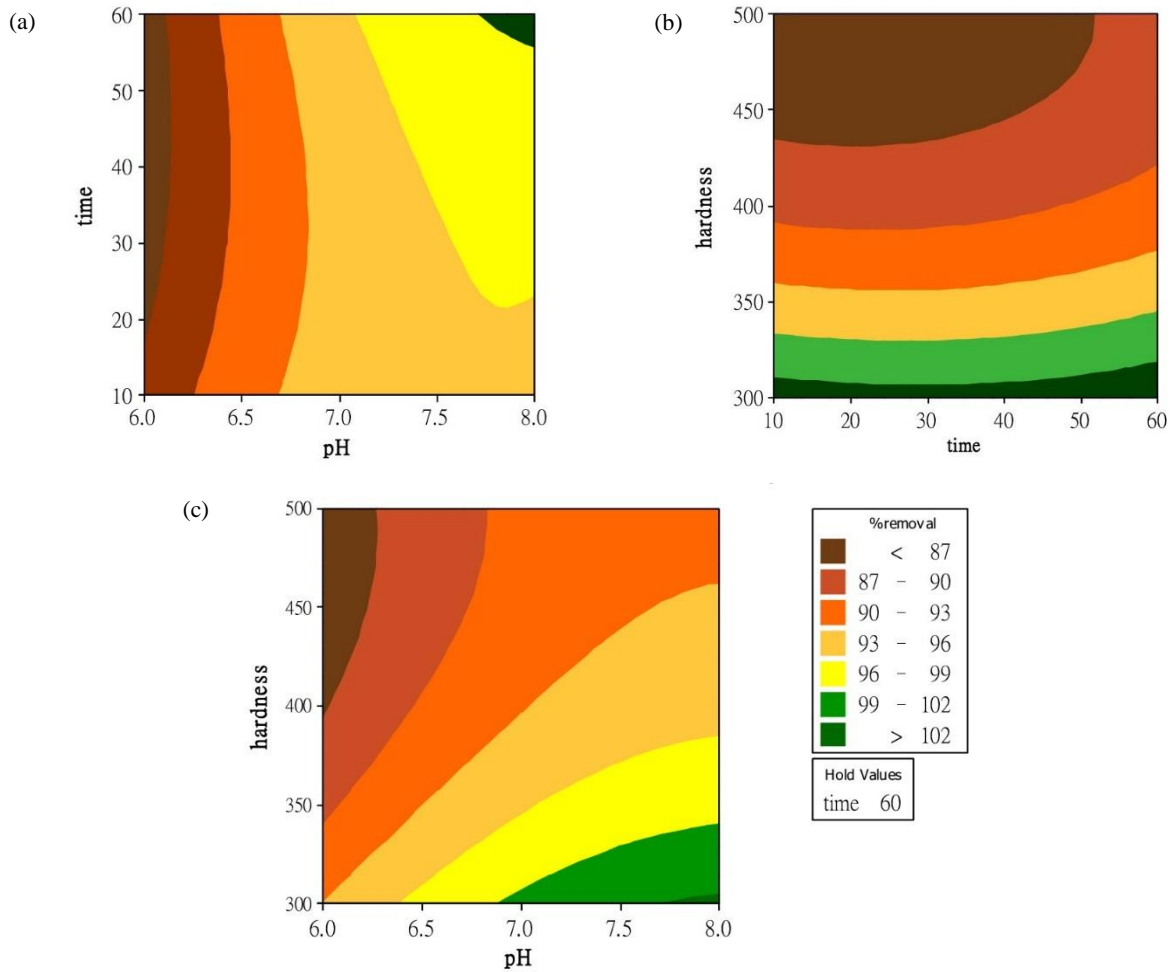


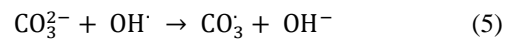
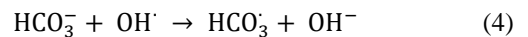
Figure 1. Contour plot of iron removal on variable affected (a) pH vs time; (b) time vs hardness; and (c) pH vs hardness (Experimental conditions: O_3 generation=0.57 mg/min, iron concentration=109 mg/L).

The effect of time and pH on iron removal at a fixed hardness at 300 mg/L as $CaCO_3$ clearly showed that iron removal favored high pH. According to previous studies, under alkaline pH conditions, iron(II) oxidized to iron(III) and subsequent formation of ferric hydroxide (Abraham et al., 2020). In the ozonation process, high pH is attributed to the decomposition of ozone and consequently the generation of the hydroxyl radicals (OH^\bullet), which was a very powerful radical and reacted with iron (Sukmilin et al., 2019). For these reasons, at pH 8 with ozone applied to oxidized iron from the groundwater, the removal efficiency of iron was almost 100 %.

The reaction time did not affect iron removal by ozonation due to ozone acting as a strong oxidant. Ozone could rapidly oxidize iron(II) to iron(III). For this reason, reaction time had no effect on iron removal by ozonation.

When the hardness in the groundwater was increased, the oxidation of iron decreased. The results showed that at 60 minutes, as the hardness as $CaCO_3$

increased from 300 to 500 mg/L, the removal efficiency of iron decreased. According to a previous study Araby et al. (2009), carbonate and bicarbonate can act as ozone radical scavengers as shown in Equation 4 and Equation 5.



From Equation 4 and Equation 5, bicarbonate and carbonate are strong scavengers for hydroxyl radicals (Hachemi et al., 2013). Therefore, the ozonation process with high hardness could slow down decomposition of ozone in the groundwater. For this reason, at hardness 300 mg/L as $CaCO_3$, the removal efficiency of iron was nearly 100%. It might suggest, when the hardness increased, the oxidation of iron decreased. Conversely, when pH increased, iron removal increased. The results showed that high efficiency of removing iron occurred at high pH and

low hardness. In other words, high pH and low hardness could remove iron almost 100%.

3.4 Condition optimization and confirmation test

The compared results between experimental data and the predicted data, calculated using Equation 3, is shown in Table 5.

Table 5 showed the maximum predicting iron removal percentage was about 99% at an initial iron concentration of 109 mg/L, initial solution pH of 6.99, contact time 10 min, hardness 300 mg/L as CaCO₃ and ozone concentration 0.57 mg/min. The optimum conditions were calculated from Equation 3. The optimum conditions were 10 min, pH 6.99 and hardness 300 mg/L. The optimum iron removal

efficiency of the experiment was 98.45%, which was close to the target iron removal efficiency (99%). The percentage of error was 0.558%. Therefore, the Quadratic model was accurate. According to a previous study, the optimum condition to remove iron from simulated groundwater was a pH between 9-10. The percentage of removal iron was 96% (Araby et al., 2009) which was close to the test results. This showed that the RSM model could be effectively used to predict the optimal conditions for iron removal in real groundwater. Therefore, the ozonation process was efficient for removal of iron from groundwater as a pre-treatment process before continuing to other processes such as filtration and ion-exchange in the water treatment.

Table 5. Experimental design matrix and iron removal from the experimental data compared to the predicted values.

Order	Time (min)	pH	Hardness (mg/L)	Iron removal efficiency (%)		% Error
				Experiment	Predict	
1	10	6.00	400	86.95	87.450	0.575
2	10	7.00	300	99.95	99.011	0.939
3	10	7.00	500	88.65	88.976	0.367
4	10	8.00	400	91.35	91.827	0.522
5	35	6.00	300	92.65	93.088	0.472
6	35	6.00	500	84.89	84.428	0.544
7	35	7.00	400	91.35	91.48	0.142
8	35	7.00	400	91.26	91.48	0.241
9	35	7.00	400	91.83	91.48	0.381
10	35	8.00	300	100.00	100.46	0.46
11	35	8.00	500	90.26	89.821	0.486
12	60	6.00	400	87.26	86.782	0.547
13	60	7.00	300	99.56	99.598	0.038
14	60	7.00	500	89.76	90.689	1.034
15	60	8.00	400	95.67	95.17	0.522
Optimum condition	10	6.99	300	98.45	99.0	0.558

4. CONCLUSION

The ozonation process, of which the optimum condition was identified by the BBD with the RSM, was successfully applied to remove iron from the groundwater. Furthermore, the quadratic model was proven suitable to describe the relationship between pH and hardness. The model fitted the experimental data well, with a coefficient of determination (R^2) of 98.83 % and an Adj- R^2 of 96.72%. In addition, the p-value of this model was less than 0.05, which indicates that the model was statistically significant. At the optimum condition of pH 8 and hardness of 300 mg/L, removal efficiency of iron reached 99.00%. Moreover,

the experiment revealed that iron removal was 98.45%. It can be concluded that ozonation was able to effectively oxidize iron in the groundwater as predicted by the model constructed according to the BBD. Future research is required to investigate more effective pilot-scale treating. In addition, the efficiency of disinfection and economic aspects such as operation cost and investment cost should be investigated.

ACKNOWLEDGEMENTS

The research was supported by Pranakhon Rajabhat University.

REFERENCES

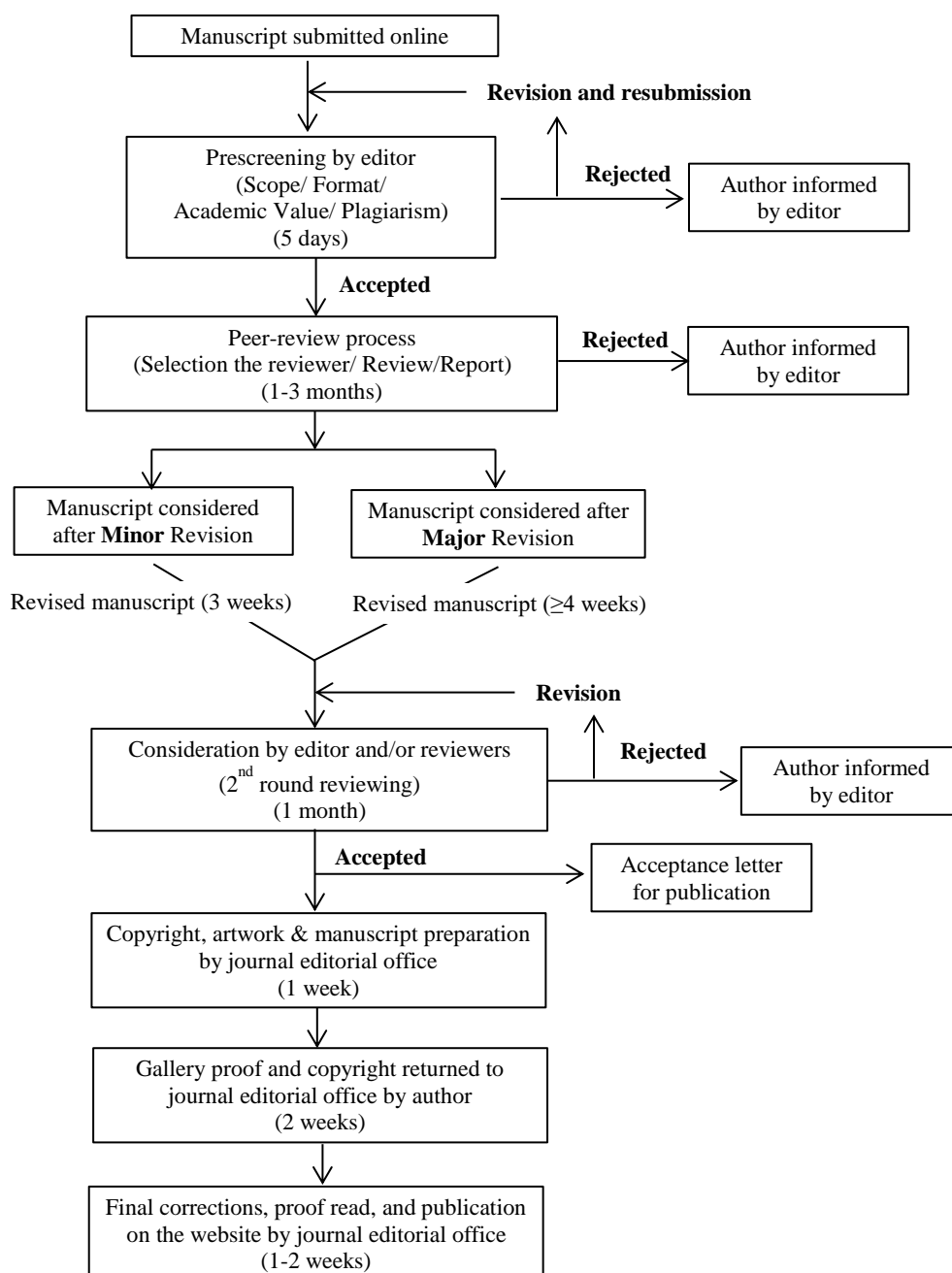
- Abraham N, James J, Banerji T, Menon R. Development of a novel groundwater iron removal system using adsorptive Fe(II) process. *Groundwater for Sustainable Development* 2020; 10:1-7.
- Aljundi IH. Bromate formation during ozonation of drinking water: A response surface methodology study. *Desalination* 2011;277:24-8.
- Araby R El, Hawash S, Diwani G El. Treatment of iron and manganese in simulated groundwater via ozone technology. *Desalination* 2009;249:1345-9.
- Chaturvedi S, Dave PN. Removal of iron for safe drinking water. *Desalination* 2012;303:1-11.
- Choothong N, Kaewvilai A, Laobuthee A, Lertworasirikul A. A novel colorimetric sensing material, poly(γ -glutamic acid)-graft-3, 4-dihydro-3-(2'-ethyl hydroxyl)-6-ethyl-1,3,2H-benzoxazine (γ -PGA-graft-ethyl-Bx), for iron(III) ions. *Sains Malaysiana* 2013;42(2):223-9.
- Das B, Hazarika P, Saikia G, Kalita H, Goswami DC, Das HB, et al. Removal of iron from groundwater by ash: A systematic study of a traditional method. *Journal of Hazardous Materials* 2007;141:834-41.
- Das B, Nandi BK. Removal of Fe (II) ions from drinking water using Electrocoagulation (EC) process: Parametric optimization and kinetic study. *Journal of Environmental Chemical Engineering* 2019;7:1-9.
- Ellis D, Bouchard C, Lantagne G. Removal of iron and manganese from groundwater by oxidation and microfiltration. *Desalination* 2000;130:255-64.
- Hachemi MEE, Naffrechoux E, Suptil J, Hausler R. Bicarbonate effect in the ozone-UV process in the presence of nitrate. *Ozone: Science and Engineering* 2013;35:3-7.
- Kumar SS, Malyan SK, Kumar A, Bishnoi NR. Optimization of fenton's oxidation by box Behnken design of response surface methodology for landfill leachate. *Journal of Material and Environmental Science* 2016;12:4456-66.
- Pentamwa P, Thiphara W, Nuangon S. Removal of hardness from groundwater by synthetic resin from waste plastics. *International Journal of Environmental Science and Development* 2011;2(6):479-83.
- Qiu P, Cui M, Kang K, Park B, Son Y, et al. Application of Box Behnken design with response surface methodology for modelling and optimizing ultrasonic oxidation of arsenite with H₂O₂. *Central European Journal of Chemistry* 2014;12(2):164-72.
- Rice EW, Baird RB, Eaton AD. *Standard Methods for the Examination of Water and Wastewater*. 23rd ed. American Public Health Association, American Water Works Association, Water Environment Federation; 2017.
- Sukmilin A, Boonchom B, Jarusuttirak C. Catalytic ozonation using iron-doped water treatment sludge as a catalyst for treatment of phenol in synthetic wastewater. *Environment and Natural Resources Journal* 2019;17(2):87-95.
- Tayeb A, Tony MA, Mansour SA. Application of Box Behnken factorial design for parameters optimization of basic dye removal using nano hematite photo fenton. *Applied Water Science* 2018;8(138):1-9.
- Thaweechai T, Kaewvilai A. Benzoxazine grafted poly(γ -glutamic acid) functional material: Synthesis, characterization and photophysical properties. *Materials Chemistry and Physics* 2019;227:117-22.
- World Health Organization (WHO). *World Health Organization Guidelines for Drinking Water Quality, Recommendations*. Geneva, Switzerland: WHO; 1984. p. 79.

INSTRUCTION FOR AUTHORS

Publication and Peer-reviewing processes of Environment and Natural Resources Journal

Environment and Natural Resources Journal is a peer reviewed and open access journal that is published twice a year (January-June and July-December). Manuscripts should be submitted online at <https://ph02.tci-thaijo.org/index.php/ennrj/about/submissions> by registering and logging into this website. Submitted manuscripts should not have been published previously, nor be under consideration for publication elsewhere (except conference proceedings papers). A guide for authors and relevant information for the submission of manuscripts are provided in this section and also online at: <https://ph02.tci-thaijo.org/index.php/ennrj/author>. All manuscripts are refereed through a **double-blind peer-review** process.

Submitted manuscripts are reviewed by outside experts or editorial board members of **Environment and Natural Resources Journal**. This journal uses double-blind review, which means that both the reviewer and author identities are concealed from the reviewers, and vice versa, throughout the review process. Steps in the process are as follows:



The Environment and Natural Resources Journal (EnNRJ) accepts 2 types of articles for consideration of publication as follows:

- *Original Research Article*: Manuscripts should not exceed 3,500 words (excluding references).
- *Review Article (by invitation)*: This type of article focuses on the in-depth critical review of a special aspect in the environment and also provides a synthesis and critical evaluation of the state of the knowledge of the subject. Manuscripts should not exceed 6,000 words (excluding references).

Submission of Manuscript

Cover letter: Key points to include:

- Statement that your paper has not been previously published and is not currently under consideration by another journal
- Brief description of the research you are reporting in your paper, why it is important, and why you think the readers of the journal would be interested in it
- Contact information for you and any co-authors
- Confirmation that you have no competing interests to disclose

Manuscript-full: Manuscript (A4) must be submitted in Microsoft Word Files (.doc or .docx). Please make any identifying information of name(s) of the author(s), affiliation(s) of the author(s). Each affiliation should be indicated with superscripted Arabic numerals immediately after an author's name and before the appropriate address. Specify the Department/School/Faculty, University, Province/State, and Country of each affiliation.

Manuscript-anonymized: Manuscript (A4) must be submitted in Microsoft Word Files (.doc or .docx). Please remove any identifying information, such as authors' names or affiliations, from your manuscript before submission and give all information about authors at title page section.

Reviewers suggestion (mandatory): Please provide the names of 3 potential reviewers with the information about their affiliations and email addresses. *The recommended reviewers should not have any conflict of interest with the authors. Each of the reviewers must come from a different affiliation and must not have the same nationality as the authors.* Please note that the editorial board retains the sole right to decide whether or not the recommended potential reviewers will be selected.

Preparation of Manuscript

Manuscript should be prepared strictly as per guidelines given below. The manuscript (A4 size page) must be submitted in Microsoft Word (.doc or .docx) with Times New Roman 12 point font and a line spacing of 1.5. *The manuscript that is not in the correct format will be returned and the corresponding author may have to resubmit.* The submitted manuscript must have the following parts:

Title should be concise and no longer than necessary. Capitalize first letters of all important words, in Times New Roman 12 point bold.

Author(s) name and affiliation must be given, especially the first and last names of all authors, in Times New Roman 11 point bold.

Affiliation of all author(s) must be given in Times New Roman 11 point italic.

Abstract should indicate the significant findings with data. A good abstract should have only one paragraph and be limited to 250 words. Do not include a table, figure or reference.

Keywords should adequately index the subject matter and up to six keywords are allowed.

Text body normally includes the following sections: 1. Introduction 2. Methodology 3. Results and Discussion 4. Conclusions 5. Acknowledgements 6. References

Reference style must be given in Vancouver style. Please follow the format of the sample references and citations as shown in this Guide below.

Unit: The use of abbreviation must be in accordance with the SI Unit.

Format and Style

Paper Margins must be 2.54 cm on the left and the right. The bottom and the top margin of each page must be 1.9 cm.

Introduction is critically important. It should include precisely the aims of the study. It should be as concise as possible with no sub headings. The significance of problem and the essential background should be given.

Methodology should be sufficiently detailed to enable the experiments to be reproduced. The techniques and methodology adopted should be supported with standard references.

Headings in Methodology section and Results and Discussion section, no more than three levels of headings should be used. Main headings should be typed (in bold letters) and secondary headings (in bold and italic letters). Third level headings should be typed in normal and no bold, for example;

2. Methodology

2.1 Sub-heading

2.1.1 Sub-sub-heading

Results and Discussion can be either combined or separated. This section is simply to present the key points of your findings in figures and tables, and explain additional findings in the text; no interpretation of findings is required. The results section is purely descriptive.

Tables Tables look best if all the cells are not bordered; place horizontal borders only under the legend, the column headings and the bottom.

Figures should be submitted in color; make sure that they are clear and understandable. Please adjust the font size to 9-10, no bold letters needed, and the border width of the graphs must be 0.75 pt. (*Do not directly cut and paste them from MS Excel.*) Regardless of the application used, when your electronic artwork is finalized, please 'save as' or convert the images to TIFF (or JPG) and separately send them to EnNRJ. The images require a resolution of at least 300 dpi (dots per inch). If a label needed in a figure, its font must be "Times New Roman" and its size needs to be adjusted to fit the figure without borderlines.

All Figure(s) and Table(s) should be embedded in the text file.

Conclusions should include the summary of the key findings, and key take-home message. This should not be too long or repetitive, but is worth having so that your argument is not left unfinished. Importantly, don't start any new thoughts in your conclusion.

Acknowledgements should include the names of those who contributed substantially to the work described in the manuscript but do not fulfill the requirements for authorship. It should also include any sponsor or funding agency that supported the work.

References should be cited in the text by the surname of the author(s), and the year. This journal uses the author-date method of citation: the last name of the author and date of publication are inserted in the text in the appropriate place. If there are more than two authors, "et al." after the first author's name must be added. Examples: (Frits, 1976; Pandey and Shukla, 2003; Kungsuwas et al., 1996). If the author's name is part of the sentence, only the date is placed in parentheses: "Frits (1976) argued that . . ."

Please be ensured that every reference cited in the text is also present in the reference list (and vice versa).

In the list of references at the end of the manuscript, full and complete references must be given in the following style and punctuation, arranged alphabetically by first author's surname. Examples of references as listed in the References section are given below.

Book

Tyree MT, Zimmermann MH. Xylem Structure and the Ascent of Sap. Heidelberg, Germany: Springer; 2002.

Chapter in a book

Kungsuwan A, Ittipong B, Chandrakachang S. Preservative effect of chitosan on fish products. In: Steven WF, Rao MS, Chandrakachang S, editors. Chitin and Chitosan: Environmental and Friendly and Versatile Biomaterials. Bangkok: Asian Institute of Technology; 1996. p. 193-9.

Journal article

Muenmee S, Chiemchaisri W, Chiemchaisri C. Microbial consortium involving biological methane oxidation in relation to the biodegradation of waste plastics in a solid waste disposal open dump site. *International Biodeterioration and Biodegradation* 2015;102:172-81.

Published in conference proceedings

Wiwattanakantang P, To-im J. Tourist satisfaction on sustainable tourism development, amphawa floating market Samut songkhram, Thailand. *Proceedings of the 1st Environment and Natural Resources International Conference*; 2014 Nov 6-7; The Sukosol hotel, Bangkok: Thailand; 2014.

Ph.D./Master thesis

Shrestha MK. Relative Ungulate Abundance in a Fragmented Landscape: Implications for Tiger Conservation [dissertation]. Saint Paul, University of Minnesota; 2004.

Website

Orzel C. Wind and temperature: why doesn't windy equal hot? [Internet]. 2010 [cited 2016 Jun 20]. Available from: <http://scienceblogs.com/principles/2010/08/17/wind-and-temperature-why-doesn/>.

Report organization:

Intergovernmental Panel on Climate Change (IPCC). IPCC Guidelines for National Greenhouse Gas Inventories: Volume 1-5. Hayama, Japan: Institute for Global Environmental Strategies; 2006.

Remark

** Please be note that manuscripts should usually contain at least 15 references and some of them must be up-to-date research articles.*

** Please strictly check all references cited in text, they should be added in the list of references. Our Journal does not publish papers with incomplete citations.*

Copyright transfer

The copyright to the published article is transferred to Environment and Natural Resources Journal (EnNRJ) which is organized by Faculty of Environment and Resource Studies, Mahidol University. The accepted article cannot be published until the Journal Editorial Officer has received the appropriate signed copyright transfer.

Online First Articles

The article will be published online after receipt of the corrected proofs. This is the official first publication citable with the Digital Object Identifier (DOI). After release of the printed version, the paper can also be cited by issue and page numbers. DOI may be used to cite and link to electronic documents. The DOI consists of a unique alpha-numeric character string which is assigned to a document by the publisher upon the initial electronic publication. The assigned DOI never changes.

Environment and Natural Resources Journal (EnNRJ) is licensed under a Attribution-NonCommercial 4.0 International (CC BY-NC 4.0)





Mahidol University
Wisdom of the Land



Research and Academic Service Section, Faculty of Environment and Resource Studies, Mahidol University
999 Phutthamonthon 4 Rd, Salaya, Nakhon Pathom 73170, Phone +662 441-5000 ext. 2108 Fax. +662 441 9509-10
E-mail: ennjournal@gmail.com Website: <https://www.tci-thaijo.org/index.php/ennrj>

